

**Reliability-based design for buckling strength of
stiffened steel plates: ultimate and serviceability
limit states**

(補剛板の信頼性理論の基づく設計：終局限界強度と使用性限界強度)



埼玉大学大学院理工学研究科（博士後期課程）
理工学専攻（主指導教員 奥井義昭）

Mahmudur Rahman

March 2019

**Reliability-based design for buckling strength of stiffened
steel plates: ultimate and serviceability limit states**

(補剛板の信頼性理論の基づく設計：終局限界強度と使用性限
界強度)

by

Mahmudur Rahman

A dissertation submitted to the Saitama University in partial fulfillment of the
requirements for the degree of

DOCTOR OF PHILOSOPHY

Examination Committee

Professor Yoshiaki Okui (Principal Supervisor)

Professor Yasunao Matsumoto

Professor Takeshi Maki

Professor Masahiko Osada

Department of Civil and Environmental Engineering

Saitama University

Saitama, Japan

March 2019

Acknowledgements

It was a great opportunity for me to continue my Doctoral study immediately after my Masters study in the Saitama University under the ADB-JSP, which is probably the first example of this kind. Thanks to the ADB-JSP and Saitama University for providing me such opportunity.

I would like to express my sincere gratitude to my supervisor, Prof. Yoshiaki Okui, for his continuous support, guidance and inspiration. From him, I learned to think in-depth for finding some solution of a critical problem. It was not possible to complete this research without his advices. Constructive comments during the Lab seminars from Prof. Yasunao Matsumoto and Assistant Prof. Dang Ji helped me a lot to enrich the research. I also acknowledge Prof. A.F.M. Saiful, BUET who encouraged me to study in Saitama University and Prof. Monjur Hossain, KUET who enlightened me with the fundamental principles of doing research during my undergraduate study.

This was a joint research work of Saitama University (SU), Muroran Institute of Technology (MIT), and Nagaoka National College of Technology (NNCT), supported by The Japan Iron and Steel Federation. Contribution from Associate Prof. Masato Komuro, MIT and Associate Prof. Yasuhiro Miyazaki, NNCT are greatly acknowledged. For some of the numerical analysis, appreciation towards Mr. Daiki Miazaki, Mr. Shoji Takahiro, and Mr. Atif Anwer, former students of Saitama University and Ms. Azusa Numata, graduate student of MIT.

Finally, special thanks to my wife and my son for their eternal love and encouragement.

Mahmudur Rahman
06 March, 2019
Saitama, Japan

Dedicated to my Parents

Abstract

The strengths of longitudinally continuous stiffened steel plates under uniaxial compression were investigated by employing a combination of numerical and probabilistic approaches. The probabilistic compressive strengths were obtained for two different limit states, i.e. the Ultimate Limit State (ULS) and the Serviceability Limit State (SLS). For slender stiffened plates, the SLS is particularly important because large out-of-plane deflection occurs due to elastic buckling, before reaching the ultimate strength. Due to lack of specific criteria to determine the compressive strength at SLS, a rational criterion has been proposed based on elastic buckling strength and fabrication tolerance.

Three different stiffened plate models with three, two, and one flat plate longitudinal stiffeners, corresponding to Model-1, Model-2, and Model-3 were considered for the study, where Model-1 and Model-2 shows column-like behavior (small post-buckling strength) and Model-3 exhibits plate-like behavior (significant post-buckling strength reserve). The plates of both normal and high-performance steel (SBHS) were taken into account, and their thickness was varied from 10 to 90 mm. The compressive strengths at ULS and SLS were determined from nonlinear elasto-plastic finite element analysis (FEA), where both material and geometric nonlinearity were taken into account. As a source of variability of the compressive strengths, variation of the initial out-of-plane deflection and residual stress were considered simultaneously in the FEA. The probabilistic distribution of the compressive strengths for Model-1 and Model-2 were obtained through Monte Carlo simulations in association with the response surface method. The response surface function is a second order polynomial of the independent random variables, i.e. the initial out-of-plane deflections and the residual stresses. For Model-3, an approximate estimation procedure was followed to obtain the first-order mean values. The first order variances were also estimated approximately, employing the Taylor series finite difference (TSFD) method. Based on the

obtained probabilistic information, partial safety factors were proposed, considering the mean value strengths as the nominal strengths, as an example.

The study results were compared with different design codes e.g. JSMB, AASHTO, Eurocode, and Canadian Code. Comparing to the ULS strengths for Model-1 and Model-2 with a 5% non-exceedance probability indicate that the JSMB, AASHTO, and Canadian Code provides significantly conservative design, specifically for stiffened plates with high reduced slenderness parameters. However, in the middle range of reduced slenderness parameters, AASHTO and Canadian Code predicts overestimated strengths for Model-3. All of the three Models showed better agreement with the Eurocode than other design specifications. Nevertheless, a scope for improvement of the Eurocode was addressed by considering continuous stiffened panels (in the longitudinal direction) rather than an isolated panel. The uniqueness of this research is that the effect of thick plates and SBHS steels were included. Furthermore, rather than deterministic strengths, probabilistic strengths are provided for column-like behavior and plate-like behavior, which can be used as an important reference for developing a reliability-based design strength curve.

Keywords: *Stiffened steel plates, column-like behavior, plate-like behavior, initial imperfection, SBHS steels, FEA, ULS, SLS, response surface, Monte Carlo simulation.*

Table of Contents

Acknowledgements	iv
Abstract	vi
Table of Contents	viii
List of Figures	xi
List of Tables	xv
Chapter 1: Introduction	17
1.1 General.....	17
1.2 Historic steel box girder bridge collapse	18
1.3 Code provisions for buckling strength.....	20
1.3.1 JSHB.....	20
1.3.2 AASHTO	22
1.3.3 Canadian Code.....	24
1.3.4 Eurocode	25
1.4 Basic concept of reliability-based design	26
1.5 Identification of problems	28
1.6 Research objectives and scope	29
1.7 Outline of the dissertation	30
Chapter 2: Probabilistic compressive strength of stiffened steel plates exhibiting column-like behavior: ULS and SLS	33
2.1 Introduction	33
2.2 Description of the models for numerical analysis	35
2.2.1 Geometric configuration.....	35
2.2.2 Boundary conditions.....	36
2.2.3 Material model.....	37
2.3 Deterministic finite element analysis (FEA)	38
2.3.1 Elastic buckling analysis	38
2.3.2 Nonlinear elasto-plastic analysis	40
2.3.3 Effect of initial local out-of-plane deflection	42
2.3.4 Parametric study	43
2.4 FEA results and response surface for ULS.....	45
2.4.1 ULS and stress-strain curves	45
2.4.2 Effect of variation of initial imperfections	46
2.4.3 Response surface for ULS	48
2.5 FEA results and response surface for SLS	51
2.5.1 The SLS and its determination criteria	51
2.5.2 Effect of variation of initial imperfection.....	54

2.5.3 Response surface for SLS	54
2.6 Probabilistic analysis and PSFs	56
2.6.1 Monte Carlo simulation (MCS).....	56
2.6.2 Proposal for PSFs	59
2.7 Discussion.....	60
2.8 Conclusion.....	63

Chapter 3: Probabilistic column-like compressive strength considering the effect of longitudinal edge support: ULS and SLS

3.1 Introduction	65
3.2 Deterministic FEA.....	67
3.2.1 Model geometry, boundary conditions, and material model	67
3.2.2 Elastic buckling analysis	69
3.2.3 Verification of the nonlinear FEA result	70
3.2.4 Mesh size dependency analysis	72
3.2.5 Effect of local initial out-of-plane deflection	73
3.2.6 Parametric study	75
3.3 FEA results for ULS.....	75
3.3.1 Effect of reduced slenderness parameter R_R	76
3.3.2 Effect of plate thickness	76
3.3.3 Effect of material grade	77
3.4 FEA results for SLS.....	78
3.4.1 Variation of buckling modes for slender plates.....	78
3.4.2 Normalized stress vs. out-of-plane deflection curves.....	79
3.4.3 SLS determination criterion	80
3.5 Probabilistic analysis	81
3.5.1 Response surface: ULS and SLS	81
3.5.2 Monte Carlo simulation (MCS): ULS and SLS	85
3.5.3 Partial safety factors: ULS and SLS	87
3.6 Discussion.....	88
3.7 Conclusion.....	90

Chapter 4: Probabilistic compressive strength of stiffened plates exhibiting plate-like behavior: ULS and SLS.....

4.1 Introduction	91
4.2 Selection of stiffened plate models.....	93
4.3 Numerical analysis	95
4.3.1 Model geometry, boundary conditions, and material model	95
4.3.2 Elastic buckling analysis	96
4.3.3 Nonlinear elasto-plastic FEA.....	97
4.3.4 Nonlinear FEA result for ULS.....	98
4.3.5 Nonlinear FEA result for SLS	99
4.3.6 Effect of local initial out-of-plane deflection	100

4.3.7 Parametric analysis	101
4.4 Experimental verification	102
4.4.1 Experimental model.....	102
4.4.2 Initial out-of-plane deflection measurement.....	103
4.4.3 Measurement of residual stress.....	104
4.4.4 Test setup.....	105
4.4.5 Numerical simulation of the experimental model	106
4.4.6 Result verification	107
4.5 Approximate solution for probabilistic strengths: ULS and SLS.....	109
4.5.1 Estimation of first order mean and first order variance.....	110
4.5.2 Probabilistic compressive strengths: ULS and SLS	112
4.5.3 Partial safety factors: ULS and SLS	113
4.6 Discussion.....	114
4.7 Conclusion.....	116
Chapter 5: Summary and recommendations for future study	119
5.1 Summary.....	119
5.2 Recommendations for future study	122
References	124
APPENDIX A.....	130
Detailed dimensions of the Model-1 stiffened plates	130
APPENDIX B	131
Detailed dimensions of the Model-2 stiffened plates	131
APPENDIX C.....	132
Detailed dimensions of the Model-3 stiffened plates	132
APPENDIX D.....	133
FEA Results for Model-1	133
APPENDIX E	151
FEA Results for Model-2	151
APPENDIX F.....	166
FEA Results for Model-3	166

List of Figures

Fig. 1.1	Stiffened plate used in the bottom flange of steel box Girder Bridge.	18
Fig. 1.2	The collapse of (a) Milford Haven Bridge in England and (b) Koblenz Bridge in Germany [8, 11].	19
Fig. 1.3	Stiffened plate under axial compression.	21
Fig. 2.1	Stiffened plates with (a) plate-like and (b) column-like behaviors used in the bottom flange of a box-girder bridge.	34
Fig. 2.2	Stiffened plate model (Model-1).	36
Fig. 2.3	Boundary conditions of Model-1.	36
Fig. 2.4	Idealized stress-stain relations for different steel grades.	38
Fig. 2.5	Elastic buckling modes of Model-1: (a) whole-plate mode and (b) local mode.	39
Fig. 2.6	Initial out-of-plane deflection shape: (a) whole-plate deflection and (b) local deflection.	40
Fig. 2.7	Residual stress distribution pattern for (a) a panel plate and (b) a stiffener.	41
Fig. 2.8	Stiffened plate model selection process for the parametric study.	43
Fig. 2.9	Graphical representation of initial imperfection combinations for Model-1.	45
Fig. 2.10	Variation in ultimate strength with respect to R_R	46
Fig. 2.11	Effect of variation of imperfection magnitudes on ultimate buckling strength: (a) variation of x_1 magnitude while $x_2 = \mu$ and $x_3 = 0$; (b) variation of x_2 magnitude while $x_1 = \mu$ and $x_3 = 0$; (c) variation of x_3 magnitude while $x_1 = \mu$ and $x_2 = \mu$	47
Fig. 2.12	Response surfaces (RS) for σ_{ULS}/σ_y at $R_R = 1.0$. (a) RS 1: variation of x_1 and x_2 for the case in which $x_3 = 0$; (b) RS 2: variation of x_2 and x_3 for the case in which $x_1 = \mu$, and (c) RS 3: variation of x_3 and x_1 for the case in which $x_2 = \mu$	50
Fig. 2.13	Normalized stress versus out-of-plane deflection curves: (a) whole-plate deflection and (b) local deflection.	52

Fig. 2.14	Effect of variation of imperfection magnitudes on SLS strength: (a) variation of x_1 magnitude while $x_2 = \mu$ and $x_3 = 0$; (b) variation of x_2 magnitude while $x_1 = \mu$ and $x_3 = 0$; (c) variation of x_3 magnitude while $x_1 = \mu$ and $x_2 = \mu$	53
Fig. 2.15	Response surfaces (RS) for σ_{SLS}/σ_y at $R_R = 1.4$. (a) RS 1: variation of x_1 and x_2 for the case in which $x_3 = 0$; (b) RS 2: variation of x_2 and x_3 for the case in which $x_1 = \mu$, and (c) RS 3: variation of x_3 and x_1 for the case in which $x_2 = \mu$	55
Fig. 2.16	Probability density functions for (a) normalized compressive residual stress (x_1), (b) normalized initial out-of-plane whole-plate deflection (x_2), and (c) normalized initial out-of-plane local deflection (x_3).	57
Fig. 2.17	Relative frequency distribution for (a) normalized ultimate strength (σ_{ULS}/σ_y) and (b) normalized SLS strength (σ_{SLS}/σ_y) at $R_R = 1.2$	58
Fig. 2.18	Results for ULS obtained by MCS, compared with various design codes and experimental study.....	61
Fig. 2.19	Probabilistic ULS and SLS strengths obtained from MCS.	62
Fig. 3.1	JSHB strength curve and experimental results of Kanai et al.	66
Fig. 3.2	Geometric configuration of Model-2.....	68
Fig. 3.3	Boundary conditions of Model-2.....	68
Fig. 3.4	Buckling modes and σ_e/σ_y values for Model-2 stiffened plate with $R_R = 0.8$, $t = 30$ mm and steel grade SBHS500.....	69
Fig. 3.5	Geometry and strain gauge location of test specimen (after Komatsu et al. [53]).	70
Fig. 3.6	Normalized stress (σ/σ_y) versus normalized local strain ($\varepsilon_l/\varepsilon_y$) curves from experiment and FE analysis.....	71
Fig. 3.7	Ultimate buckling mode from FEA.....	72
Fig. 3.8	Mesh dependency analysis result.....	73
Fig. 3.9	Combination of initial imperfections for Model-2.	75
Fig. 3.10	Effect of R_R on normalized stress-strain curves for mean values of the residual stress and initial deflection, and a thickness of 30 mm.....	76

Fig. 3.11	Effect of plate thickness on normalized ultimate buckling strength for mean values of the residual stress and initial deflection, and for material grades SM570 and SBHS500.....	77
Fig. 3.12	Effect of material grade on normalized ultimate buckling strength for mean values of the residual stress and initial deflection, and a thickness of 20 mm. 78	
Fig. 3.13	Variation of buckling modes with respect to the initial imperfections. Symbol A, B and C denotes whole-plate, local and coupled buckling mode respectively.	79
Fig. 3.14	Normalized compressive stress versus normalized out-of-plane deflection curves: (a) Curve Type-1 and (b) Curve Type-2.	80
Fig. 3.15	Flowchart for the SLS determination criterion of Model-2.....	81
Fig. 3.16	(a) Response surface for ULS, (b) Effect of variation of residual stress for a mean value of the initial deflection and (c) Effect of variation of initial deflection for a mean value of the residual stress, for different steel grades at $R_R = 1.0$	83
Fig. 3.17	(a) Response surface for SLS, (b) Effect of variation of residual stress for a mean value of the initial deflection and (c) Effect of variation of initial deflection for a mean value of the residual stress, for different steel grades at $R_R = 1.0$	84
Fig. 3.18	Convergence of mean value and standard deviation for σ_{SLS}/σ_y at $R_R = 1.0$. 85	
Fig. 3.19	Relative frequency distribution for Model-2 stiffened plates at $R_R = 1.2$ (a) normalized ultimate strength (σ_{ULS}/σ_y) and (b) normalized SLS strength (σ_{SLS}/σ_y).	86
Fig. 3.20	Comparison of MCS results for ULS of Model-2 stiffened plates.	88
Fig. 3.21	Comparison of probabilistic ULS and SLS strengths of Model-2 stiffened plates.	89
Fig. 4.1	Stiffened plates used in the bottom flange of a narrow box girder.....	91
Fig. 4.2	Actual steel box girder bridge data for the aspect ratio of bottom flanges.....	94
Fig. 4.3	Effect of aspect ratio on the plate-like behavior.....	94
Fig. 4.4	Geometric configuration of Model-3.....	95
Fig. 4.5	Boundary conditions for Model-3.	96

Fig. 4.6	Buckling modes and σ_e/σ_y values for Model-2 stiffened plate with $R_R = 1.0$, $t = 15$ mm and steel grade SM490Y.	97
Fig. 4.7	Effect of R_R on normalized stress-strain curves for Model-3 stiffened plates with SBHS700 steel grade and for mean values of the x_1 , x_2 , and x_3	99
Fig. 4.8	Effect of R_R on the SLS strengths of Model-3 stiffened plates with SBHS700 steel grade and for mean values of the x_1 , x_2 , and x_3	100
Fig. 4.9	General configuration of experimental model (units in mm).	102
Fig. 4.10	Initial out-of-plane deflection measurement: (a) Gridlines, (b) Measurement arrangement (Picture ref: [67]).	103
Fig. 4.11	Contour plot of measured Initial out-of-plane deflection (units in mm).	104
Fig. 4.12	Measured and idealized residual stress distribution in the panel plate.	105
Fig. 4.13	Test setup in the fatigue testing machine with a static load capacity of 6,000kN.	105
Fig. 4.14	Position of displacement dial gauges and elastic strain gauges.....	106
Fig. 4.15	Simulation of initial out-of-plane deflection in the panel plate.....	107
Fig. 4.16	Comparison of FEA and Test result at the ULS.	108
Fig. 4.17	Comparison of FEA and Test result at the SLS.....	109
Fig. 4.18	Effect of material grades on the mean value strengths at (a) ULS and (b) SLS	113
Fig. 4.19	Comparison of probabilistic ULS strengths with different design codes.	115
Fig. 4.20	Comparison of probabilistic ULS and SLS strengths of Model-3 stiffened plates.....	116
Fig. 5.1	Comparison of the probabilistic compressive strengths for three different stiffened plate models at (a) ULS and (b) SLS.....	121
Fig. 5.2	Considered sections for R_R and $\bar{\lambda}$	122

List of Tables

Table 1.1	Historic steel box girder bridge collapse [8, 10].	19
Table 1.2	The relationship between P_f and β .	28
Table 2.1	Yield strength [MPa] for different steel grades.	37
Table 2.2	Elastic buckling analysis result for Model-1.	39
Table 2.3	Statistical parameters for initial imperfections obtained from previous studies.	41
Table 2.4	Effect of addition of initial local out-of-plane deflection (x_3) in Model-1.	42
Table 2.5	Initial imperfection combinations for Model-1.	44
Table 2.6	Regression parameters for ULS at various values of R_R .	49
Table 2.7	Regression parameters for SLS for various values of R_R .	56
Table 2.8	Mean values and standard deviations for σ_{ULS}/σ_y and σ_{SLS}/σ_y obtained from MCS.	59
Table 2.9	Partial safety factors for ULS and SLS strengths assuming that the nominal strength is equal to the mean strength.	60
Table 3.1	Geometric and material properties of the test specimen.	70
Table 3.2	Combination of imperfections for Case-1 and Case-2.	74
Table 3.3	Comparison of ultimate buckling strengths for Case-1 and Case-2 [54].	74
Table 3.4	Regression parameters for Model-2 stiffened plates at ULS and SLS.	82
Table 3.5	Mean values and standard deviations of σ_{ULS}/σ_y and σ_{SLS}/σ_y for Model-2.	87
Table 3.6	PSFs for Model-2 ULS and SLS strengths assuming that the nominal strength is equal to the mean strength.	87
Table 4.1	Effect of initial out-of-plane deflection modes on Model-3.	101
Table 4.2	Geometric and material properties of the right web of the box column.	103
Table 4.3	Initial imperfection combinations for Model-3.	111
Table 4.4	Mean values and standard deviations of σ_{ULS}/σ_y and σ_{SLS}/σ_y for Model-3.	112
Table 4.5	PSFs for Model-3 ULS and SLS strengths assuming that the nominal strength is equal to the mean value strength.	114

[This page is left intentionally blank]

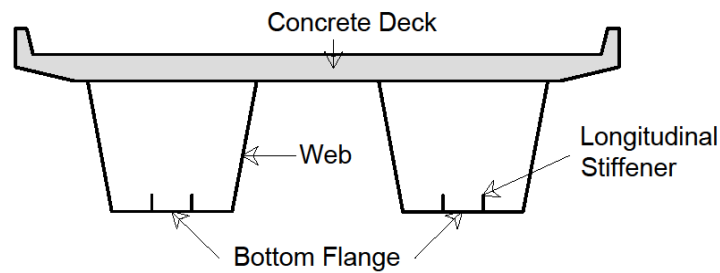
1.1 General

The application of stiffened steel plates can be found in many civil engineering as well as marine structures. Stiffened steel plates form the primary elements of box girder bridges, bridge decks, box columns, and pylons for cable bridges, ship decks, hulls, and other offshore structures that require a high strength-to-weight ratio [1-7]. In the design of a stiffened plate, it is important to pay special attention to the compressive load carrying capacity, because the thin plates exhibit local buckling under compression and may fail with sudden collapse [5]. Hence, the design strength of a stiffened plate is usually governed by its buckling strength.

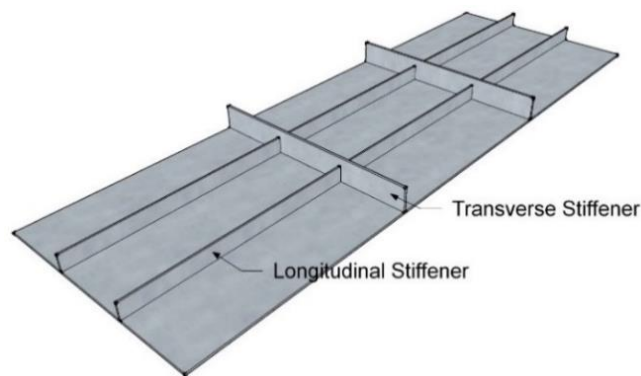
Among different types of steel structures, the area of interest of this research is focused on the steel bridges, particularly the bottom flange of a steel box girder bridge. An example of stiffened plate use in the bottom flange is illustrated in Fig. 1.1. In the continuous support zone of a steel box girder bridge, the bottom flange is subjected to axial compressive load and design of the bottom flange in such case is governed by the buckling strength of the stiffened steel plate.

The stability and buckling behavior of stiffened plates under compression is somewhat complicated because the resistance to compression is sensitive to a large number of parameters, such as the reduced slenderness parameter, the relative stiffness of stiffeners, the plate and stiffener geometry, and the boundary conditions. Furthermore, the same stiffened plate can have a different response in buckling behavior due to differences in the shape and magnitude of initial geometric imperfections and residual stresses that are generated during the fabrication process. For a complete understanding of the buckling behavior and

assessment of load-bearing capacity, it is important to consider the effect of all of the influential parameters.



(a) Section of a typical steel box girder bridge



(b) Stiffened plate used as a bottom flange

Fig. 1.1 Stiffened plate used in the bottom flange of steel box Girder Bridge.

1.2 Historic steel box girder bridge collapse

Before the 1960s, the design philosophy of steel bridges was limited to designing the member components separately and using traditional bolted connections to form trusses or plate girders, where buckling was avoided following the permissible slenderness ratio of the member sections [8]. Inspired by the advanced aircraft engineering, welded box girders with stiffened plates evolved as a leading innovation for bridges in the 1960s. During this period, steel box girder bridges were designed and constructed in Germany, England, and Australia. However, the design was carried out following the old design specification [9] which was not capable of recognizing the special aspects of the welded box sections.

Table 1.1 Historic steel box girder bridge collapse [8, 10].

Country	Name of Bridges	Year of Collapse
Austria	Fourth Danube Bridge	1969
England	Milford Haven Bridge	1970
Germany	Koblenz Bridge	1970
Australia	West Gate Bridge	1970
Germany	Rhine River Bridge	1971
Germany	Zeulenroda Bridge	1973



(a)



(b)

Fig. 1.2 The collapse of (a) Milford Haven Bridge in England and (b) Koblenz Bridge in Germany [8, 11].

Unlike simple beam, boxes are torsionally stiff. Furthermore, the distribution of tension, compression, and shear stresses in the deck, webs, and bottom flange are more complex as local and overall buckling develops in webs and flanges and stresses are redistributed. The severity of underestimating the compressive load carrying capacity resulted in a fatal collapse of several large steel box girder bridges in the 1970s. Table 1.1 presents a list of reported historic steel box girder bridge collapse [8, 10]. Figure 1.2(a) and 1.2(b) shows the collapsed Milford Haven Bridge in England and Koblenz Bridge in Germany, respectively. In both cases, the bottom flange of the steel box girder near the support zone buckled.

The collapses during the 1970s led to extensive research on buckling behavior and the ultimate load carrying capacity of stiffened steel plates [5]. For example, the Merrison Committee [12] was formed in England which facilitated theoretical and experimental

research and produced the interim design and workmanship rules, IDWR. Today, different design specifications have a different provision for predicting the ultimate buckling strength. The following section provides a review of four different design specifications on the buckling strength of stiffened plates used in the bottom flange of a steel box girder bridge. The design specifications discussed are- i) Japanese Specification for Highway Bridges (hereinafter JSHB [13]), ii) AASHTO LRFD Bridge Design Specifications (hereinafter AASHTO [14]), iii) Canadian Highway Bridge Design Code (hereinafter Canadian Code [15]), and iv) Eurocode 3: Design of steel structures (hereinafter Eurocode [16]).

1.3 Code provisions for buckling strength

1.3.1 JSHB

The standard ultimate strength curve of a stiffened plate, conforming to the relative stiffness requirement of longitudinal stiffeners, is given by the following formula

$$\frac{\sigma_{cr}}{\sigma_y} = 1.0 \quad (\text{if } R_R \leq 0.5) \quad (1.1-1)$$

$$\frac{\sigma_{cr}}{\sigma_y} = 1.5 - R_R \quad (\text{if } 0.5 < R_R \leq 1.0) \quad (1.1-2)$$

$$\frac{\sigma_{cr}}{\sigma_y} = \frac{0.5}{R_R^2} \quad (\text{if } 1.0 < R_R) \quad (1.1-3)$$

wherein, σ_{cr} is the ultimate buckling strength of stiffened plate, σ_y represents the yield strength of steel and R_R corresponds to the reduced slenderness parameter, defined by

$$R_R = \frac{b}{t} \sqrt{\frac{\sigma_y}{E} \frac{12(1-\nu^2)}{\pi^2 k_r}} \quad (1.2)$$

herein, b is the overall width of the plate; t is the thickness of the stiffened plate; E and ν are the modulus of elasticity, and Poisson's ratio, respectively, of the steel. The buckling coefficient, k_r , is equal to $4n^2$, where n is the number of subpanels divided by the number of adjacent longitudinal stiffeners.

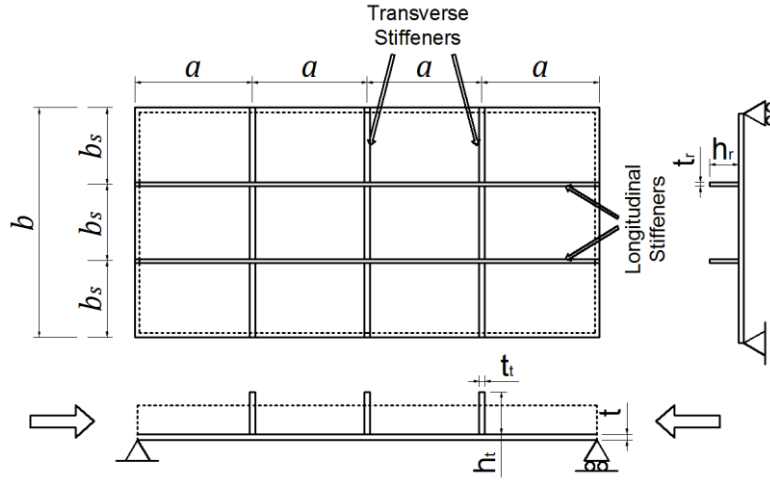


Fig. 1.3 Stiffened plate under axial compression.

Considering four sides simply supported boundary condition (as shown in Fig. 1.3), the required relative stiffness for a flat longitudinal stiffener ($\gamma_{l,req}$), to avoid whole-plate buckling, is derived based on elastic buckling theory and given by the following equations

If $\alpha \leq \alpha_0$

$$\gamma_{l,req} = 4\alpha^2 n \left(\frac{t_0}{t} \right)^2 (1 + n\delta_l) - \frac{(\alpha^2 + 1)}{n}; \quad \text{for } t \geq t_0 \quad (1.3-1)$$

$$\gamma_{l,req} = 4\alpha^2 n (1 + n\delta_l) - \frac{(\alpha^2 + 1)}{n}; \quad \text{for } t < t_0 \quad (1.3-2)$$

If $\alpha > \alpha_0$

$$\gamma_{l,req} = \frac{1}{n} \left[\left\{ 2n^2 \left(\frac{t_0}{t} \right)^2 (1 + n\delta_l) - 1 \right\}^2 - 1 \right]; \quad \text{for } t \geq t_0 \quad (1.4-1)$$

$$\gamma_{l,req} = \frac{1}{n} \left[\left\{ 2n^2 (1 + n\delta_l) - 1 \right\}^2 - 1 \right]; \quad \text{for } t < t_0 \quad (1.4-2)$$

Herein, the aspect ratio is the ratio of panel length to total width, given by $\alpha = a/b$; the critical aspect ratio expressed as $\alpha_0 = \sqrt[4]{1 + n\gamma_l}$, where n is the number of subpanels and γ_l is the relative stiffness of the longitudinal stiffener given by

$$\gamma_l = I_l / (bt^3/11) \quad (1.5)$$

wherein, I_l is the moment of inertia for a longitudinal stiffener. The moment of inertia is calculated with respect to the bottom of the longitudinal stiffener. Furthermore, in Eqs. 1.3 and 1.4, δ_l denotes the cross-sectional area ratio for the longitudinal stiffener to panel plate (A_l/bt), where A_l is the cross-sectional area of one longitudinal stiffener. The critical thickness of the panel plate to avoid local buckling is denoted by t_0 and given by

$$t_0 = \frac{b}{n\pi} \sqrt{\frac{12(1-\nu^2)\sigma_y}{E}} \quad (1.6)$$

where the symbols are the same as those in Eq. 1.2.

In this specification, it was assumed that the plate element used for a stiffened plate generally have a small thickness, and the stiffened plate is not rigid enough to satisfy the edge-support conditions of a plate. It was also mentioned that the standard ultimate strength curve was set for the small R_R range to cover the experimental values conducted by the Public Works Research Institute of Japan. In the range of large R_R , it was also set on the safe side considering the stiffened plate is susceptible to out of plane deformation and toughness reduction.

1.3.2 AASHTO

The nominal buckling strength of a longitudinally stiffened steel plate at the bottom flange of a box girder (compression flange) is given by the following equations

$$\frac{\sigma_{nc}}{\sigma_y} = R_b R_h \Delta \quad \left(\text{if } \lambda_f \leq R_1 \sqrt{\frac{kE}{\sigma_y}} \right) \quad (1.7-1)$$

$$\left. \begin{aligned} \frac{\sigma_{nc}}{\sigma_y} &= R_b R_h \left[\Delta - \left(\Delta - \frac{\sigma_{yr}}{R_h \sigma_y} \right) \left\{ 1 - \sin \left[\frac{\pi}{2} \left(\frac{R_2 - \frac{b}{t} \sqrt{\frac{\sigma_y}{kE}}}{R_2 - R_1} \right) \right] \right\} \right] \\ &\left(\text{if } R_1 \sqrt{\frac{kE}{\sigma_y}} < \lambda_f \leq R_2 \sqrt{\frac{kE}{\sigma_y}} \right) \end{aligned} \right\} \quad (1.7-2)$$

$$\frac{\sigma_{nc}}{\sigma_y} = \frac{0.9ER_b k \sigma_y}{\left(\frac{b}{t}\right)^2} - \frac{R_b f_v^2 k \sigma_y}{0.9Ek_s^2} \left(\frac{b}{t}\right)^2 \quad \left(\text{if } \lambda_f > R_2 \sqrt{\frac{kE}{\sigma_y}} \right) \quad (1.7-3)$$

in which, σ_{nc} is the nominal buckling strength, R_b and R_h are the web load-shedding and hybrid factor respectively (both values are 1.0 for axially compressive stiffened plates), Δ is a factor considering the influence of torsional shear stress ($\Delta = 1.0$ for axially compressive stiffened plates) and $\lambda_f = b/t$, is the slenderness ratio of the stiffened plate. Furthermore,

$$R_1 = \frac{0.57}{\sqrt{\frac{1}{2} \left[\Delta + \sqrt{\Delta^2 + 4 \left(\frac{f_v}{\sigma_y} \right)^2 \left(\frac{k}{k_s} \right)^2} \right]}} \quad (1.8)$$

and

$$R_2 = \frac{1.23}{\sqrt{\frac{1}{1.2} \left[\frac{\sigma_{yr}}{\sigma_y} + \sqrt{\left(\frac{\sigma_{yr}}{\sigma_y} \right)^2 + 4 \left(\frac{f_v}{\sigma_y} \right)^2 \left(\frac{k}{k_s} \right)^2} \right]}} \quad (1.9)$$

where f_v is the St. Venant torsional shear stress ($f_v = 0$ for axially compressive stiffened plates), σ_{yr} is the compression-flange stress accounting for residual stress effects ($\sigma_{yr} = 0.6\sigma_y$).

The plate buckling coefficient for uniform normal stress and shear stress are k and k_s respectively, and determined as follows

$$\left. \begin{aligned} k &= \left(\frac{8I_l}{bt^3} \right)^{\frac{1}{3}} && \text{(for } n = 2) \\ k &= \left(\frac{0.894I_l}{bt^3} \right)^{\frac{1}{3}} && \text{(for } n = 3) \end{aligned} \right\} \quad (1.10)$$

and

$$k_s = \frac{5.34 + 2.84 \left(\frac{I_l}{bt^3} \right)^{\frac{1}{3}}}{(n+2)^2} \leq 5.34 \quad (1.11).$$

The determination of k and k_s are assumed based on simply-supported boundary conditions at the edges of the stiffened plate.

The nominal buckling strength determination formula of AASHTO (Eq. 1.7) is divided into three regions, representing three distinct behavior of stiffened plates based on the slenderness

ratio. Eq. 1.7-1 represents the full yielding of the plate. This region corresponds to the stocky plates, which does not buckles but yields under compression. Eq. 1.7-3 is for slender plates that go under elastic buckling, represented by the Euler hyperbola. In between these two regions, there is a transition curve in between full yielding and elastic buckling, where the effect of residual stress and initial imperfections is prominent. The nominal buckling strength in this region is defined in Eq. 1.7-2 by a sine curve.

1.3.3 Canadian Code

The design criteria for longitudinally stiffened plates at the compression flanges of box girder are based on the theory of elastic stability in this specification. Similar to AASHTO, the nominal buckling strength curve corresponds to the three modes of stiffened plate behavior i.e., yielding, inelastic, and elastic instability, represented by the following equations

$$\frac{\sigma_{nc}}{\sigma_y} = 1.0 \quad \left(\text{for } \frac{b_s}{t} \leq 255 \sqrt{\frac{k_1}{\sigma_y}} \right) \quad (1.12-1)$$

$$\frac{\sigma_{nc}}{\sigma_y} = 0.592\sigma_y \left[1 + 0.687 \sin \frac{\pi C_s}{2} \right] \quad \left(\text{for } 255 \sqrt{\frac{k_1}{\sigma_y}} < \frac{b_s}{t} \leq 550 \sqrt{\frac{k_1}{\sigma_y}} \right) \quad (1.12-2)$$

$$\frac{\sigma_{nc}}{\sigma_y} = \frac{18k_1 \times 10^4}{\left(\frac{b_s}{t} \right)^2} \quad \left(\text{for } \frac{b_s}{t} > 550 \sqrt{\frac{k_1}{\sigma_y}} \right) \quad (1.12-3)$$

where b_s is the width of a subpanel as shown in Fig. 3, C_s is a simplified term and k_1 is the buckling coefficient respectively, given by

$$C_s = \frac{550\sqrt{k_1} - \left(\frac{b_s}{t} \right) \sqrt{\sigma_y}}{295\sqrt{k_1}} \quad (1.13)$$

$$\left. \begin{aligned} k_1 &= \left(\frac{8I_l}{b_s t^3} \right)^{\frac{1}{3}} \leq 4.0 && \text{(for } n = 2) \\ k_1 &= \left(\frac{14.3I_l}{b_s t^3 (n-1)^4} \right)^{\frac{1}{3}} \leq 4.0 && \text{(for } n > 3) \end{aligned} \right\} \quad (1.14)$$

It is interesting to note that, both AASHTO and Canadian code emphasizes one longitudinal stiffener (without the need of a transverse stiffener). If the number of stiffeners is increased beyond one, according to the specifications, the moment of inertia required to increase the buckling strength increases dramatically and becomes nearly impractical. Therefore, both Canadian code and AASHTO recommends to use one longitudinal stiffener and the number should not exceed two.

1.3.4 Eurocode

According to the effective width method, Eurocode 3 considers the concept of an effective section which is reduced from the original section to take into account the effect of local buckling of subpanels, local buckling of longitudinal stiffeners, and overall buckling of the stiffened plate. The effective area of the stiffened plate under compression is taken as follows

$$A_{c,eff} = \rho_c A_{c,eff,loc} + \sum b_{edge,eff} t \quad (1.15)$$

where $A_{c,eff}$ is the effective section area of all the stiffeners and subpanels; ρ_c is the reduction factor accounting for overall buckling which is determined by interpolating between reduction factor for plate-like behavior, ρ and reduction factor for column-like behavior, χ_c , and ρ_c is given by

$$\rho_c = (\rho - \chi_c) \xi (2 - \xi) + \chi_c \quad (1.16)$$

where

$$\xi = \frac{\sigma_{cr,p}}{\sigma_{cr,c}} - 1 \quad \text{but } 0 \leq \xi \leq 1 \quad (1.17)$$

in which, ξ is the interpolation factor, determined from $\sigma_{cr,p}$, the elastic critical plate-like buckling stress and $\sigma_{cr,c}$, the elastic critical column-like buckling stress. The procedure for obtaining the critical buckling stresses and the reduction factors, ρ and χ_c , are described in detail in Eurocode 3.

In Eq. 1.15, $A_{c,eff,loc}$ is the effective section area of all the stiffeners and subpanels that are in the compression zone except the effective edge parts of width $b_{edge,eff}$ and given by

$$A_{c,eff,loc} = A_{sl,eff} + \sum_c \rho_{loc} b_{c,loc} \quad (1.18)$$

where $A_{sl,eff}$ is the deducted effective section of the longitudinal stiffener due to local buckling; $b_{c,loc}$ is the width of the compressed part of each subpanel, and ρ_{loc} is the reduction factor for each subpanel accounting for local buckling.

The final compressive strength of the stiffened plate is obtained as follows

$$P_u = \frac{A_{c,eff} \sigma_y}{\gamma_{M1}} \quad (1.19)$$

where $A_{c,eff}$ is the effective cross-sectional area of the compression zone of the stiffened panel in Eq. 1.15 and γ_{M1} is the partial factor for the structural stability.

It is important to note that, unlike JSHB, AASHTO, and Canadian Code, Eurocode discusses two distinct types of behavior of a stiffened plate under compression, i.e. a plate-like behavior and a column-like behavior. It provides a plate-like buckling strength and a column-like buckling strength and interpolates between the plate-like and column-like buckling to determine the final strength.

1.4 Basic concept of reliability-based design

The present practice in developing structure design codes is to develop a reliability-based design criteria with partial safety factors (PSF) for different limit states, e.g. the ultimate limit state, the serviceability limit state etc. Hence, understanding the basic concept of reliability-based design is important.

According to the general principles on reliability for structures [17], the fundamental requirements to design structures or structural elements is that they are suited for their use during the design working life and in an economic way. In particular, they shall fulfill three requirements with *appropriate degrees of reliability* which are a) serviceability limit state requirement, b) ultimate limit state requirement, and c) structural integrity requirement. The *degrees of reliability* may be selected according to the consequences of the failure of the structures. Explicitly, there are three consequences categories (CC) which are defined as follows [17, 18]:

- Consequences Category CC1 - risk to life is low, economic, social and environmental consequences small or negligible;
- Consequences Category CC2 - risk to life is medium, economic, social and environmental consequences considerable; and
- Consequences Category CC3 - risk to life is high, economic, social and environmental consequences very great.

Interestingly, it is possible that within the same structural system, different structural components may have different consequences categories and therefore requires different degrees of reliability.

Depending upon the *degree of reliability* in structural design, the reliability-based design procedures are generally classified in the following four levels [19] based on the extent of information available for probabilistic calculations.

- *Level I procedure (first-moment method)*: This method is also known as Partial Safety Factor based method, where a predefined set of characteristic or nominal values are assigned to a number of random variables, governing the design equation. The characteristic value of each variable is determined from the level II reliability analysis. Most of the design codes, such as ASHTO and Eurocode, are based on this level.
- *Level II procedure (second-moment method)*: In this procedure, the stochastic variables are modeled by the mean values and the standard deviations, and by the correlation coefficients between the random variables. The reliability index method is an example of a level II method.
- *Level III procedure (full probabilistic)*: These methods utilize the complete probability distribution functions of all relevant quantities (loads, load effects and limit values) for calculation of the probability of failure P_f associated to each load and each mode of failure. These probabilities are then combined into an overall probability of failure.
- *Level IV procedure*: *Level IV* procedure considers the combination of probability of failure and its consequences (cost) issues. This procedure is followed for the structures with prodigious consequences on failure.

The Eurocode defines three reliability classes RC1, RC2, and RC3 based on the β reliability index concept, corresponding to the three consequences categories CC1, CC2 and CC3. The

relationship between the probability of failure P_f and reliability index β is given in Table 1.2 [18].

Table 1.2 The relationship between P_f and β .

P_f	β
10^{-1}	1.28
10^{-2}	2.32
10^{-3}	3.09
10^{-4}	3.72
10^{-5}	4.27
10^{-6}	4.75
10^{-7}	5.20

1.5 Identification of problems

After reviewing different design codes and previous research, four important issues motivated the author to conduct the present study. First, earlier research, either experimental [3, 20-24] or numerical [25-32], basically dealt with relatively thin plates (approximately 10 mm thick). However, the use of thick plates is common in present-day bridge construction. For example, since 1996, the JSHB limit for the maximum thickness of steel plates that can be used in steel bridge construction has increased from 50 mm to 100 mm [33-34]. Nevertheless, the effect of using such thick plates is unknown with respect to load carrying capacity.

Second, due to higher performances with respect to tensile strength, toughness, weldability, and corrosion resistance [35], the use of Steel for Bridge High-performance Structures (SBHS) is advantageous compared to other conventional steels for long-span bridge construction [36]. However, SBHS has different inelastic behavior as compared to ordinary steels, including smaller ductility, almost no yield plateau, and a greater yield-to-tensile strength ratio [37]. The strength equation of the latest JSHB code [13] recently included SBHS500 steels. Nevertheless, the strength equation is based on the experimental results of Kanai et al. [38], which focus on plate-like buckling only. Furthermore, the inelastic behavior of SBHS500 is similar to that of ordinary SM570 steels, whereas SBHS700 is quite

different, i.e., it has no yield plateau. Hence, investigating the effects of both SBHS500 and SBHS700 is essential.

Third, numerous studies have been conducted in order to determine the ultimate strength corresponding to the ultimate limit state (ULS). Conversely, although important for efficient structural design, the serviceability limit state (SLS) was less frequently studied. Stiffened plates with a large reduced slenderness parameter R_R exhibit a large out-of-plane deflection due to elastic buckling, which may occur before reaching the ultimate strength [38]. Since serviceability is not a direct indicator of structural safety, design with respect to SLS criteria are primarily based on past experience [39]. For stiffened plates, criteria based on elastic buckling followed by large out-of-plane deflections are often considered for the SLS design [40, 41]. From a serviceability point of view, restriction of out-of-plane deflection exceeding the fabrication tolerance, within the elastic range, is important [42].

Fourth, most modern structural design codes, i.e., AASHTO [14], Eurocode [16], and JSDB [13], currently employ probability-based limit state design methods, in which partial safety factors (PSFs) are assigned to account for uncertainties originating from individual sources. In order to propose PSFs, it is necessary to obtain probabilistic information for the compressive strength, such as a mean value and a standard deviation.

1.6 Research objectives and scope

Considering the limitations stated above, the main objectives of the current research is to establish a reliability-based design framework through investigating the probabilistic compressive strengths at both ultimate limit states (ULS) and serviceability limit states (SLS). In doing so, three different stiffened plate models with three, two, and one flat plate longitudinal stiffeners, corresponding to Model-1, Model-2, and Model-3 respectively, are taken into account. Furthermore, two different distinct behavior of stiffened plates under compression, i.e. the column-like behavior and the plate-like behavior are discussed within these three models.

The geometric configuration of the models is selected in such a way that Model-1 and Model-2 exhibit the column-like behavior and Model-3 demonstrates the plate-like behavior. The relative stiffness of the longitudinal stiffeners for each model conforms to the required relative stiffness, as specified by the JSHB.

After obtaining the probabilistic information, such as a probability density function, a mean value and a standard deviation of compressive strengths at ULS and SLS, an example calculation procedure for the proposal of partial safety factors based on reliability index concept is presented for each of the three models.

1.7 Outline of the dissertation

Chapter 1 provides a background of the study with information of some historic bridge collapses that initiated extensive research in this field. Insight about the basic concept of reliability-based design as well as limitations of different design specifications and past studies are also discussed. Finally, the scope and objectives of the research are identified.

Chapter 2 discusses the column-like behavior of stiffened steel plates, represented by Model-1. The compressive strengths at ULS and SLS were determined from nonlinear elasto-plastic FE analysis, where both material and geometric nonlinearity were taken into account. The probabilistic distribution of the strengths was obtained through Monte Carlo simulation, in association with a response surface method.

Chapter 3 investigates the effect of longitudinal edge support (from the webs of the box girder) on column-like behavior. In this chapter, probabilistic compressive strengths at ULS and SLS are obtained for Model-2, which exhibits column-like behavior and assumes simply supported boundary conditions along the longitudinal edges.

Chapter 4 concentrates on narrow steel box girder bridges where the bottom flange of the box girder has a large aspect ratio and usually composed of one longitudinal stiffener. This kind of stiffened plates shows plate-like behavior where the plates possess a large post-buckling strength reserve. Model-1 is selected to produce plate-like behavior. First-order

mean values of the compressive strengths at ULS and SLS were obtained through an approximate solution procedure, while the first-order variance was evaluated using *Taylor series finite difference* (TSFD) estimation procedure.

Chapter 5 discusses the major findings of this study, compares the results of three different stiffened plate models, and provides directions for future research.

[This page is left intentionally blank]

Probabilistic compressive strength of stiffened steel plates exhibiting column-like behavior: ULS and SLS

2.1 Introduction

Depending on the aspect ratio and the level of stiffening, stiffened plates may exhibit two distinct types of behavior: a plate-like behavior and a column-like behavior. Plate-like buckling refers to the global buckling of the entire panel along with the longitudinal stiffeners, where the stiffened plates possess a significant post-buckling strength reserve [43]. In such cases, the longitudinal edge support contributes to the development of a catenary action in the transverse direction (as shown in Fig. 2.1(a)) and thus allows the plate to carry a further load after buckling. However, wide stiffened plates with low aspect ratio ($\alpha \leq 1.0$) exhibit column-like buckling that does not have any post-buckling strength reserve, because the curvature in the transverse direction is low and the catenary action is weak (see Fig. 2.1(b)).

In the case of column-like buckling, the effect of longitudinal edge support is negligible. The stiffened plate is considered as a series of unconnected compression struts, where a “strut” consists of a longitudinal stiffener and the associated subpanel width between two stiffeners [44]. The column behavior is simply achieved by removing the effect of longitudinal edge supports [45].

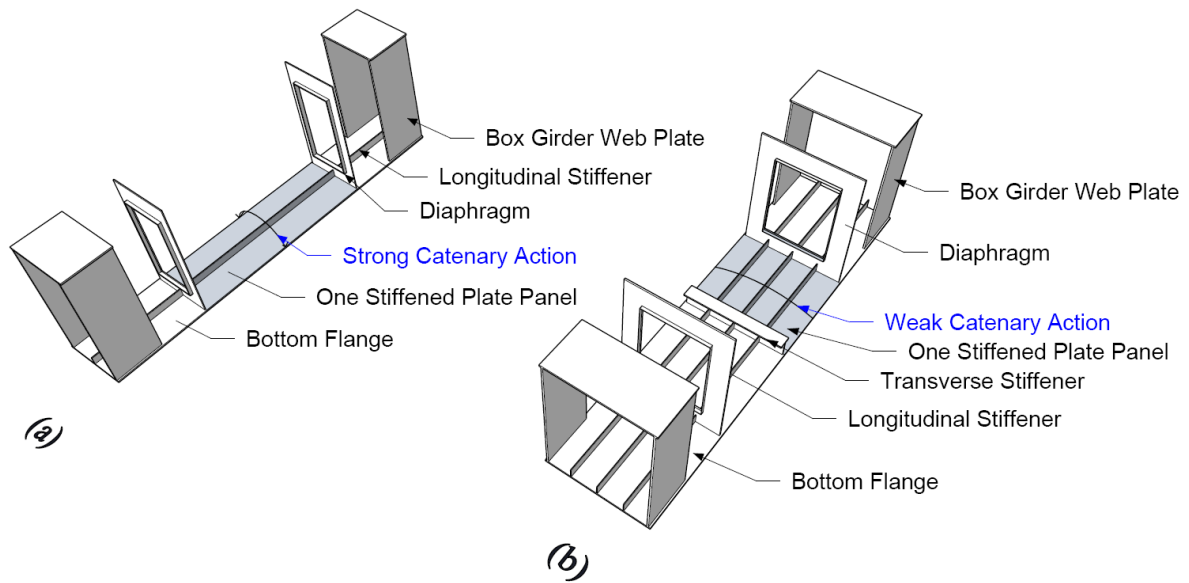


Fig. 2.1 Stiffened plates with (a) plate-like and (b) column-like behaviors used in the bottom flange of a box-girder bridge.

Aside from Eurocode [16], most design specifications [14-15], including the JSMB [13], neither distinguish between plate-like and column-like behavior nor concentrates on the diminished post-buckling strength aspect of a wide multi-stiffened plate—and even Eurocode has room for improvement. Johansson and Veljkovic [46] reported that, in the effective width method, after attaining the maximum load by a plate in compression, there is a sharp drop in resistance, which may be correct for an isolated panel. However, in the case of a continuous plate, where one panel is connected to other panels that have not reached their yield strength, the drop in the resistance will be small and controlled by these other panels. Hence, it is important to consider the continuity of the stiffened plate in the longitudinal direction, rather than considering an isolated panel.

Furthermore, Braun [47] pointed out that, for column-like buckling, the sensitivity of initial geometric imperfection is higher than that of plate-like buckling. Therefore, it is also necessary to consider the effect of shape and magnitude variation of initial geometric imperfections.

In association with the general problems identified in Section 1.5 of Chapter 1, this Chapter investigates the probabilistic distribution of compressive strengths at ULS as well as SLS for longitudinally continuous stiffened steel plates, exhibiting column-like behavior i.e. the

Model-1. Compressive strengths were determined from nonlinear elasto-plastic FE analysis, where both material and geometric nonlinearity were taken into account. In the parametric analysis, the reduced slenderness parameter (R_R) was varied from 0.4 to 1.4, and for each R_R , thick plates and high-performance steels (SBHS) were considered along with thin plates and ordinary steels. The probabilistic distribution of the strengths was obtained through Monte Carlo simulation (MCS), in association with a response surface method. The response surface function comprises three independent variables, upon which the uncertainties in estimating the compressive strength of a certain stiffened plate depend, i.e., the residual stress, the initial out-of-plane whole-plate deflection, and the initial out-of-plane local deflection.

2.2 Description of the models for numerical analysis

2.2.1 Geometric configuration

Stiffened steel plates, as shown in Fig. 2.2, with an aspect ratio ($\alpha = a/b = 1$) and with three equidistant flat-type longitudinal stiffeners, satisfying the relative stiffness requirement of JSHB ($\gamma_l/\gamma_{l,req} = 1$) were considered in the present study. Here, a is the length of the plate, i.e., the distance between two transverse stiffeners, b is the width of the plate, γ_l is the relative stiffness of the longitudinal stiffeners, and $\gamma_{l,req}$ is the relative stiffness required in order to avoid whole-plate buckling, which is derived based on the elastic buckling theory and discussed in the subsection 1.3.1.

Considering i) the continuity of the plate along the longitudinal direction, ii) removal of the effect of longitudinal edge support, and iii) symmetric loading and boundary conditions, a strut model, as shown in the shaded part of Fig. 2.2, was selected from the full stiffened plate for numerical analysis.

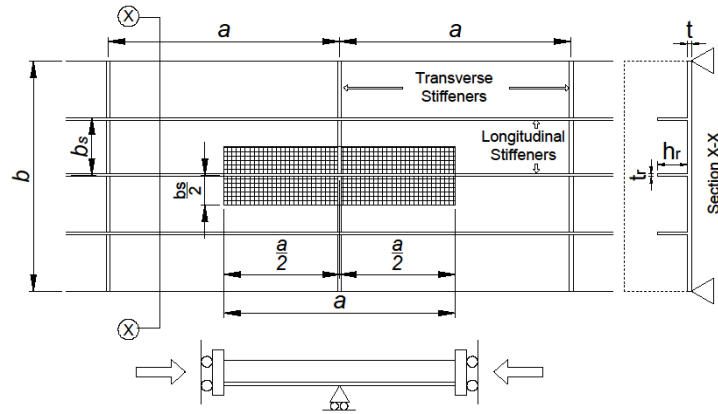


Fig. 2.2 Stiffened plate model (Model-1).

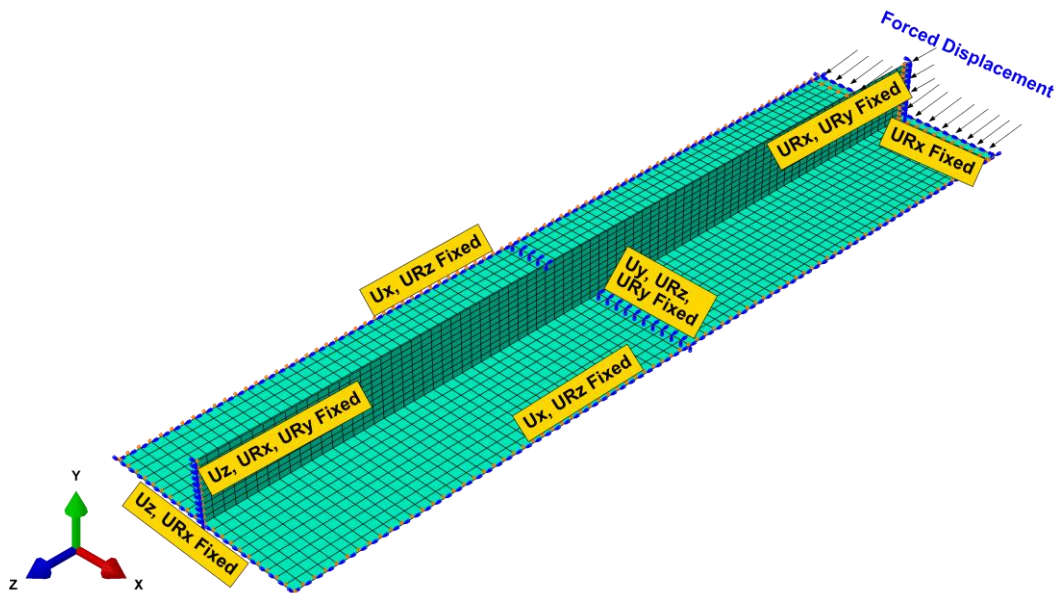


Fig. 2.3 Boundary conditions of Model-1.

2.2.2 Boundary conditions

The boundary conditions for the strut model are illustrated in Fig. 2.3. In this figure U_x , U_y , and U_z denote translation along the X, Y, and Z axes, respectively, and UR_x , UR_y , and UR_z denote the rotational degrees of freedom around the X, Y, and Z axes, respectively. In order to achieve the column-like behavior, the effect of longitudinal edge support on the stiffened plate was ignored, and, in the strut model, a continuous boundary condition in the transverse direction was considered.

As mentioned earlier, the model is also continuous along the longitudinal direction. In order to simulate the continuous boundary condition, the translational movement was restricted along the direction of continuity, and rotational movement was restricted with respect to the axis of the section cut.

The transverse stiffener was assumed to have sufficient rigidity, i.e., does not buckle before the panel plate or the longitudinal stiffeners. Instead of modeling a transverse stiffener, boundary conditions representing sufficient rigidity were applied along the nodal line intersecting the panel plate and transverse stiffener, which reduces the computational time. The compressive load was applied through a forced displacement, which ensures the application of equal and uniform compressive stress in the panel plate and stiffener simultaneously.

2.2.3 Material model

The yield strengths of the four material grades considered herein are presented in Table 2.1 (obtained from [34] and [48]). For all of the material grades, the modulus of elasticity and Poisson's ratio were considered as a deterministic standardized value, i.e., 200 GPa and 0.3, respectively. Since the present study proposes PSFs for member capacity, it is important to ignore variations in material properties, i.e., yield strength, modulus of elasticity, and Poisson's ratio.

Table 2.1 Yield strength [MPa] for different steel grades.

Steel Grade	Plate thickness (mm)			
	$t \leq 16$	$16 < t \leq 40$	$40 < t \leq 75$	$t > 75$
SM490Y	365	355	335	325
SM570	460	450	430	420
SBHS500	500	500	500	500
SBHS700	700	700	700	700

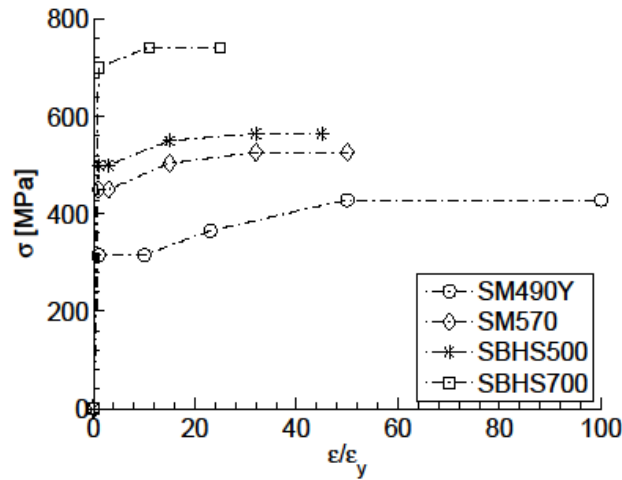


Fig. 2.4 Idealized stress-strain relations for different steel grades.

The inelastic characteristics of the four material grades were determined from idealized uniaxial stress-strain (σ - ϵ) relationships, as shown in Fig. 2.4, based on test data [49]. It is important to note that, like SM570, SBHS500 has a small yield plateau, whereas SBHS700 does not have any yield plateau. In the numerical analysis, Mises plasticity, the associated flow rule, and the isotropic strain hardening theory were used to model the material nonlinearity.

2.3 Deterministic finite element analysis (FEA)

Finite element analyses were carried out in order to obtain the deterministic compressive strengths at the ULS and SLS. ABAQUS [50] commercial FEA software was used for modeling, analysis, and post-processing. The plate and stiffeners were modeled using a four-node, quadrilateral, stress-displacement shell element S4R, which uses a reduced integration method and is suitable for large displacement analysis.

2.3.1 Elastic buckling analysis

Eigenvalue buckling analysis was carried out in order to determine the elastic buckling modes and elastic buckling strengths (σ_e) of Model-1. Two important buckling modes, i.e., the whole-plate mode and the local mode, are depicted in Figs. 2.5(a) and 2.5(b), respectively. The whole-plate mode epitomizes one half-sine wave shape buckling of the panel plate along

with the longitudinal stiffener, whereas the local mode refers to the local buckling in one subpanel. Table 2.2 shows an example of the elastic buckling analysis results for various reduced slenderness parameters (R_R) for material grade SM570 and a plate thickness of 30 mm. The local buckling mode was observed as the first buckling mode, except at $R_R = 0.4$.

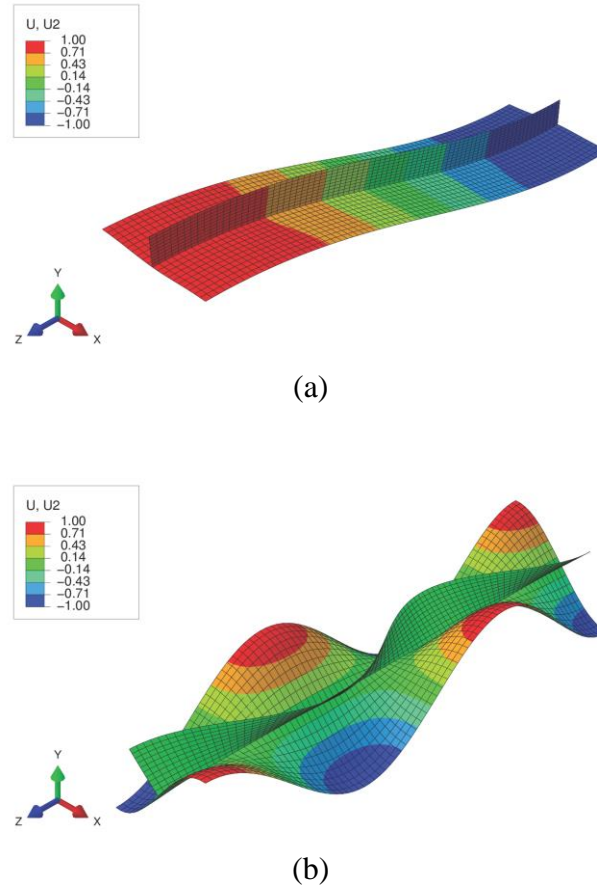


Fig. 2.5 Elastic buckling modes of Model-1: (a) whole-plate mode and (b) local mode.

Table 2.2 Elastic buckling analysis result for Model-1.

R_R	Local Mode			Whole Plate mode		
	Mode No.	σ_e (Mpa)	σ_e/σ_y	Mode No.	σ_e (Mpa)	σ_e/σ_y
0.4	2	1799.3	4.00	1	1091.9	2.43
0.6	1	895.7	1.95	2	915.1	1.99
0.8	1	523.6	1.16	4	547.5	1.22
1.0	1	344.5	0.77	3	352.5	0.78
1.2	1	243.7	0.54	4	249.5	0.55
1.4	1	180.1	0.40	4	184.9	0.41

2.3.2 Nonlinear elasto-plastic analysis

Both the material and geometric nonlinearity were taken into account in the subsequent FEA. The material nonlinearity was specified based on the idealized inelastic characteristics of various steel grades, as shown earlier in Fig. 2.4. The geometric nonlinearity considers a large deflection in order to solve the equivalent equations. The nonlinear analysis was carried out in two steps. In the first step, initial imperfections were simulated to represent the initial condition, and, in the second step, compressive loading was applied through forced displacement.

In the first step, residual stresses and initial out-of-plane deflections of two different shapes, i.e., a) whole-plate deflection and b) local deflection, as shown in Fig. 2.6, were simulated simultaneously in the FE model. The residual stresses were included directly in each element through a “predefined field” in ABAQUS, following the idealized stress distribution pattern, shown in Fig. 2.7. There is an internal equilibrium state between the residual compressive and tensile stresses in the idealized distribution pattern.

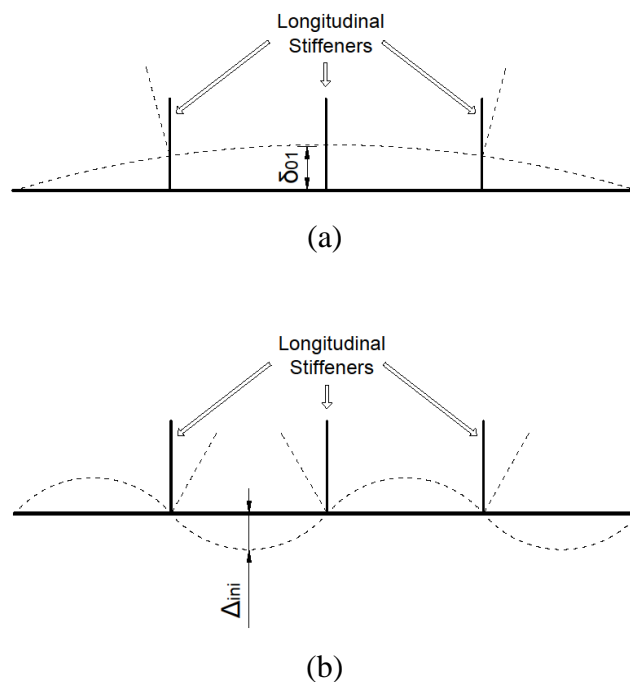


Fig. 2.6 Initial out-of-plane deflection shape: (a) whole-plate deflection and (b) local deflection.

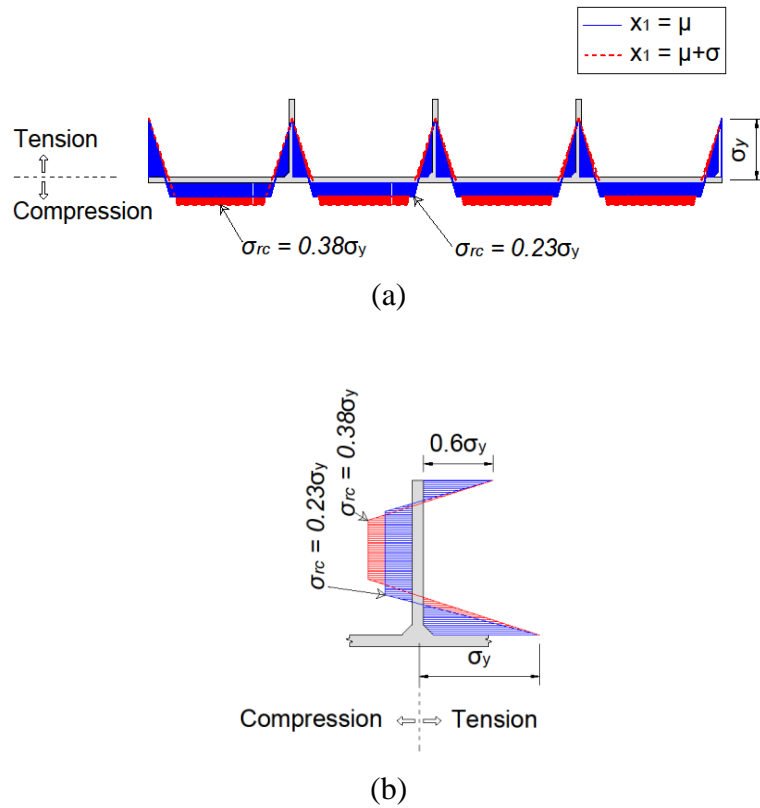


Fig. 2.7 Residual stress distribution pattern for (a) a panel plate and (b) a stiffener.

Table 2.3 Statistical parameters for initial imperfections obtained from previous studies.

Imperfections	Mean (μ)	Standard deviation (σ)
$x_1 = \sigma_{rc} / \sigma_y$	0.230	0.145
$x_2 = 1000\delta_{01} / a$	0.096	0.426
$x_3 = 150 \Delta_{ini} / b_s$	0.138	0.107

Initial out-of-plane deflections of two shapes were simulated using the deflected nodal coordinates of relevant elastic buckling modes scaled to the desired magnitude of out-of-plane deflection. The simultaneous simulation of imperfections was implemented for a series of different possible combinations (described in detail in Subsection 2.3.4) among the imperfections based on reported statistical data. Table 2.3 presents the statistical data obtained from previous studies [51, 27, and 52]. Here, σ_{rc} is the residual compressive stress, δ_{01} is the initial out-of-plane whole-plate deflection, Δ_{ini} is the initial out-of-plane local deflection, and b_s is the width of a subpanel between two longitudinal stiffeners. The variables x_1 , x_2 , and x_3 represents the non-dimensional imperfections i.e. residual stress,

initial whole-plate out-of-plane deflection, and initial local out-of-plane deflection (see Table 2.3).

The nonlinear FEA technique was validated with respect to experimental results previously reported by Komatsu et al. [53], and details of the verification are described in Chapter 3. When the reported initial imperfections in the experiment were taken into account in the FEA, the FE results agreed very well with the experimental results in terms of ultimate buckling strength as well as the load-deflection curve pattern. The ultimate buckling strength obtained from FEA was only 1.16% lower than the experimental value.

2.3.3 Effect of initial local out-of-plane deflection

Table 2.4 Effect of addition of initial local out-of-plane deflection (x_3) in Model-1.

Material	R_R	x_1	x_2	x_3	σ_{ULS}/σ_y	σ_{ULS} reduction due to the addition of x_3
SM490Y	0.8	μ	$\mu + \sigma$	0	0.823	
		μ	$\mu + \sigma$	$\mu + \sigma$	0.778	5.47%
	1.0	μ	$\mu + \sigma$	0	0.702	
		μ	$\mu + \sigma$	$\mu + \sigma$	0.658	6.27%
SM570	0.8	μ	$\mu + \sigma$	0	0.827	
		μ	$\mu + \sigma$	$\mu + \sigma$	0.785	5.08%
	1.0	μ	$\mu + \sigma$	0	0.702	
		μ	$\mu + \sigma$	$\mu + \sigma$	0.659	6.13%
SBHS500	0.8	μ	$\mu + \sigma$	0	0.821	
		μ	$\mu + \sigma$	$\mu + \sigma$	0.783	4.63%
	1.0	μ	$\mu + \sigma$	0	0.728	
		μ	$\mu + \sigma$	$\mu + \sigma$	0.674	7.42%
SBHS700	0.8	μ	$\mu + \sigma$	0	0.802	
		μ	$\mu + \sigma$	$\mu + \sigma$	0.792	1.25%
	1.0	μ	$\mu + \sigma$	0	0.722	
		μ	$\mu + \sigma$	$\mu + \sigma$	0.675	6.51%

* Plate thickness $t = 30$ mm

As mentioned earlier, the column-like buckling model is sensitive to initial imperfections [47]. From a previous study [54], it is established that the effect of x_1 and x_2 is significant. However, for column-like buckling, it is also important to investigate the effect of x_3 . As such, the effect of x_3 was investigated for Model-1 and was found to be significant, especially for $R_R = 0.8$ and 1.0. The addition of x_3 to x_1 and x_2 yields an ultimate strength

(σ_{ULS}) that is 5 to 7% lower, as shown in Table 2.4. Consequently, x_1 , x_2 , and x_3 were considered simultaneously in Model-1.

2.3.4 Parametric study

A large-scale parametric study was conducted in order to investigate the effects of various influential parameters on the column-like buckling strength. A total of 83 stiffened plate models with various material grades (SM490Y, SM570, SBHS500, and SBHS700), R_R values (0.4 to 1.4, with increments of 0.2), and plate thicknesses (10 to 90 mm) were analyzed numerically. Detail dimensions of the stiffened plate models are listed in Appendix A. The stiffened plate models were chosen such that, R_R varied for each material grade, and there was a variation in plate thickness for each R_R value. Figure 2.8 describes the model selection plan for the parametric study.

Furthermore, in order to address the uncertainties originating from initial imperfections, each of the stiffened plate models was analyzed for 36 different combinations of initial imperfections, consisting x_1 , x_2 , and x_3 , as listed in Table 2.5. The combinations were based on the mean values (μ) and standard deviations (σ) of x_1 , x_2 , and x_3 . Figure 2.9 presents the imperfection combinations graphically, where a circular dot represents one imperfection combination. A total of 2,988 nonlinear elasto-plastic FEAs were carried out in the present study and the results are presented in Appendix D.

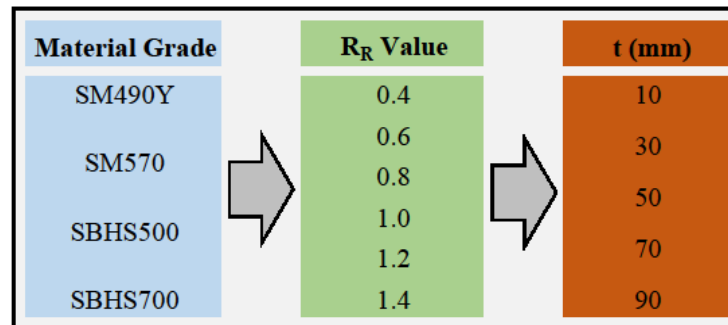


Fig. 2.8 Stiffened plate model selection process for the parametric study.

Table 2.5 Initial imperfection combinations for Model-1.

Comb.	Index	$x_1 = \sigma_{rc}/\sigma_y$	$x_2 = 1000\delta_{01}/a$	$x_3 = 150 \Delta_{ini} /b_s$			
1	C130	$\mu - \sigma$	0.085	μ	0.096	0	0.000
2	C131	$\mu - \sigma$	0.085	μ	0.096	$\mu + 2\sigma$	0.351
3	C132	$\mu - \sigma$	0.085	μ	0.096	$\mu + 8\sigma$	0.990
4	C160	$\mu - \sigma$	0.085	$\mu + 3\sigma$	1.375	0	0.000
5	C161	$\mu - \sigma$	0.085	$\mu + 3\sigma$	1.375	$\mu + 2\sigma$	0.351
6	C162	$\mu - \sigma$	0.085	$\mu + 3\sigma$	1.375	$\mu + 8\sigma$	0.990
7	C220	μ	0.230	$\mu - \sigma$	-0.330	0	0.000
8	C221	μ	0.230	$\mu - \sigma$	-0.330	$\mu + 2\sigma$	0.351
9	C222	μ	0.230	$\mu - \sigma$	-0.330	$\mu + 8\sigma$	0.990
10	C230	μ	0.230	μ	0.096	0	0.000
11	C231	μ	0.230	μ	0.096	$\mu + 2\sigma$	0.351
12	C232	μ	0.230	μ	0.096	$\mu + 8\sigma$	0.990
13	C240	μ	0.230	$\mu + \sigma$	0.522	0	0.000
14	C241	μ	0.230	$\mu + \sigma$	0.522	$\mu + 2\sigma$	0.351
15	C242	μ	0.230	$\mu + \sigma$	0.522	$\mu + 8\sigma$	0.990
16	C250	μ	0.230	$\mu + 2\sigma$	0.949	0	0.000
17	C251	μ	0.230	$\mu + 2\sigma$	0.949	$\mu + 2\sigma$	0.351
18	C252	μ	0.230	$\mu + 2\sigma$	0.949	$\mu + 8\sigma$	0.990
19	C310	$\mu + \sigma$	0.375	$\mu - 2\sigma$	-0.757	0	0.000
20	C311	$\mu + \sigma$	0.375	$\mu - 2\sigma$	-0.757	$\mu + 2\sigma$	0.351
21	C312	$\mu + \sigma$	0.375	$\mu - 2\sigma$	-0.757	$\mu + 8\sigma$	0.990
22	C330	$\mu + \sigma$	0.375	μ	0.096	0	0.000
23	C331	$\mu + \sigma$	0.375	μ	0.096	$\mu + 2\sigma$	0.351
24	C332	$\mu + \sigma$	0.375	μ	0.096	$\mu + 8\sigma$	0.990
25	C430	$\mu + 2\sigma$	0.520	μ	0.096	0	0.000
26	C431	$\mu + 2\sigma$	0.520	μ	0.096	$\mu + 2\sigma$	0.351
27	C432	$\mu + 2\sigma$	0.520	μ	0.096	$\mu + 8\sigma$	0.990
28	C460	$\mu + 2\sigma$	0.520	$\mu + 3\sigma$	1.375	0	0.000
29	C461	$\mu + 2\sigma$	0.520	$\mu + 3\sigma$	1.375	$\mu + 2\sigma$	0.351
30	C462	$\mu + 2\sigma$	0.520	$\mu + 3\sigma$	1.375	$\mu + 8\sigma$	0.990
31	C540	$\mu + 3\sigma$	0.665	$\mu + \sigma$	0.522	0	0.000
32	C541	$\mu + 3\sigma$	0.665	$\mu + \sigma$	0.522	$\mu + 2\sigma$	0.351
33	C542	$\mu + 3\sigma$	0.665	$\mu + \sigma$	0.522	$\mu + 8\sigma$	0.990
34	C560	$\mu + 3\sigma$	0.665	$\mu + 3\sigma$	1.375	0	0.000
35	C561	$\mu + 3\sigma$	0.665	$\mu + 3\sigma$	1.375	$\mu + 2\sigma$	0.351
36	C562	$\mu + 3\sigma$	0.665	$\mu + 3\sigma$	1.375	$\mu + 8\sigma$	0.990

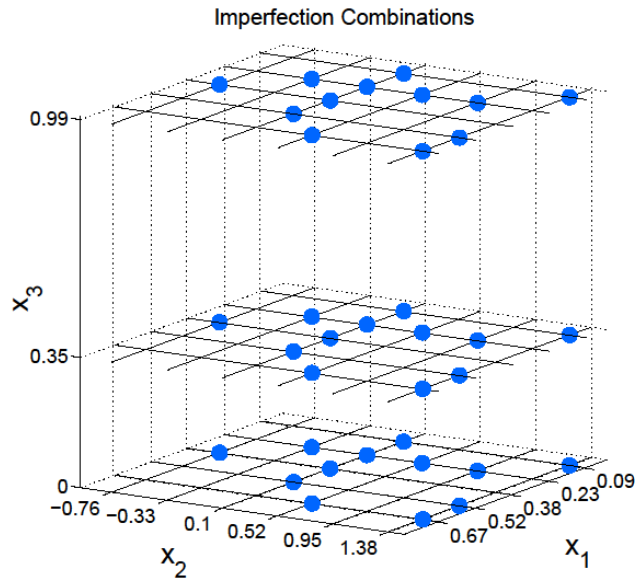


Fig. 2.9 Graphical representation of initial imperfection combinations for Model-1.

2.4 FEA results and response surface for ULS

2.4.1 ULS and stress-strain curves

The ultimate load carrying capacity, which is determined from the maximum load, is referred to as the ultimate buckling strength, which represents the ULS. Normalized average stress vs. strain ($\sigma/\sigma_y - \varepsilon/\varepsilon_y$) curves for six stiffened plates with the same imperfection combination ($x_1 = \mu, x_2 = \mu, x_3 = \mu + 2\sigma$) and six different R_R values are presented in Fig. 2.10 as an example. Here, σ and σ_y represent the average compressive stress and the yield stress, respectively, and ε and ε_y denote the average applied axial strain and the yield strain, respectively. Note that all models exhibit snap-through buckling behavior, irrespective of reduced slenderness parameter R_R . With increasing R_R , the ultimate strength decreases, as expected.

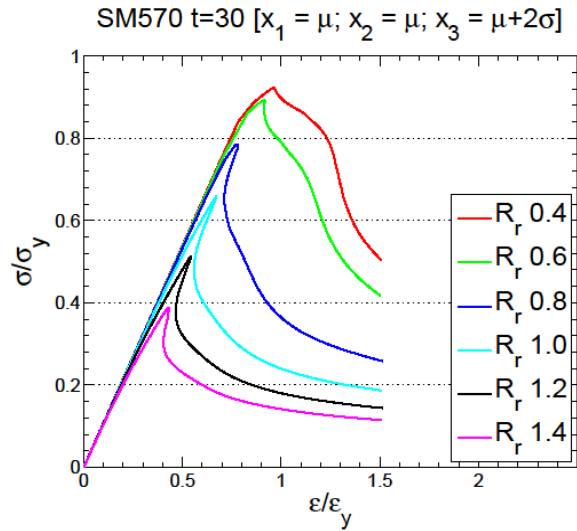
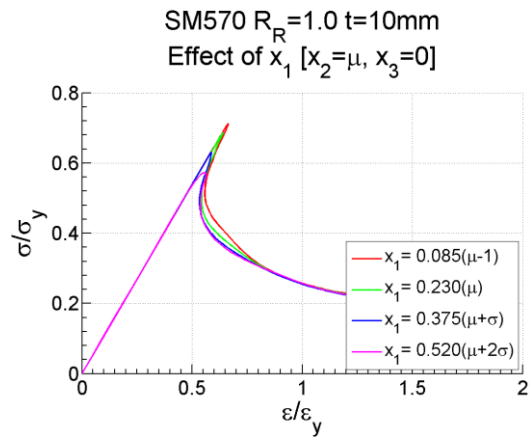


Fig. 2.10 Variation in ultimate strength with respect to R_R .

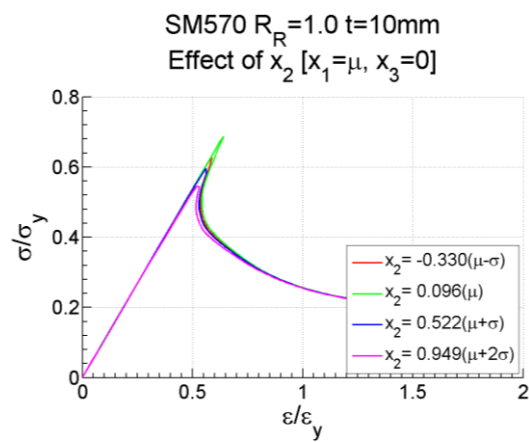
2.4.2 Effect of variation of initial imperfections

To investigate the effect of variation of initial imperfections on ultimate buckling strength, normalized stress-strain curves are plotted in Fig. 2.11 as an instance of a stiffened plate with a reduced slenderness parameter $R_R = 1.0$, plate thickness $t = 10$ mm and material grade SM570. Figs. 2.11(a), (b) and (c) demonstrates the effect of x_1 , x_2 and x_3 *individually*. While presenting the variation of one imperfection, the other two are kept constant. For example, in Fig. 2.11(a) the effect of variation of residual stress (x_1) magnitude is presented, while the magnitude of two other imperfection i.e. x_2 and x_3 are set to a constant value of μ and zero respectively.

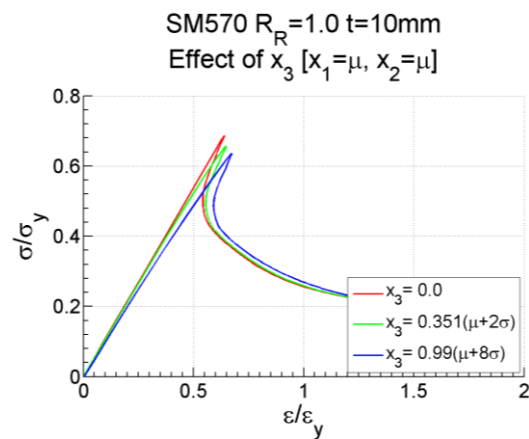
It is observed that with the increase of magnitude of each type of imperfections, the ultimate buckling strength decreased. Furthermore, it can be seen that x_1 is the most sensitive imperfection followed by x_2 and x_3 for this particular stiffened plate.



(a)



(b)



(c)

Fig. 2.11 Effect of variation of imperfection magnitudes on ultimate buckling strength: (a) variation of x_1 magnitude while $x_2 = \mu$ and $x_3 = 0$; (b) variation of x_2 magnitude while $x_1 = \mu$ and $x_3 = 0$; (c) variation of x_3 magnitude while $x_1 = \mu$ and $x_2 = \mu$.

2.4.3 Response surface for ULS

The ultimate buckling strength response with respect to the variations in initial imperfections as well as variations due to different material grade and the plate thickness is investigated for various values of R_R . The response surface method [55, 56] was used to identify the response, where the ultimate buckling strength is expressed as a response function of the three initial imperfections x_1 , x_2 , and x_3 . A second-order polynomial response surface function, as shown below, is used in the present study:

$$\frac{\sigma_{ULS}}{\sigma_y} = \sum p_{ijk} x_1^i x_2^j x_3^k; \quad (i = 0 \sim 2; j = 0, 2; k = 0, 2; i + j + k \leq 6) \quad (2.1)$$

where σ_{ULS} is the ultimate buckling strength, and p_{ijk} are the coefficients of the polynomial, as determined by a nonlinear multiple regression analysis. The sample dataset of the regression analysis at a certain R_R includes the σ_{ULS} data for all of the material grades and all of the thickness variations.

Since positive and negative values of x_2 or x_3 of the same magnitude yield the same ultimate strength, the initial out-of-plane deflections for the whole-plate mode (x_2) and the local mode (x_3) are approximated as an even function in Eq. 2.1. A positive value of the out-of-plane deflection (x_2 or x_3) indicates that the deflection is toward the stiffener, whereas a negative value of the out-of-plane deflection indicates that the deflection is opposite to the stiffener.

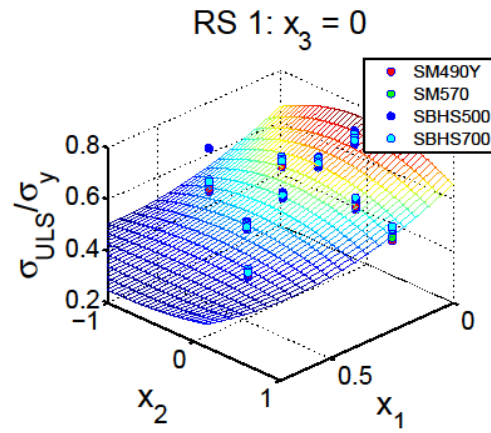
In fact, the initial out-of-plane deflections were approximated from corresponding elastic buckling modes, where a positive value in one panel/subpanel appears with a corresponding negative value in the adjacent panel/subpanel. Hence, the positive or negative sign of x_2 or x_3 does not affect the ultimate buckling strength. The regression coefficients calculated for different R_R values are listed in Table 2.6.

Since the response surface function comprises three variables, the response of σ_{ULS} is presented in Fig. 2.12 with respect to two variables, while the third variable is maintained constant. Figure 2.12(a) shows the response surface with respect to x_1 and x_2 for the case in

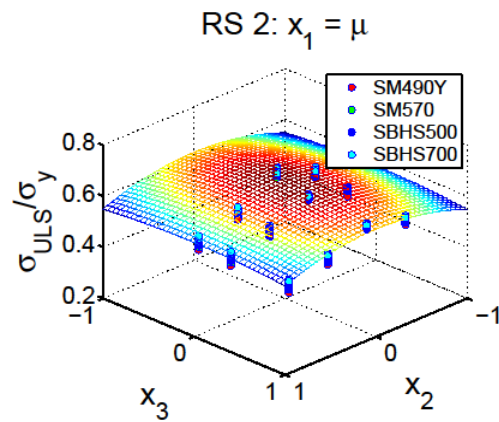
which $x_3 = 0$. Similarly, Fig. 2.12(b) shows the response surface regarding x_2 and x_3 for the case in which $x_1 = \mu$, and Fig. 2.12(c) shows variation in x_3 and x_1 for the case in which $x_2 = \mu$. In these figures, the mesh grid represents the response surface function, and the circular dots denote the FEA results. The response surface function is later used in the MCS to obtain the probabilistic strength.

Table 2.6 Regression parameters for ULS at various values of R_R .

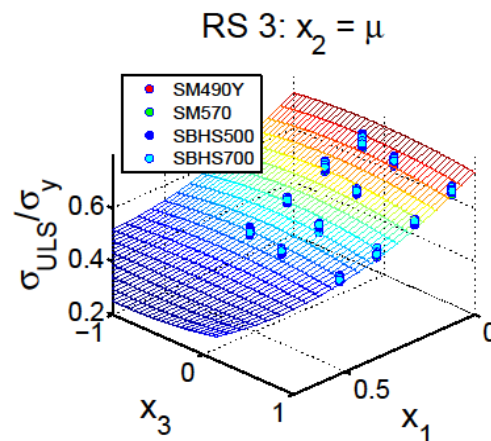
Regression Parameters		R_R					
		0.4	0.6	0.8	1.0	1.2	1.4
Coefficient of determination	R^2	0.720	0.856	0.925	0.889	0.811	0.879
Regression Coefficients	p_{000}	1.024	1.035	0.959	0.759	0.544	0.397
	p_{100}	-0.424	-0.705	-0.890	-0.498	-0.123	-0.040
	p_{200}	0.423	0.677	0.743	0.247	-0.084	-0.092
	p_{020}	-0.029	-0.074	-0.119	-0.100	-0.051	-0.028
	p_{002}	-0.017	-0.070	-0.080	-0.023	0.010	0.004
	p_{120}	-0.151	-0.008	0.161	0.024	-0.128	-0.116
	p_{102}	0.081	0.205	0.162	-0.088	-0.120	-0.006
	p_{220}	0.188	0.028	-0.090	0.115	0.247	0.189
	p_{202}	-0.098	-0.225	-0.125	0.149	0.126	-0.018
	p_{022}	0.003	0.024	0.035	0.007	-0.009	-0.002
	p_{122}	-0.026	-0.065	-0.078	0.062	0.075	0.002
	p_{222}	0.034	0.073	0.050	-0.110	-0.085	0.010



(a)



(b)



(c)

Fig. 2.12 Response surfaces (RS) for σ_{ULS}/σ_y at $R_R = 1.0$. (a) RS 1: variation of x_1 and x_2 for the case in which $x_3 = 0$; (b) RS 2: variation of x_2 and x_3 for the case in which $x_1 = \mu$, and (c) RS 3: variation of x_3 and x_1 for the case in which $x_2 = \mu$.

2.5 FEA results and response surface for SLS

2.5.1 The SLS and its determination criteria

Unlike ULS, the SLS for stiffened plates under compression is a relatively less frequently studied topic, despite its importance for efficient structural design. In a recent study [57], the authors discussed the SLS for compressive stiffened plates, considering the effect of longitudinal edge support. The SLS is important for stiffened plates with large reduced slenderness parameters (R_R) because large out-of-plane plastic deformations occur before the plates reach their ultimate strength. An experimental investigation [38] revealed that plastic deformation occurs at nearly half of the ultimate load for stiffened plates with $R_R \geq 1.2$. There are provisions in some design codes for restricting this large out-of-plane deflection from a serviceability point of view. For example, checking the SLS related to out-of-plane deflection is necessary for the Nordic code [58] for stiffened plates with a span-to-thickness ratio greater than 120.

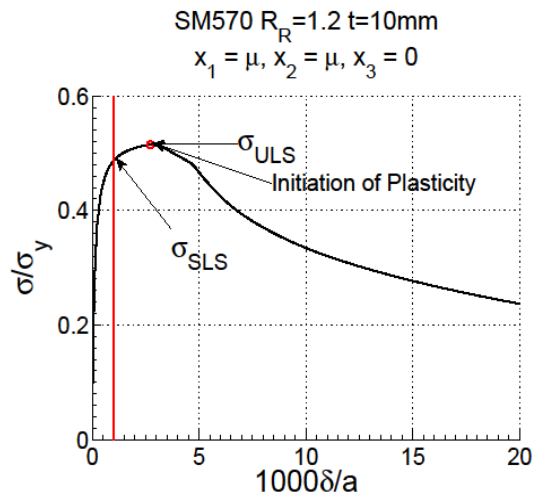
Fabrication tolerance is often used as a limiting criterion for excessive out-of-plane deflection. For example, in Eurocode, while validating the plate buckling check, test results, including large out-of-plane deflection, exceeding the fabrication tolerance were discarded [46]. Nara and Komatsu [27] reported the fabrication tolerance in the JSHB code. For whole-plate out-of-plane deflection shape, $\delta \leq a/1000$, and for local out-of-plane deflection shape, $\Delta \leq b_s/150$, where δ and Δ are the highest out-of-plane deflection magnitude after loading for the whole-plate and the local deflection shape, respectively.

In this research, the compressive strength at SLS (σ_{SLS}) was investigated for stiffened plates with $R_R \geq 1.0$, where σ_{SLS} was defined in the elastic range (e.g., plasticity does not occur), as the strength corresponding to the fabrication tolerance, as follows:

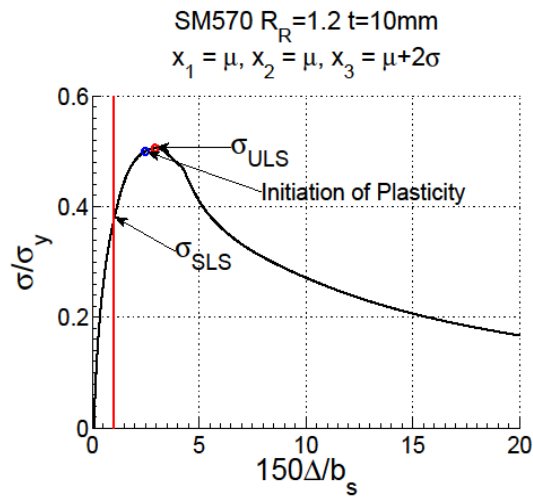
$$\sigma_{SLS} = \begin{cases} \text{for whole-plate deflection, } \sigma \text{ at } \delta = \frac{1000}{a} \\ \text{for local deflection, } \sigma \text{ at } \Delta = \frac{150}{b_s} \end{cases} \quad (2.2)$$

where σ represents the corresponding stresses at fabrication tolerance. After checking the onset of plasticity, σ_{SLS} was confirmed to remain within the elastic range. Figures 2.13(a) and

2.13(b) describe the determination of compressive strengths at SLS from normalized stress versus out-of-plane deflection curves, as an example. In these figures, the fabrication tolerance is indicated by a vertical red line. The SLS strength is the stress value corresponding to the intersection point between the vertical line and the normalized stress versus out-of-plane deflection curve. The initiation of plasticity occurred between σ_{SLS} and σ_{ULS} .

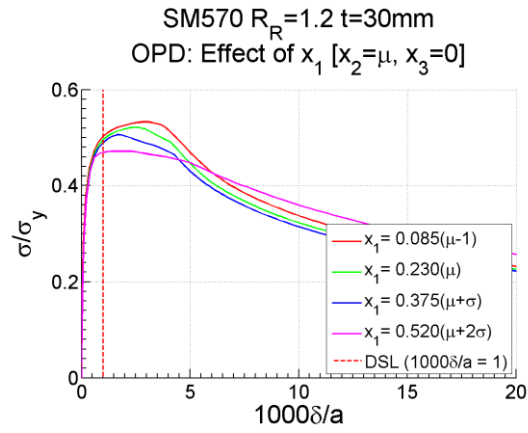


(a)

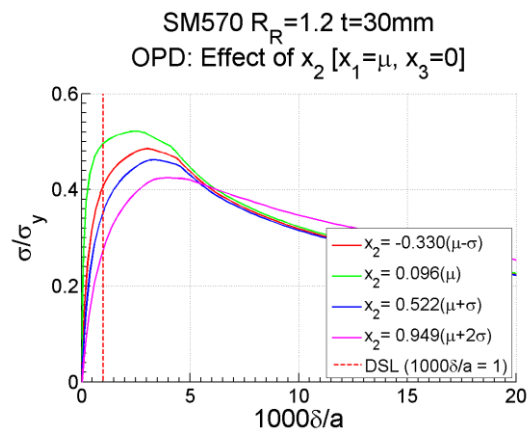


(b)

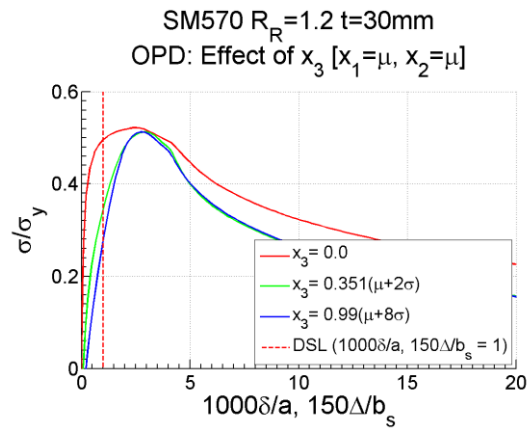
Fig. 2.13 Normalized stress versus out-of-plane deflection curves: (a) whole-plate deflection and (b) local deflection.



(a)



(b)



(c)

Fig. 2.14 Effect of variation of imperfection magnitudes on SLS strength: (a) variation of x_1 magnitude while $x_2 = \mu$ and $x_3 = 0$; (b) variation of x_2 magnitude while $x_1 = \mu$ and $x_3 = 0$; (c) variation of x_3 magnitude while $x_1 = \mu$ and $x_2 = \mu$.

2.5.2 Effect of variation of initial imperfection

The effect of variation of initial imperfections are investigated for SLS as well. Normalized stress – out-of-deflection curves are plotted in Fig. 2.14, following a similar way of explanation as in Fig. 2.11. Figs. 2.14 (a), (b) and (c) presents the effect of x_1 , x_2 and x_3 *individually* for a stiffened plate with a reduced slenderness parameter $R_R = 1.2$, plate thickness $t = 30$ mm and material grade SM570.

In Fig. 2.14(c), there are two horizontal axes. One corresponds to the normalized whole-plate out-of-plane deflection (after loading) and another corresponds to the normalized local out-of-plane deflection (after loading). The reason is, there are two different buckling modes observed in the FEA results. Whole-plate mode observed for the initial imperfection combinations with a zero value of x_3 , while local mode observed for the nonzero value of x_3 . Analyzing Figs. 2.14 (a), (b) and (c), it can be seen that x_2 is the most sensitive imperfection at SLS for this particular stiffened plate, followed by x_3 and x_1 .

2.5.3 Response surface for SLS

After determining the σ_{SLS} according to Subsection 2.5.1, the response of the σ_{SLS} due to variations in initial imperfections, material grade, and the plate thickness is investigated for stiffened plates with $R_R \geq 1.0$ using the response surface function described in Eq. 2.1. Table 2.7 shows the regression coefficients of the response surface functions at different R_R values obtained through nonlinear multiple regression analysis. Figures 2.15(a), (b), and (c) show the responses of σ_{SLS} with respect to two variables while the third variable constant. The order of exposition is the same as that for Figs. 2.12(a), (b), and (c), respectively.

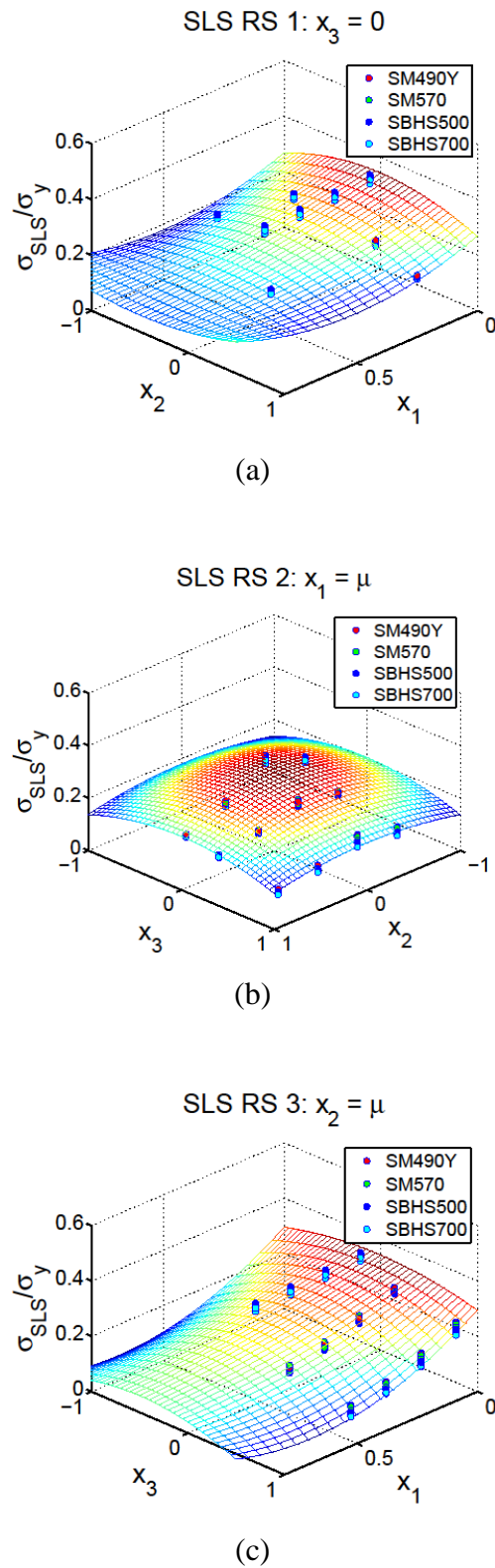


Fig. 2.15 Response surfaces (RS) for σ_{SLS}/σ_y at $R_R = 1.4$. (a) RS 1: variation of x_1 and x_2 for the case in which $x_3 = 0$; (b) RS 2: variation of x_2 and x_3 for the case in which $x_1 = \mu$, and (c) RS 3: variation of x_3 and x_1 for the case in which $x_2 = \mu$.

Table 2.7 Regression parameters for SLS for various values of R_R .

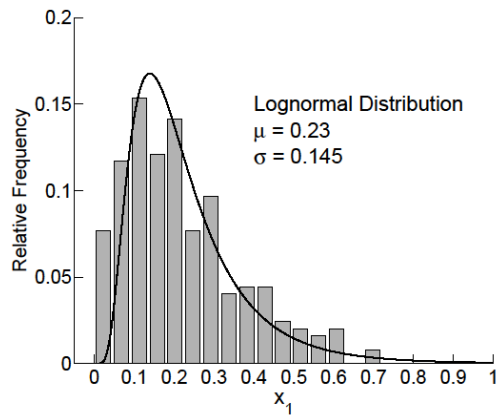
Regression Parameters		R_R		
		1.0	1.2	1.4
Coefficient of determination	R^2	0.839	0.752	0.764
Regression Coefficients	p ₀₀₀	0.672	0.460	0.345
	p ₁₀₀	-0.399	-0.201	-0.229
	p ₂₀₀	0.090	0.008	0.094
	p ₀₂₀	-0.151	-0.098	-0.077
	p ₀₀₂	-0.179	-0.103	-0.050
	p ₁₂₀	-0.188	-0.209	-0.127
	p ₁₀₂	-0.254	-0.360	-0.375
	p ₂₂₀	0.481	0.401	0.256
	p ₂₀₂	0.384	0.382	0.346
	p ₀₂₂	0.069	0.032	0.015
	p ₁₂₂	0.148	0.271	0.217
	p ₂₂₂	-0.305	-0.392	-0.280

2.6 Probabilistic analysis and PSFs

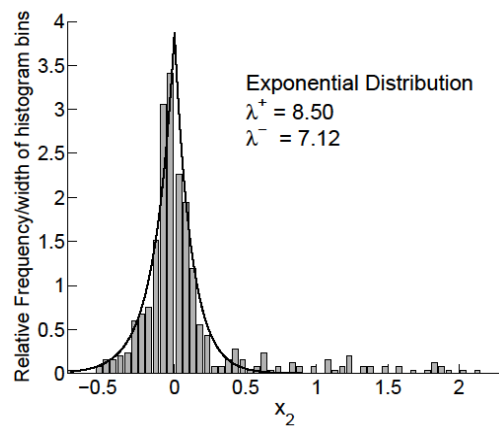
Using the response surfaces, MCSs were carried out in order to obtain probabilistic information of compressive strengths at different R_R values, for both SLS and ULS. Partial safety factors were proposed based on the obtained probabilistic information.

2.6.1 Monte Carlo simulation (MCS)

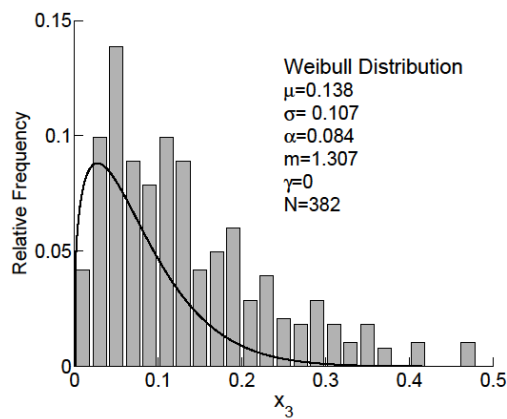
In the MCS, x_1 , x_2 , and x_3 were considered to be three independent random variables. In the first realization, one set of random values for x_1 , x_2 , and x_3 were generated in accordance with their respective probability density functions (PDFs), as reported in previous studies [51, 27, and 52]. The set of random values was then placed in the response surface function (Eq. 2.1) in order to determine the normalized compressive strength at ULS (σ_{ULS}/σ_y) or SLS (σ_{SLS}/σ_y), for that set of initial imperfections. The realizations continued until the convergence of the MCS result, i.e., until the mean value and standard deviation of σ_{ULS}/σ_y or σ_{SLS}/σ_y , obtained from several realizations, become convergent. A total of 100,000 realizations were required in order to obtain a convergent MCS result.



(a)

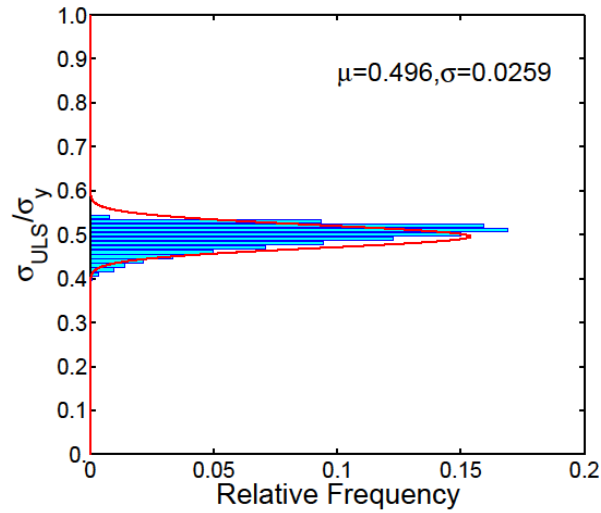


(b)

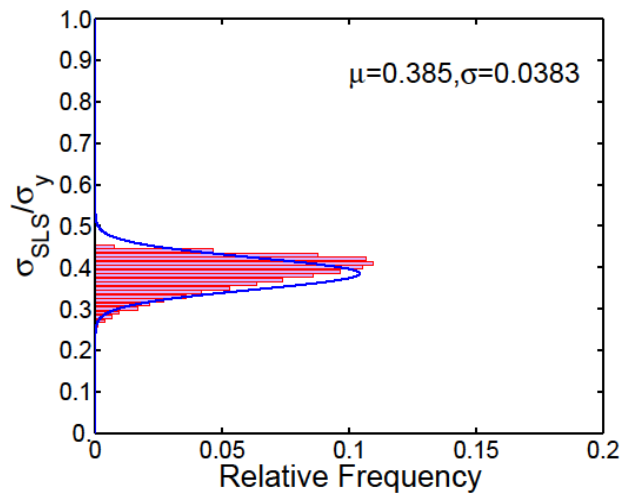


(c)

Fig. 2.16 Probability density functions for (a) normalized compressive residual stress (x_1), (b) normalized initial out-of-plane whole-plate deflection (x_2), and (c) normalized initial out-of-plane local deflection (x_3).



(a)



(b)

Fig. 2.17 Relative frequency distribution for (a) normalized ultimate strength (σ_{ULS}/σ_y) and (b) normalized SLS strength (σ_{SLS}/σ_y) at $R_R = 1.2$.

The PDFs for x_1 , x_2 , and x_3 are shown in Figs. 2.16 (a), (b), and (c), respectively. The PDF for x_1 follows a lognormal distribution, and that for x_2 conforms to a special distribution consisting of two exponential distributions with rate parameters $\lambda^+ = 8.50$ and $\lambda^- = 7.12$, where the $+/-$ signs in the superscripts denote positive and negative deflections, respectively. Positive means a deflection toward the stiffener, while negative means a deflection opposite to the stiffener. Details of this distribution is discussed elsewhere [54]. The PDF for x_3 fits a Weibull distribution. The parameters of the PDFs are shown in the

respective figures, where the solid bars indicate the observation data, and the curved lines represent the PDFs.

After performing MCS for each value of R_r , the relative frequency distributions of σ_{ULS}/σ_y and σ_{SLS}/σ_y were plotted. Figures 2.17(a) and 2.17(b) show an example of the relative frequency distributions plotted for ULS and SLS, respectively, at $R_r = 1.2$. The histogram of the relative frequency was fitted with a normal distribution using the mean and standard deviation obtained from the MCS. The probabilistic information, e.g., mean values and standard deviations for σ_{ULS}/σ_y and σ_{SLS}/σ_y are tabulated in Table 2.8 for various values of R_r .

Table 2.8 Mean values and standard deviations for σ_{ULS}/σ_y and σ_{SLS}/σ_y obtained from MCS.

Steel grades	Statistical parameter	σ_{ULS}/σ_y						σ_{SLS}/σ_y		
		R_R								
		0.4	0.6	0.8	1.0	1.2	1.4	1.0	1.2	1.4
SM490Y	μ	0.957	0.894	0.781	0.634	0.488	0.373	0.554	0.387	0.282
	σ	0.026	0.042	0.058	0.049	0.028	0.018	0.061	0.038	0.031
SM570	μ	0.932	0.904	0.783	0.632	0.482	0.371	0.540	0.380	0.279
	σ	0.034	0.048	0.059	0.048	0.025	0.016	0.057	0.038	0.031
SBHS500	μ	0.943	0.906	0.789	0.649	0.519	0.372	0.546	0.400	0.279
	σ	0.027	0.041	0.061	0.045	0.028	0.016	0.057	0.038	0.031
SBHS700	μ	0.946	0.909	0.794	0.652	0.491	0.372	0.546	0.373	0.268
	σ	0.026	0.046	0.058	0.047	0.023	0.014	0.056	0.039	0.030
Combined all steel	μ	0.945	0.903	0.787	0.642	0.496	0.372	0.546	0.385	0.277
	σ	0.028	0.044	0.059	0.046	0.026	0.016	0.058	0.038	0.031

2.6.2 Proposal for PSFs

Partial safety factors are adopted in most modern design codes in order to account for uncertainties originating from different sources. Member factors and material factors are two commonly used important PSFs. The present study focuses on the member factor, which discusses the uncertainty in the member's load carrying capacity.

Partial safety factors are proposed for both ULS and SLS for various R_r values, for stiffened plate members exhibiting column-like behavior. The reliability indexing method is used to calculate the PSFs. The assumption for using the reliability indexing method is that the probability density functions (PDFs) for σ_{ULS}/σ_y and σ_{SLS}/σ_y are normally distributed, as

shown earlier in Fig. 2.17. For a normally distributed PDF, the target reliability index (β_T) is 1.64, 1.88, and 2.33 for 5%, 3%, and 1% probability of non-exceedance (p_f), respectively. Eq. 2.3 describes the relationship between the PSF and the reliability index:

$$\mu - \beta_T \sigma = \frac{1}{\gamma} f_N \quad (2.3)$$

where μ and σ are the mean and the standard deviation of the normalized strengths σ_{ULS}/σ_y or σ_{SLS}/σ_y , respectively, γ is the PSF, and f_N is the corresponding nominal strength. *If the nominal strength is considered to be the mean value strength*, then the corresponding PSFs for probabilities of non-exceedance (p_f) of 5%, 3%, and 1% are presented in Table 2.9, *as an example*. It was found that PSFs for ULS at $R_r = 0.8$ and 1.0 are higher than those at other R_r values, while the PSF for SLS at $R_r = 1.4$ is the highest.

Table 2.9 Partial safety factors for ULS and SLS strengths assuming that the nominal strength is equal to the mean strength.

Limit States	R_r	μ	σ	f_N	PSFs (γ)		
					$p_f = 1\%$	$p_f = 3\%$	$p_f = 5\%$
ULS	0.4	0.945	0.028	0.945	1.074	1.059	1.051
	0.6	0.903	0.044	0.903	1.128	1.101	1.087
	0.8	0.787	0.059	0.787	1.211	1.164	1.140
	1.0	0.642	0.046	0.642	1.202	1.157	1.134
	1.2	0.496	0.026	0.496	1.139	1.109	1.094
	1.4	0.372	0.016	0.372	1.108	1.086	1.074
SLS	1.0	0.546	0.058	0.546	1.328	1.249	1.211
	1.2	0.385	0.038	0.385	1.302	1.230	1.195
	1.4	0.277	0.031	0.277	1.350	1.264	1.223

2.7 Discussion

The probabilistic ultimate buckling strength (corresponding to the ULS) of Model-1 is compared with the experimental results and various design codes, e.g., JSHB, AASHTO, Canadian Code, and Eurocode, in Fig. 2.18. Experimental results were obtained from various previous studies compiled by Niwa [59]. In this figure, MCS results are shown by vertical error bars for various values of R_r , where the bottom error bars indicate a 5% non-

exceedance probability ($p_f = 5\%$), midpoints represent the mean value strength, and the top error bars denote 95% non-exceedance probability ($p_f = 95\%$) for the ultimate buckling strengths. Predictions from Eurocode are shown for three different strengths, i.e. the plate-like buckling strength, the column-like buckling strength, and the interpolated final strengths. In order to discuss a rational comparison among different sources, all of the results shown in Fig. 2.18 corresponds to the same configuration of the stiffened plate considered for the Model-1, i.e., a stiffened plate with three equidistant longitudinal stiffeners and conforming to the JSHB specified required relative stiffness of longitudinal stiffeners.

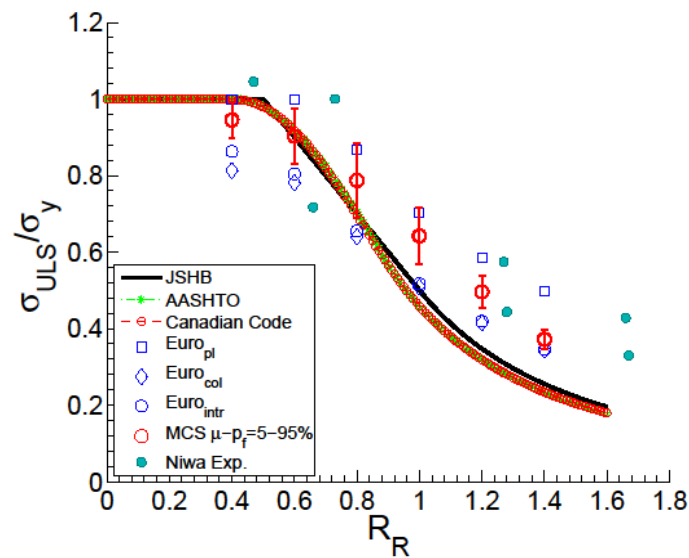


Fig. 2.18 Results for ULS obtained by MCS, compared with various design codes and experimental study.

Figure 2.18 shows that the AASHTO and Canadian Code provide almost identical results, which match well the JSHB results for $R_R \leq 0.8$ but predict an approximately 8% lower strength than the JSHB for $R_R > 0.8$. Note that the JSHB, AASHTO, and Canadian Code overestimate strength by around 9 to 11% for $R_R < 0.8$ and underestimated strength by 23 to 35% for $R_R > 0.8$, as compared to the MCS result with $p_f = 5\%$. This tendency of the JSHB strength curve has been reported in previous studies [54, 60]. Furthermore, it is well reported that, for stiffened plates with more than one longitudinal stiffener, AASHTO provides significantly conservative design [23, 61].

Among the various design codes shown in Fig. 2.18, Eurocode column-like buckling strengths show better agreement with the MCS results with $p_f = 5\%$, as expected. However, the Eurocode column-like buckling strengths are still lower than the MCS results for $p_f = 5\%$. This can be explained as the effect of the continuity of a stiffened plate in the longitudinal direction, which is considered herein but is not considered in Eurocode, which instead considers a single panel. It is clear that the stiffened plate, which is continuous in the longitudinal direction, will have higher strength than a single panel.

Experimental results, obtained from various previous studies (compiled by Niwa [59]), show a large variation in ultimate strength, even in the same range of R_R . This might be the effect of variations in imperfections in the different plates, differences in the experimental boundary set up, etc. Nevertheless, most of the experimental results are higher than the design codes and the MCS results.

The probabilistic SLS strengths are compared with the probabilistic ULS strengths, obtained from the MCS, as well as with the deterministic ULS strength of JSHB, as shown in Fig. 2.19. The mean values of the SLS strengths at $R_R = 1.0, 1.2,$ and 1.4 are 18%, 29%, and 34% lower than those of the ULS strengths, respectively. In addition, the coefficient of variation of SLS strengths is higher than that of ULS strengths. For a 5% non-exceedance probability, the SLS strengths are lower than the current JSHB ULS strengths.

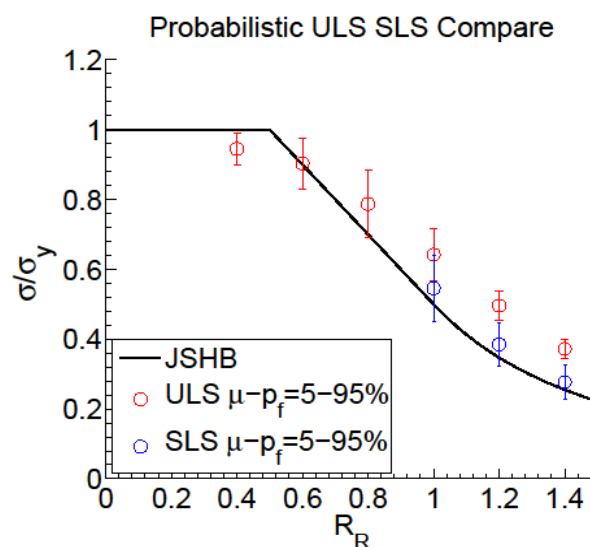


Fig. 2.19 Probabilistic ULS and SLS strengths obtained from MCS.

2.8 Conclusion

Chapter 2 addressed the column-like behavior of longitudinally continuous stiffened steel plates and investigated probabilistic compressive strengths at ULS and SLS. Stiffened plates with an aspect ratio of $a = 1.0$ and three flat plate equidistant longitudinal stiffeners, satisfying the relative stiffness requirement of JSHB were considered. The compressive strengths were obtained through nonlinear elasto-plastic FEA using ABAQUS commercial software. A total of 2,988 FEA were carried out in order to address the effect of varying parameters, e.g., initial out-of-plane deflections, residual stress, plate thickness, material grade, and reduced slenderness parameter. A response surface function was estimated from the nonlinear FEA results in order to take into account the variability of initial imperfections. Monte Carlo simulations were performed in association with the response surface in order to obtain the probabilistic strengths.

The probabilistic ULS strengths were compared with various design codes. The JSHB, AASHTO, and Canadian Code were found to overestimate strengths for $R_R < 0.8$ and to be significantly conservative for $R_R > 0.8$, as compared to the ULS strengths with $p_f = 5\%$. However, Eurocode column-like buckling strengths are in good agreement with the ULS strengths corresponding to $p_f = 5\%$. Comparing the SLS strength and the ULS strengths, the mean SLS strengths at different R_R values are approximately 63 to 82% of the mean ULS strengths. The SLS strengths with $p_f = 5\%$ are lower than the current ULS strengths of the JSHB.

The uniqueness of this Chapter is that rather than deterministic strengths, probabilistic strengths are provided for column-like behavior, which can be used as an important reference for developing a reliability-based design strength curve. Furthermore, continuous stiffened panels (in the longitudinal direction) are discussed rather than an isolated panel, addressing scope for improvement of Eurocode.

[This page is left intentionally blank]

Probabilistic column-like compressive strength considering the effect of longitudinal edge support: ULS and SLS

3.1 Introduction

The standard ultimate strength curve of the current Japanese specification (JSHB) for a stiffened plate is mainly based on the research of Kanai and Otsuka [38]. Kanai and Otsuka carried out experiments on 43 stiffened plates under uniaxial loading and proposed the ultimate strength curve. Among the 43 stiffened plates, more than 80% of the plates (35 stiffened plates) were of two longitudinal stiffeners, which indicates that the current specification concentrates on stiffened plates with 2 equidistant flat plate longitudinal stiffeners, satisfying the relative stiffness requirement of JSHB ($\gamma_1/\gamma_{1,req} = 1$).

Other than Kanai and Otsuka, many Japanese researchers investigated the ultimate buckling strength of stiffened steel plates during the 1970-80s. The effect of initial imperfections was examined by several studies. For example, Komatsu et al. [21] measured the initial deflection and residual stress for 28 stiffened plate specimens including high-strength steel. Komatsu et al. [52] reported statistical data for the initial deflection of steel bridge members and investigated the effect of initial deflection on the ultimate buckling strength. Furthermore, Komatsu and Nara [26] enhanced the research by discretizing the fundamental modes of initial deflection and their individual effect on the ultimate strength.

The study during the 1970s that proposed probabilistic buckling strength was conducted by Nara and Komatsu [27]. They proposed ultimate buckling strength curves corresponding to 1%, 5% and 10% probability of non-exceedance. In their study, as a source of variability of the buckling strengths, only the stochastic variation of the initial out-of-plane deflection was considered. However, the variation of residual stress was not taken into account.

In general, the limitations of the past researches during 1970-80s is that, they did not consider the effect of thick plates and SBHS steels, which are in frequent use today. Moreover, only the deterministic ultimate buckling strength, corresponding to ULS, was the target. However, Kanai and Otsuka [38] pointed out the issue of large out-of-plane plastic deformation of slender stiffened plates that motivated the authors to investigate the SLS as well. Based on the experiments, Kanai and Otsuka reported that test specimens with large reduced slenderness parameter ($R_R = 1.2$) yield large out-of-plane plastic deformation, which occurs at nearly half of the ultimate load. As a consequence, they recommended that while designing the slender stiffened plates, instead of ultimate strength out-of-plane deflection limit should be considered as an important issue. This is the reason why the JSHB strength curve is predominantly conservative for $R_R \geq 1.0$, as shown in Fig. 3.1.

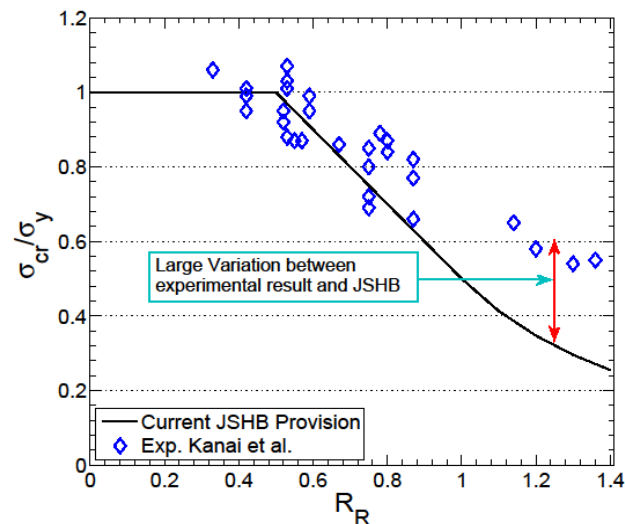


Fig. 3.1 JSHB strength curve and experimental results of Kanai et al.

There is one more issue that is important while assessing the compressive strength at ULS and SLS. In actual condition, the stiffened plates at the bottom flange of a steel box girder bridge are simply supported on two sides along the longitudinal edges, by the webs of the box girder. Moreover, the plates are continuous along the longitudinal direction. In experimental set up, it is very difficult to obtain a perfect simply supported boundary condition as well as the continuity along the longitudinal direction. Numerical simulation and analysis is therefore, a promising alternative to investigate the real behaviors accurately, provided there is a validity of the numerical results.

Taking into account the limitations described above, in addition to the issues identified before in Subsection 1.5 of Chapter 1, this Chapter, therefore, investigates the probabilistic distribution of the compressive strengths for a *continuous, two sides simply supported*, longitudinally stiffened plates with 2 equidistant flat plate stiffeners, which is hereinafter named as “Model-2”. The aspect ratio of the Model-2 plates was selected $\alpha = a/b = 1$ to produce column-like buckling and relative stiffness of the longitudinal stiffeners satisfies the relative stiffness requirement of JSHB ($\gamma_1/\gamma_{1,req} = 1$).

The probabilistic compressive strengths are investigated not only for ULS but also for SLS. Due to lack of specific criteria to determine the compressive strengths at SLS, this Chapter also proposes a rational criterion for determination of SLS strengths of Model-2 stiffened plates based on elastic buckling strength and the limit of unacceptable deformation [57].

Similar to Model-1, a stochastic variation of the initial out-of-plane deflections, as well as the residual stresses, were considered simultaneously for Model-2. Moreover, not only the normal steel grades but also the high-performance steel (SBHS) were taken into account. The plate thickness was varied from 10 to 90 mm. The probabilistic distribution of the compressive strengths was obtained through Monte Carlo simulation, in association with a response surface method. Finally, the probabilistic strengths were compared with different design codes and previous studies. The comparison revealed that for Model-2, the JSHB, AASHTO, and Canadian Code provide significantly conservative design, while Nara’s [27] results and Eurocode interpolated strengths matches well with a 5% non-exceedance probability for compressive strength at ULS. To be noted that, content of this Chapter has been published in two different journal articles by the author [54, 57].

3.2 Deterministic FEA

3.2.1 Model geometry, boundary conditions, and material model

The geometric configuration of the Model-2 stiffened plates is presented through a schematic diagram in Fig. 3.2. Due to symmetric geometric and loading conditions, and in order to reduce the computational time, half of the stiffened plate model (the shaded rectangular area in Fig. 3.2) was considered for the FEA instead of the full model. The modeling procedure in ABAQUS is similar to that of Model-1 as described earlier in Section 2.3 of Chapter-2.

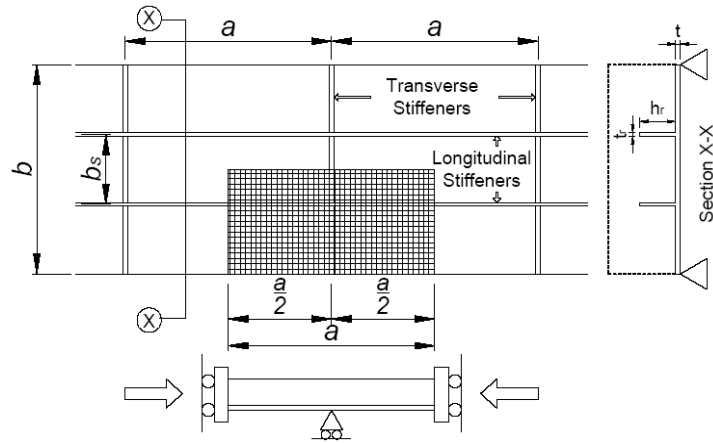


Fig. 3.2 Geometric configuration of Model-2.

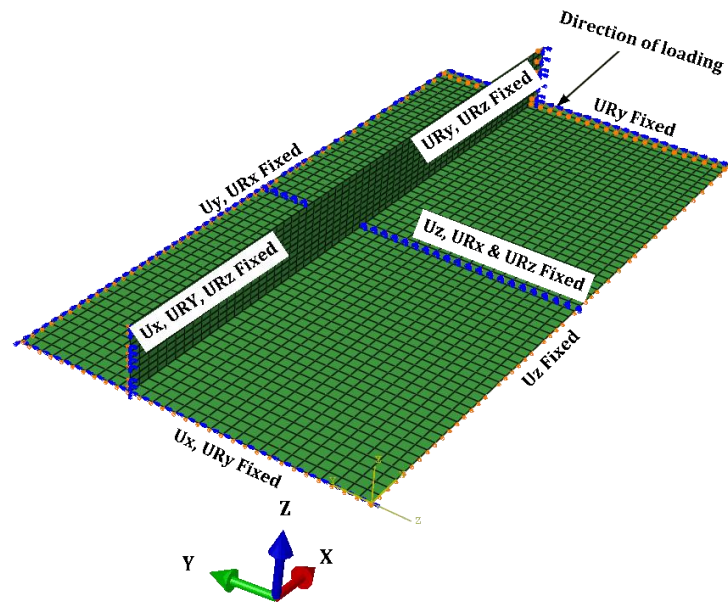


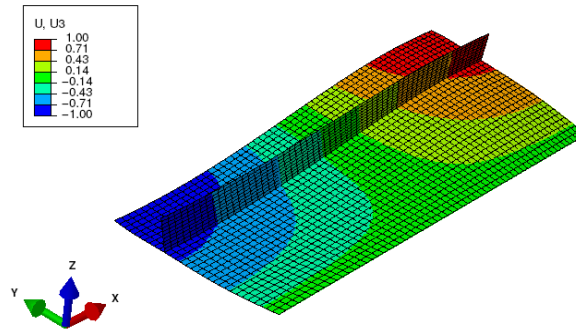
Fig. 3.3 Boundary conditions of Model-2.

Fig. 3.3 illustrates the boundary conditions of Model-2. In this figure U_x , U_y , and U_z denote translation along the X, Y, and Z axes, respectively, and UR_x , UR_y , and UR_z denote the rotational degrees of freedom around the X, Y, and Z axes, respectively. Unlike Model-1, boundary conditions corresponding to a simple support were applied along the longitudinal edge of Model-2. However, boundary conditions for the continuity in longitudinal and transverse direction, for the transverse stiffener (assuming sufficient rigidity), and for the application of forced displacement were similar to that of Model-1.

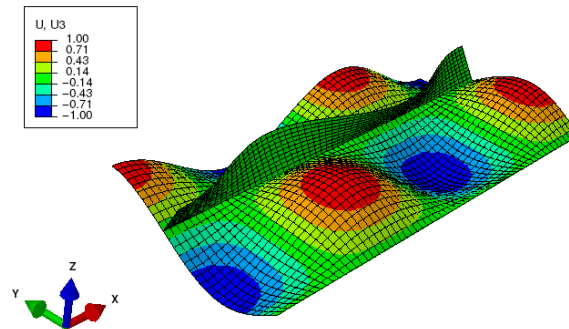
Four different material grades, i.e. SM490Y, SM570, SBHS500, and SBHS700 were considered for this study. The elastic and inelastic characteristics of the four material grades were same as that of Model-1, as described in Subsection 2.2.3 of Chapter 2.

3.2.2 Elastic buckling analysis

Prior to nonlinear analysis, eigenvalue buckling analyses were carried out to determine the elastic buckling modes and elastic buckling strengths (σ_e). A compressive load was applied through a forced displacement. Interestingly, it was found that, Model-2 stiffened plates always shows a whole-plate buckling with a single half-sine wave shape as the first buckling mode while the second mode is a local buckling in the subpanels. The first two buckling modes and the normalized elastic buckling strength (σ_e/σ_y) for a particular Model-2 stiffened plate is presented in Fig. 3.4 as an example.



(a) 1st buckling mode ($\sigma_e/\sigma_y = 1.25$).



(b) 2nd buckling mode ($\sigma_e/\sigma_y = 1.58$).

Fig. 3.4 Buckling modes and σ_e/σ_y values for Model-2 stiffened plate with $R_R = 0.8$, $t = 30$ mm and steel grade SBHS500.

3.2.3 Verification of the nonlinear FEA result

The nonlinear elasto-plastic FEA procedure is described in detail in Section 2.3.2 of Chapter 2. The same procedure has been followed for Model-2 where both material, as well as geometric nonlinearity, was considered. Mises plasticity, isotropic strain hardening theory and associated flow rule were applied to model the material nonlinearity. The nonlinear FEA result was validated with respect to a past experimental result that has been carried out by Komatsu et al. [53].

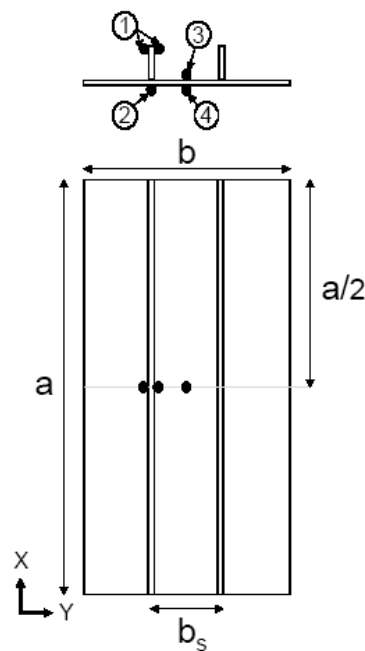


Fig. 3.5 Geometry and strain gauge location of test specimen (after Komatsu et al. [53]).

Table 3.1 Geometric and material properties of the test specimen.

(a) Geometric dimensions

a (mm)	b (mm)	b_s (mm)	t (mm)	h_r (mm)	t_r (mm)
2000	810	270	10.6	91	10.6

(b) Material properties for panel plate and longitudinal stiffeners

σ_y (MPa)	σ_T (MPa)	σ_B (MPa)	E (GPa)	ν	% of elongation
262.82	440.32	323.62	203.98	0.288	42.7

Figure 3.5 shows the geometric configuration and strain gauge locations of the selected test specimen from the study of Komatsu et al. [53]. Similar to Model-2, the selected test specimen consists of two equidistant flat plate longitudinal stiffeners. The reduced slenderness parameter (R_r) and aspect ratio (α) of the test specimen is 0.483 and 0.247 respectively. The ratio of relative stiffness to the required relative stiffness is $\gamma_1/\gamma_{1,req} = 0.375$. Table 3.1 shows the important geometric and material properties of the test specimen where σ_T and σ_B are the tensile strength and breaking strength of the steel.

Before carrying out the test, the initial imperfections in the specimen were measured. The reported highest magnitude of whole-plate initial out-of-plane deflection (δ_{01}) was 2.65 mm while the average compressive residual stress magnitude (σ_{rc}) for panel plate and stiffener was 107.76 MPa and 91.99 MPa respectively. In the numerical simulation, the magnitude of δ_{01} and σ_{rc} were considered same as the reported magnitude, following the shape and distribution pattern mentioned in Section 2.3.2 of Chapter 2. Furthermore, boundary conditions in the numerical model corresponds to a four side simply supported stiffened plate, which is similar to the experimental set up condition. Details of the experimental set up and application of loading procedure are described in detail in Komatsu et al. [53].

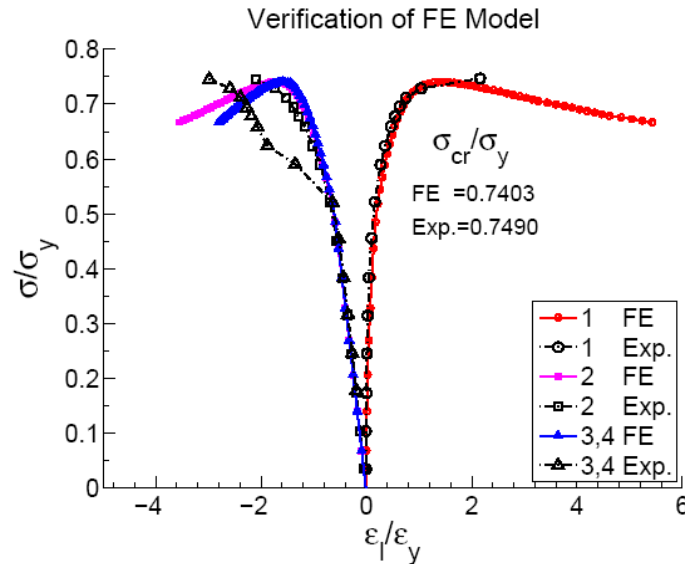


Fig. 3.6 Normalized stress (σ/σ_y) versus normalized local strain ($\varepsilon_l/\varepsilon_y$) curves from experiment and FE analysis.

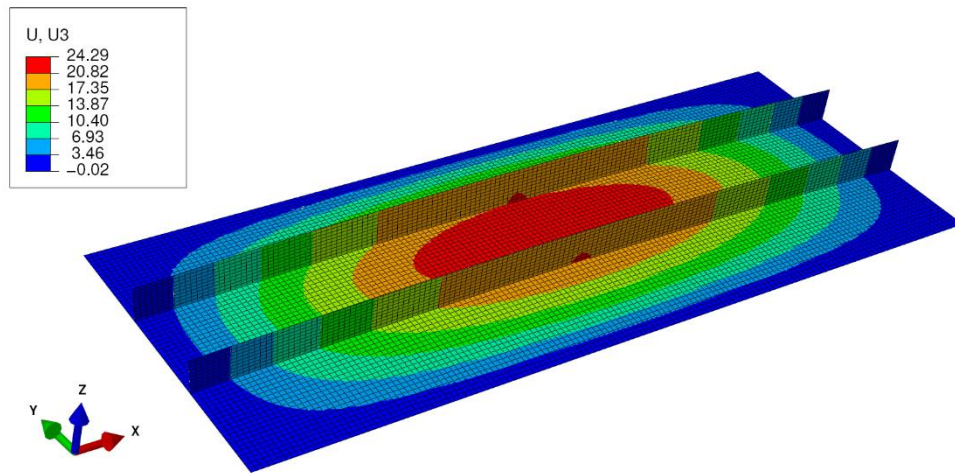


Fig. 3.7 Ultimate buckling mode from FEA.

Figure 3.6 presents the comparison between the test results and the FEA results. The normalized stress σ/σ_y versus normalized local strain $\varepsilon_l/\varepsilon_y$ curves are plotted for different strain gauge locations, i.e. the middle top and bottom position of a longitudinal stiffener, center top and bottom position of the panel plate. It was found that the ultimate buckling strength, obtained from FEA, was only 1.16% lower than that of the test result. Moreover, the trend of normalized stress-strain curves for different strain gauge locations, obtained from the FEA and experiment shows good agreement. In addition, Fig. 3.7 depicts the ultimate buckling mode, obtained from the FEA. The ultimate buckling mode from FEA is also consistent with that of the test results (as described in [53]). Therefore, the FEA results can be recognized as an alternative to the test results, provided the initial imperfections and appropriate boundary conditions are properly taken into account in the FEA.

3.2.4 Mesh size dependency analysis

The FEA result can be varied with the variation of the mesh size. The finer the mesh size, the accurate the FEA result. However, too fine mesh also requires greater computational time. Therefore, it is necessary to determine the optimum mesh size for the analysis, which is often determined from the convergence of the FEA results. For the buckling analysis with shell element, there is a thumb rule that the number of element should be at least six in the expected half wavelength of a buckle [42].

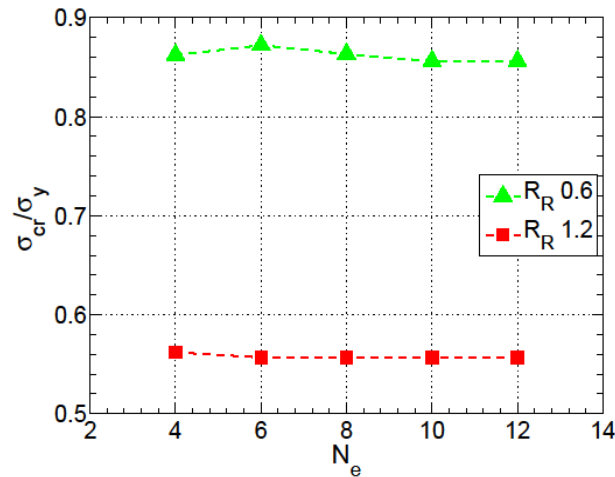


Fig. 3.8 Mesh dependency analysis result.

In this study, a mesh size dependency analysis was performed to ensure the convergence of the nonlinear elasto-plastic FEA results and the mesh size dependency analysis result has been reported in a previous study [54]. Nonlinear FEA was carried out for two different stiffened plates with different R_R values ($R_R = 0.6$ & 1.2) but same thickness ($t = 30$ mm), material grade (SM570) and initial imperfection combinations ($x_1 = \mu$, $x_2 = \mu$). Fig. 3.8 shows the result of mesh dependency analysis where N_e refers to the number of elements per half subpanel width as well as the number of elements along the height of a longitudinal stiffener. To be noted that, the subpanel width corresponds to the wavelength of the buckle with a local buckling mode. It was found that a convergent result can be obtained if N_e is greater or equal to ten. Based on this result, the value of N_e was taken equal to ten for the subsequent analysis. This result is also consistent with the thumb rule described above.

3.2.5 Effect of local initial out-of-plane deflection

Generally, the initial out-of-plane deflection with a shape of first elastic buckling mode (first eigenmode) yields the lowest ultimate buckling strength in the nonlinear FEA. Earlier, in case of Model-1, local buckling mode was the first eigenmode for most of the plates. It was, therefore, evident for Model-1 that local initial out-of-plane deflection (x_3) was necessary to consider in addition to the whole-plate initial out-of-plane deflection (x_2) and residual stress (x_1) to avoid overestimated buckling strengths from the FEA. In contrast, Model-2 has the

whole-plate buckling mode as the first eigenmode. Therefore, for Model-2, it is necessary to investigate whether x_3 should be considered along with x_1 and x_2 or not.

In this regard, two different FEA cases, i.e. Case-1 and Case-2 were considered for six different stiffened plates with different reduced slenderness parameters ($R_R = 0.4$ to 1.4). Case-1 discusses the effect of x_1 and x_2 , while Case-2 represents the effect of x_3 in addition to the x_1 and x_2 . Details of the imperfection combinations for Case-1 and Case-2 are presented in Table 3.2.

Table 3.2 Combination of imperfections for Case-1 and Case-2.

Imperfection Cases	Residual Stress x_1	Initial out-of-plane deflection	
		Whole-plate mode x_2	Local Mode x_3
Case-1	μ	$\mu+\sigma$	0
Case-2	μ	$\mu+\sigma$	$\mu+\sigma$

Table 3.3 Comparison of ultimate buckling strengths for Case-1 and Case-2 [54].

R_R	σ_{ULS}/σ_y		% difference with respect to Case-1
	Case-1	Case-2	
0.4	0.920	0.918	0.20%
0.6	0.826	0.827	-0.11%
0.8	0.760	0.753	0.92%
1.0	0.624	0.620	0.66%
1.2	0.492	0.491	0.24%
1.4	0.390	0.392	-0.38%

After carrying out the nonlinear FEAs for six different Model-2 stiffened plates with different R_R values but same material grade (SM570) and same thickness ($t = 30\text{mm}$), the results are summarized in Table 3.3, which has also been described elsewhere [54]. From this table, it was observed that the effect of addition of local initial out-of-deflection deflection (x_3) is not significant. The variation of ultimate strengths due to incorporation of the x_3 is even less than 1%. In consequence, for Model-2 stiffened plates, x_3 was not considered for the subsequent FEAs. Only the x_1 and x_2 were taken into account as the initial imperfections.

3.2.6 Parametric study

In order to address the effect of different influential parameters on the variability of the compressive strengths at ULS and SLS, it is necessary to perform a large-scale parametric study that includes the variations in plate thickness, material grade, reduced slenderness parameters, as well as the variations in the initial imperfections. For model-2, a parametric study was conducted where 96 stiffened plate models with 4 different material grades (SM490Y, SM570, SBHS500 and SBHS700) with R_R values of 0.4 to 1.4, and plate thicknesses of 10 to 90 mm were considered. Each of the stiffened plates incorporates 12 sets of initial imperfection combinations, consisting of x_1 and x_2 , as shown in Fig. 3.9. The combinations were based on the mean values (μ) and standard deviations (σ) of x_1 and x_2 . In total, 1152 number of FEAs were carried out for Model-2. Details of the dimensions of the Model-2 stiffened plates and FEA results are presented in Appendix B and Appendix E, respectively.

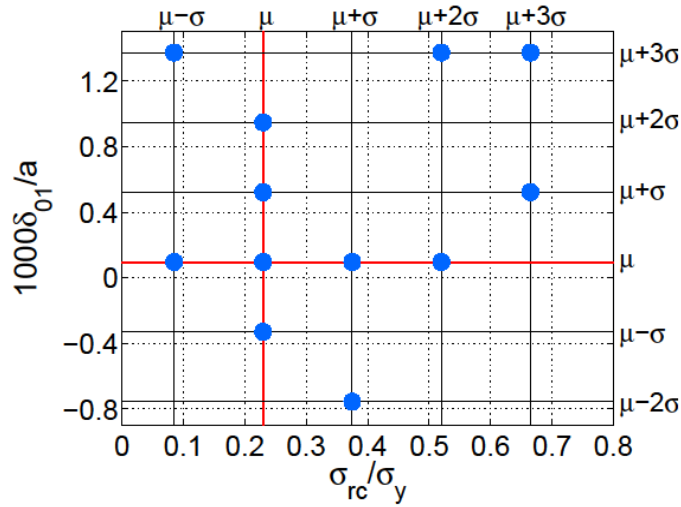


Fig. 3.9 Combination of initial imperfections for Model-2.

3.3 FEA results for ULS

This section briefly describes the effect of variation of three different parameters on the variation of ultimate buckling strengths for Model-2. The three parameters are i) the reduced slenderness parameter, ii) the plate thickness, and iii) the material grades. Detail description of the same is discussed elsewhere [54].

3.3.1 Effect of reduced slenderness parameter R_R

The normalized stress-strain curves for Model-2 stiffened plates with six different R_R values and two different material grades, i.e. the SM570 and SBHS500 are plotted in Fig. 3.10. All of the stiffened plates contains the same combination of initial imperfections ($x_1 = \mu, x_2 = \mu$). It was found that, Model-2 stiffened plates exhibit inelastic buckling for $R_R \leq 0.6$, whereas unstable snap-through behavior for $R_R \geq 0.8$. While comparing this buckling behavior between Model-1 and Model-2, it is interesting to note that, Model-1 showed snap-through buckling behavior irrespective of R_R values. In both models, with the increase of R_R values, the ultimate buckling strength decreased, as expected.

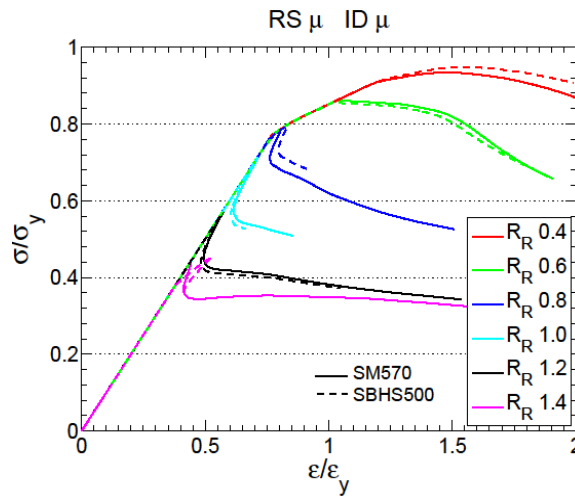


Fig. 3.10 Effect of R_R on normalized stress-strain curves for mean values of the residual stress and initial deflection, and a thickness of 30 mm.

3.3.2 Effect of plate thickness

The effect of variation of plate thickness was investigated keeping the R_R value constant. Figure 3.11 explains the result of plate thickness variation for Model-2 stiffened plates with six different R_R values and two different material grades, i.e. the SM570 and SBHS500. Analyzing the FEA results, it was found that the variation of plate thickness does not significantly affect the ultimate buckling strengths, provided the residual stress distribution along the plate thickness direction is considered constant.

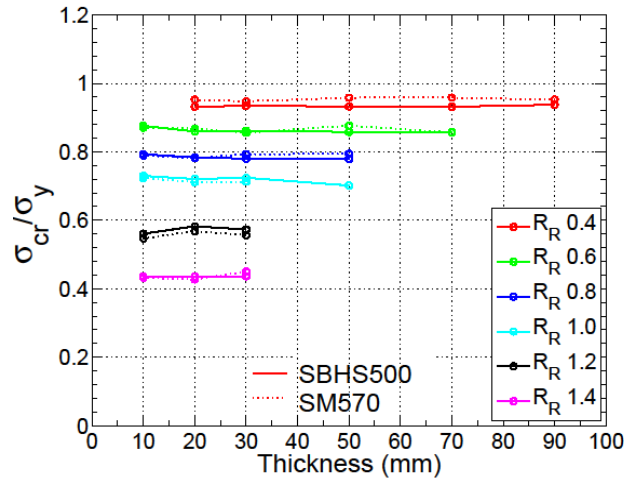


Fig. 3.11 Effect of plate thickness on normalized ultimate buckling strength for mean values of the residual stress and initial deflection, and for material grades SM570 and SBHS500.

3.3.3 Effect of material grade

Because SBHS steels have different inelastic characteristics comparing to the ordinary steels, it is obvious that their normalized ultimate buckling strength will be different. The extent of such variation due to the variation in material grade is illustrated in Fig. 3.12, which also has been reported elsewhere [54]. In this figure, normalized ultimate buckling strength for Model-2 stiffened plates with $t = 20$ mm are plotted for four different material grades and six different R_R values. It is observed that for $R_R \leq 0.6$, higher steel grades exhibit a lower load carrying capacity (σ_{ULS}/σ_y), while for $R_R \geq 0.8$ the pattern is irregular. For $R_R = 0.8$, there is no significant effect of material grade. Furthermore, SBHS700 shows a lower load carrying capacity than SBHS500 except for $R_R = 1.4$.

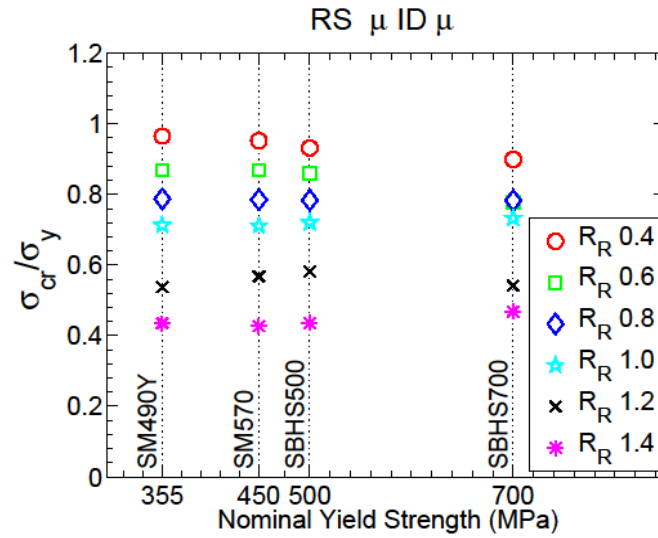


Fig. 3.12 Effect of material grade on normalized ultimate buckling strength for mean values of the residual stress and initial deflection, and a thickness of 20 mm.

3.4 FEA results for SLS

The serviceability limit state is important for stiffened plates with large reduced slenderness parameter (R_R). In this section, the scope of discussion is focused on the stiffened plates with $R_R \geq 1.0$. Before proposing a rational criteria to determine the SLS strengths for Model-2, two important behavior of slender stiffened plates are discussed in brief. Detail description of the same is also discussed in an article of the author [57].

3.4.1 Variation of buckling modes for slender plates

From the nonlinear elasto-plastic FEAs, it was observed that Model-2 stiffened plates with large reduced slenderness parameter, i.e. $R_R = 1.2$ and 1.4 exhibits different ultimate buckling modes depending upon the type and magnitude of initial imperfections (described in detail in [57]). Three different buckling modes were observed for the same stiffened plates with different imperfection combinations i.e.: i) whole-plate buckling mode, ii) local buckling mode, and iii) coupled mode of whole-plate and local buckling. Figure 3.13 illustrates an example of the variation of buckling modes for different imperfection combinations where A, B, and C denotes the whole-plate, local, and coupled buckling modes.

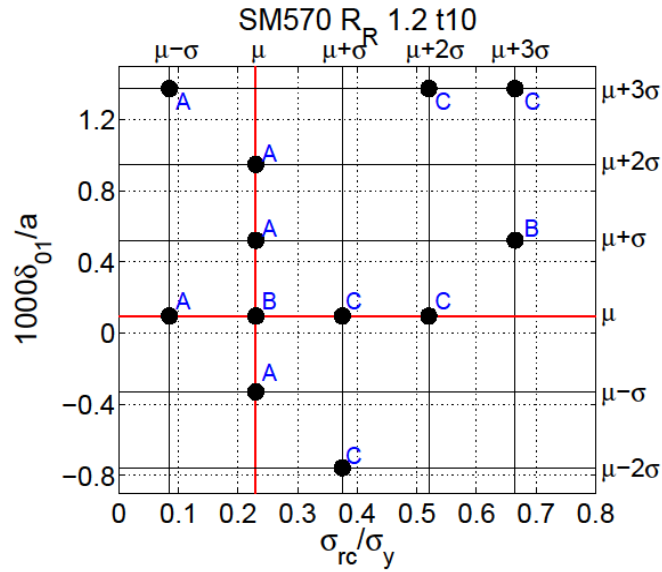
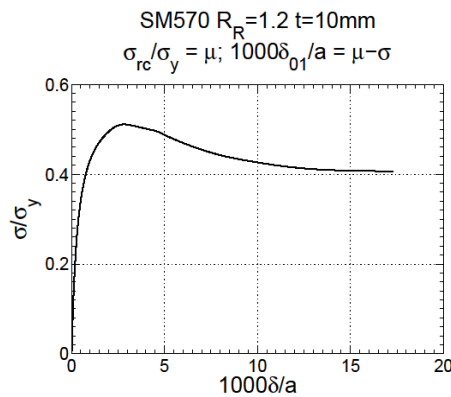


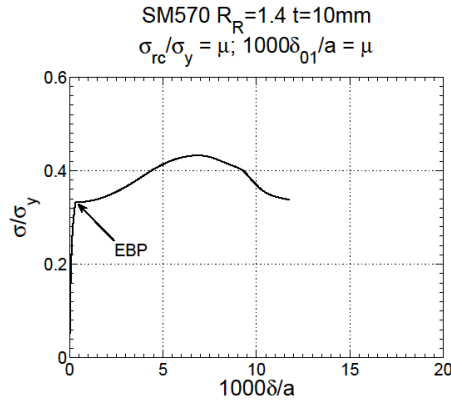
Fig. 3.13 Variation of buckling modes with respect to the initial imperfections. Symbol A, B and C denotes whole-plate, local and coupled buckling mode respectively.

3.4.2 Normalized stress vs. out-of-plane deflection curves

For the SLS, the prime concern is large out-of-plane deflection after loading. Therefore, normalized compressive stress (σ/σ_y) versus out-of-plane deflection ($1000\delta/a$ or $150\Delta/b_s$) curves were plotted in order to understand the behaviour of slender stiffened plates. Here, δ and Δ corresponds to the magnitude of out-of-plane deflection after loading for whole-plate and local buckling modes, respectively. After investigation, two different types of curves were observed as shown in Fig. 3.14. Curve Type-1 does not have a distinct elastic buckling point (EBP), while Curve Type-2 showed a clear elastic buckling point. For Model-2 stiffened plates, the SLS determination criteria is dependent upon these two types of curves.



(a) Curve Type-1



(b) Curve Type-2

Fig. 3.14 Normalized compressive stress versus normalized out-of-plane deflection curves: (a) Curve Type-1 and (b) Curve Type-2.

3.4.3 SLS determination criterion

According to ISO 2394 [17], the SLS includes three different aspects among which unacceptable deformation is one. For compressive steel plates, criterion based on elastic buckling followed by unacceptable deformation are often considered for the SLS design [41]. The SLS strengths for Model-2 stiffened plate will be proposed in this section based on the curve types as well as out-of-plane deflection limit and elastic buckling [57].

For Curve Type-1, the SLS strength σ_{SLS} is defined as the stress corresponding to the deflection serviceability limit σ_{DSL} , which is identified based on fabrication tolerance as follows:

$$\sigma_{SLS} = \sigma_{DSL} = \begin{cases} \text{for whole-plate deflection, } \sigma \text{ at } \delta = \frac{1000}{a} \\ \text{for local deflection, } \sigma \text{ at } \Delta = \frac{150}{b_s} \end{cases} \quad (3.1)$$

On the other hand, for Curve Type-2, σ_{SLS} is defined as the minimum of elastic buckling strength σ_{EBS} and stress corresponding to the deflection serviceability limit σ_{DSL} by the following equation

$$\sigma_{SLS} = \min [\sigma_{DSL}, \sigma_{EBS}] \quad (3.2)$$

The SLS determination criterion for Model-2 is presented as a flowchart in Fig. 3.15.

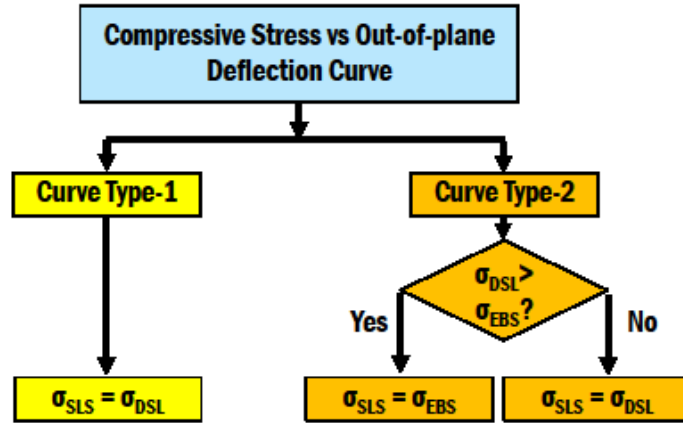


Fig. 3.15 Flowchart for the SLS determination criterion of Model-2.

3.5 Probabilistic analysis

The deterministic nonlinear FEA results were utilized to formulate the response surfaces that were later used in the probabilistic analysis. The probabilistic analysis was carried out using Monte Carlo simulation (MCS), [54, 56] where the whole-plate initial out-of-plane deflection and residual stress were considered as two independent stochastic variables.

3.5.1 Response surface: ULS and SLS

The variability of the compressive strengths (either ULS or SLS) for a single Model-2 stiffened plate depends on the variation of two independent variables, i.e. the residual stress (x_1) and the whole-plate initial out-of-plane deflection (x_2). To estimate the variability of the compressive strengths at ULS and SLS with respect to the variation of x_1 and x_2 , the following second-order polynomial response surface function of x_1 and x_2 was applied:

$$\frac{\sigma_{ULS-SLS}}{\sigma_y} = \sum p_{ij} x_1^i x_2^j; \quad (i = 0 \sim 2; \quad j = 0, 2; \quad i + j \leq 4) \quad (3.3)$$

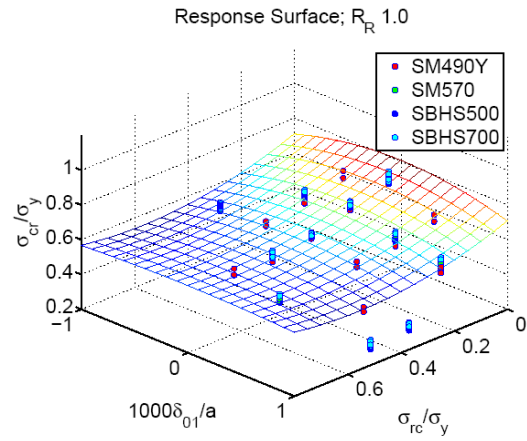
where x_1 = normalized residual stress (σ_{rc}/σ_y), x_2 = normalized initial out-of-plane deflection ($1000\delta_{01}/a$), and p_{ij} are the coefficients of the polynomial determined by a nonlinear multiple regression analysis.

The response surfaces for ULS were plotted for R_R values 0.4 to 1.4 with an increment of 0.2, while the response surfaces for SLS were plotted for R_R values 1.0, 1.2 and 1.4. In order to account for the variability of strengths due to variation in material grade as well as variation in plate thickness, the nonlinear FEA results of all the material grades and thicknesses under a certain R_R value were incorporated in the nonlinear multiple regression analysis. Therefore, a response surface for a certain R_R value includes the variation of strengths not only due to the variation of x_1 and x_2 but also the variation of material grade and plate thickness variation. Table 3.4 presents the regression parameters for the response surface functions at ULS and SLS. In addition, Figs. 3.16(a) and 3.17(a) illustrates the response surfaces at ULS and SLS, respectively, for a Model-2 stiffened plate with $R_R = 1.0$, as an example. In these figures, the mesh gridline shows the response surface and the solid dots represent the nonlinear FEA results.

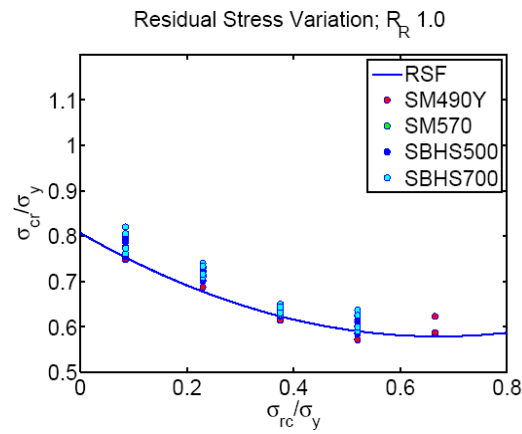
Furthermore, to clearly understand the variation in USL and SLS strengths, 2D figures were extracted from the 3D response surfaces. Figs. 3.16(b) and 3.16(c) were extracted from the Fig. 3.16(a). Fig. 3.16(b) shows the ULS strength variation with respect to the variation of x_1 while $x_2 = \mu$ and Fig. 3.16(c) depicts the ULS strength variation with respect to the variation of x_2 while $x_1 = \mu$. Similarly, Figs. 3.17(b) and 3.17(c) were extracted from the Fig. 3.17(a). Fig. 3.17(b) presents the SLS strength variation with respect to the variation of x_1 while $x_2 = \mu$ and Fig. 3.17(c) shows the SLS strength variation with respect to the variation of x_2 while $x_1 = \mu$.

Table 3.4 Regression parameters for Model-2 stiffened plates at ULS and SLS.

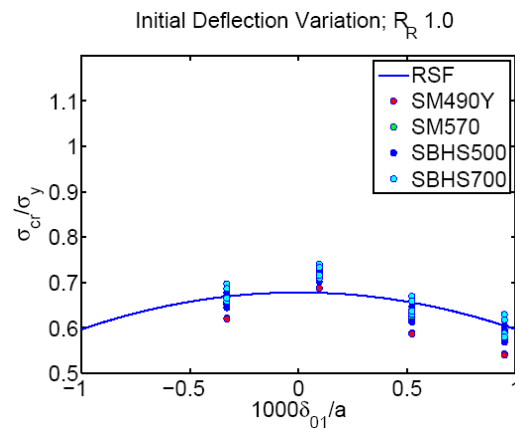
Regression Parameters		ULS						SLS		
		R_R						R_R		
		0.4	0.6	0.8	1.0	1.2	1.4	1.0	1.2	1.4
Coefficient of R^2 determination		0.710	0.704	0.777	0.843	0.786	0.796	0.889	0.715	0.747
Regression Coefficients	p_{00}	0.944	0.959	0.942	0.808	0.584	0.436	0.779	0.517	0.381
	p_{02}	-0.010	-0.039	-0.089	-0.099	-0.048	-0.027	-0.208	-0.154	-0.096
	p_{10}	-0.055	-0.537	-0.871	-0.681	-0.257	-0.102	-0.563	-0.195	-0.157
	p_{12}	-0.125	-0.017	0.114	0.070	-0.115	-0.123	-0.081	0.052	-0.138
	p_{20}	0.043	0.553	0.826	0.506	0.069	-0.045	0.251	0.032	0.043
	p_{22}	0.156	0.035	-0.094	0.038	0.231	0.213	0.381	0.130	0.257



(a)



(b)



(c)

Fig. 3.16 (a) Response surface for ULS, (b) Effect of variation of residual stress for a mean value of the initial deflection and (c) Effect of variation of initial deflection for a mean value of the residual stress, for different steel grades at $R_R = 1.0$.

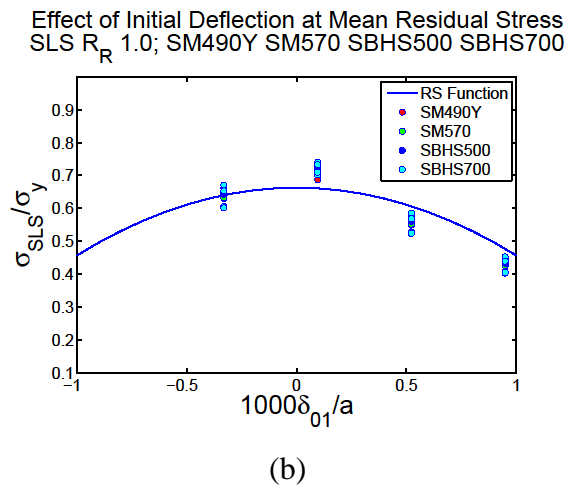
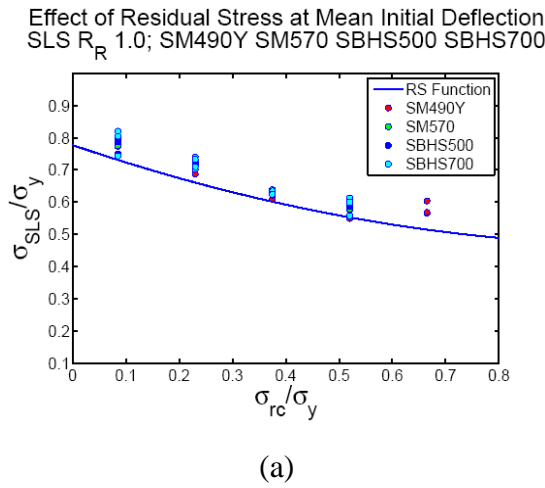
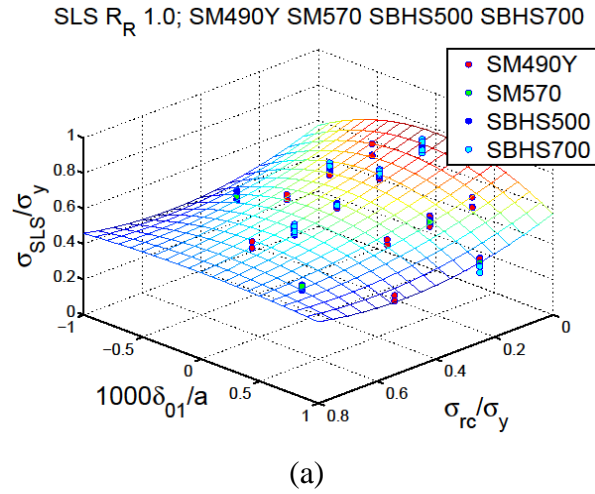


Fig. 3.17 (a) Response surface for SLS, (b) Effect of variation of residual stress for a mean value of the initial deflection and (c) Effect of variation of initial deflection for a mean value of the residual stress, for different steel grades at $R_R = 1.0$.

3.5.2 Monte Carlo simulation (MCS): ULS and SLS

In order to obtain the probabilistic distribution of compressive strengths at ULS and SLS for Model-2 stiffened plates, MCSs were carried out. In the MCSs, normalized residual stress (x_1) and normalized whole-plate initial out-of-plane deflection (x_2) were two independent stochastic variables. Random values for x_1 and x_2 were generated in accordance with their respective PDFs, as reported earlier in Figs. 2.16(a) and 2.16(b). The MCS and convergence criterion for the MCS results are the same that followed for Model-1. The only difference is, for Model-1, x_3 was also considered as a random variable in addition to x_1 and x_2 .

Figure 3.18 shows an example of the convergence of MCS result for Model-2 stiffened plates. In this figure, the mean value and standard deviation of σ_{SLS}/σ_y for stiffened plates with $R_R = 1.0$ became convergent at 100,000 realizations. Similar to Model-1, 100,000 realizations were carried out for Model-2 as well.

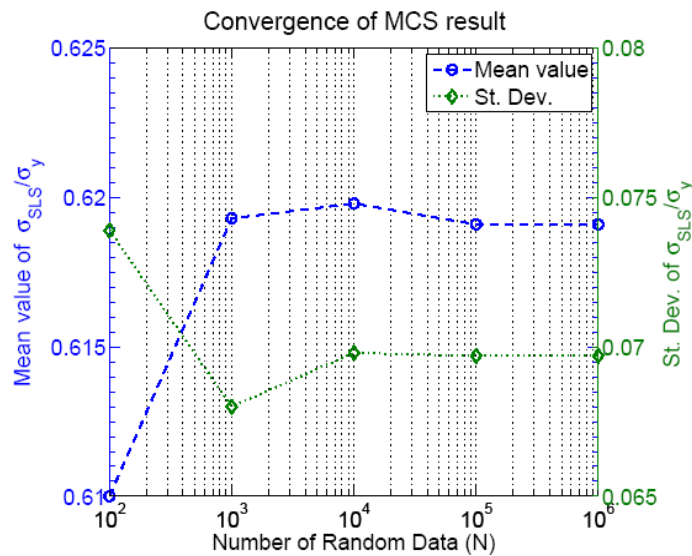
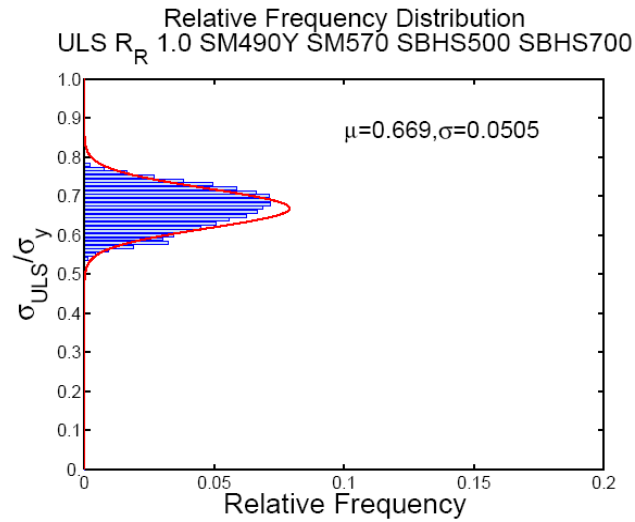


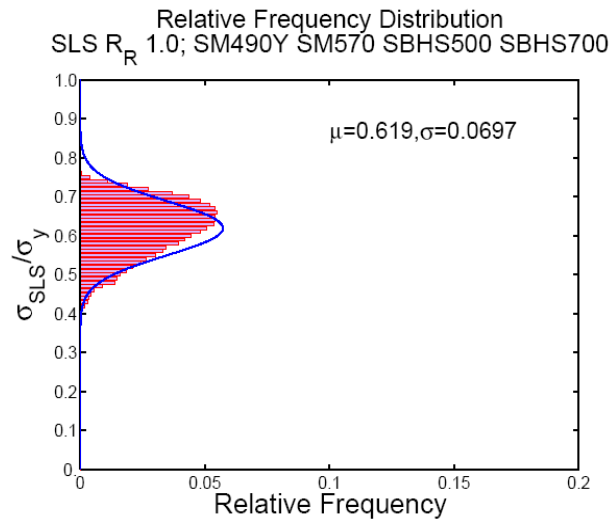
Fig. 3.18 Convergence of mean value and standard deviation for σ_{SLS}/σ_y at $R_R = 1.0$.

For a certain R_R value, after performing the MCS, 100,000 data for the σ_{ULS}/σ_y and σ_{SLS}/σ_y are obtained. To investigate the probabilistic characteristics of the aforementioned normalized strengths, relative frequency distributions of the 100,000 strength data were plotted for each R_R value. Figures 3.19(a) and 3.19(b) show an example of the relative

frequency distributions plotted for ULS and SLS, respectively, at $R_R = 1.0$. In these figures, the solid line represent the normal distribution to fit the histogram using the mean value and standard deviation obtained from the MCS. The probabilistic information, e.g., mean values and standard deviations for σ_{ULS}/σ_y and σ_{SLS}/σ_y for Model-2 stiffened plates are presented in Table 3.5 for different values of R_R .



(a)



(b)

Fig. 3.19 Relative frequency distribution for Model-2 stiffened plates at $R_R = 1.2$ (a) normalized ultimate strength (σ_{ULS}/σ_y) and (b) normalized SLS strength (σ_{SLS}/σ_y).

Table 3.5 Mean values and standard deviations of σ_{ULS}/σ_y and σ_{SLS}/σ_y for Model-2.

Steel grades	Statistical parameter	σ_{ULS}/σ_y						σ_{SLS}/σ_y		
		R_R								
		0.4	0.6	0.8	1.0	1.2	1.4	1.0	1.2	1.4
SM490Y	μ	0.951	0.887	0.760	0.627	0.487	0.384	0.573	0.413	0.304
	σ	0.010	0.037	0.059	0.065	0.039	0.026	0.112	0.079	0.054
SM570	μ	0.940	0.870	0.790	0.675	0.524	0.403	0.632	0.460	0.325
	σ	0.006	0.025	0.053	0.056	0.035	0.024	0.077	0.040	0.038
SBHS500	μ	0.921	0.871	0.784	0.679	0.545	0.404	0.633	0.467	0.330
	σ	0.008	0.030	0.054	0.056	0.041	0.021	0.077	0.052	0.038
SBHS700	μ	0.889	0.827	0.802	0.689	0.513	0.408	0.631	0.430	0.321
	σ	0.014	0.036	0.050	0.056	0.030	0.021	0.078	0.041	0.033
Combined all steel	μ	0.928	0.866	0.785	0.669	0.516	0.399	0.619	0.442	0.321
	σ	0.009	0.030	0.052	0.050	0.031	0.020	0.070	0.038	0.032

3.5.3 Partial safety factors: ULS and SLS

Assuming the compressive strengths at ULS and SLS are normally distributed, PSFs for Model-2 are calculated for several non-exceedance probability ($p_f = 5\%$, 3% , and 1%) using the reliability indexing method, as described earlier in Subsection 2.6.2 of Chapter-2. The PSFs are calculated for an example case where the nominal strength is taken equal to the mean value strength. Table 3.6 presents the calculated PSFs for both ULS and SLS of Model-2 stiffened plates with different reduced slenderness parameter R_R . It was found that PSFs at $R_R = 1.0$ is the highest than other R_R values either for ULS or SLS. In other words, it can be said that the effect of initial imperfections is dominant at $R_R = 1.0$ for Model-2.

Table 3.6 PSFs for Model-2 ULS and SLS strengths assuming that the nominal strength is equal to the mean strength.

Limit States	R_R	μ	σ	f_N	PSFs (γ)		
					$p_f = 1\%$	$p_f = 3\%$	$p_f = 5\%$
ULS	0.4	0.928	0.009	0.928	1.015	1.018	1.022
	0.6	0.866	0.030	0.866	1.061	1.071	1.089
	0.8	0.785	0.052	0.785	1.121	1.141	1.180
	1.0	0.669	0.050	0.669	1.141	1.165	1.213
	1.2	0.516	0.031	0.516	1.111	1.129	1.165
	1.4	0.399	0.020	0.399	1.090	1.105	1.133
SLS	1.0	0.619	0.070	0.619	1.228	1.270	1.358
	1.2	0.442	0.038	0.442	1.164	1.193	1.250
	1.4	0.321	0.032	0.321	1.195	1.231	1.303

3.6 Discussion

A summary of the MCS results for the ULS of Model-2 stiffened plates is presented in Fig. 3.20. Here, the MCS results are denoted by red error bar plots where the top and bottom error bars represent the 95% and 5% non-exceedance probabilities, respectively, and the midpoint represents the mean value strength. To make a rational comparison, results from other different sources are presented in the figure for stiffened plates with same configuration as of Model-2. The green solid line represents the ULS strength curve of Nara et al. [27] corresponding to a 5% non-exceedance probability. Experimental results from Kanai et al. [38] are depicted by pink circular dots. Furthermore, predictions from different design codes i.e. JSHB, AASHTO, Canadian Code, and Eurocode are also discussed, where the Eurocode predictions are presented discretely for plate-like, column-like, and interpolated buckling strength.

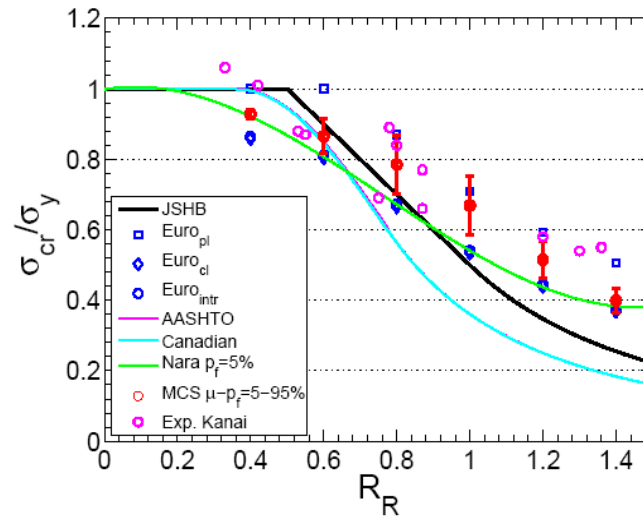


Fig. 3.20 Comparison of MCS results for ULS of Model-2 stiffened plates.

From the figure, it was observed that the MCS results for ULS strengths with a 5% non-exceedance probability agree well with those of Nara et al. and those of Eurocode, except for R_R values in the range of 0.8-1.2 [54]. In this range, the ultimate buckling strength is strongly affected by initial imperfections, which can also be confirmed from the relatively higher standard deviations of the ULS strengths. Compared to the MCS results, JSHB, AASHTO and Canadian Code overestimate the ultimate strength for $R_R \leq 0.6$, and

underestimate it for $R_R \geq 0.6$. It is interesting to note that predictions from AASHTO and Canadian Code is less than the JSHB for $R_R \geq 0.4$, which supports the statement of some previous study [23, 61] regarding strength curve of AASHTO. Experimental results of Kanai et al. shows fair agreement with MCS results in the range of $0.5 \leq R_R \leq 0.9$. Around $R_R = 0.8$, scattered experimental results were found which explains the higher standard deviation of MCS result. For $R_R \leq 0.5$ and $R_R \geq 1.2$, experimental results are higher than the MCS results.

In Fig. 3.21, the probabilistic SLS strengths of Model-2 are compared with that of the probabilistic ULS strengths, obtained from the MCS [57]. The JSHB strength curve for ULS is also presented which remarkably matches well with the SLS strengths for a 5% non-exceedance probability. The difference between the mean value strengths for SLS and ULS increases with increasing R_R . This can be clearly explained as the effect of large out-of-plane deflections, which increases with increase of R_R and produces lower strength at SLS. For example, the mean SLS strength at $R_R = 1.0$ is 92.6% of mean ULS strength, while the same at $R_R = 1.4$ is 80.4%. This result can be interpreted from a different perspective also. As the mean SLS strength at $R_R = 1.0$ becomes very close to the mean ULS strength (92.6%), it is evident that the consideration of SLS is not essential for $R_R < 1.0$.

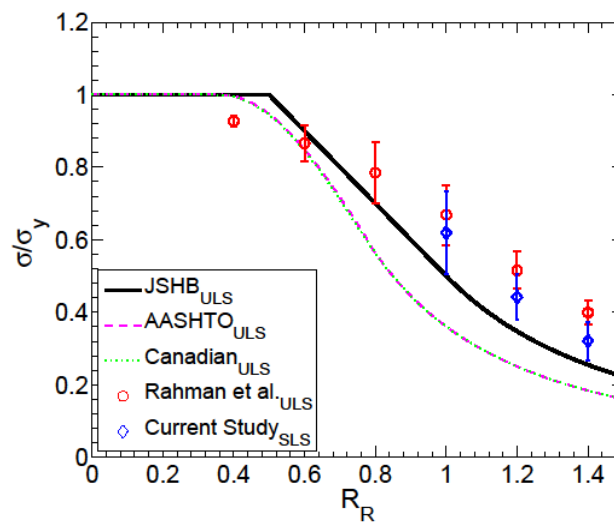


Fig. 3.21 Comparison of probabilistic ULS and SLS strengths of Model-2 stiffened plates.

3.7 Conclusion

Chapter 3 discusses the probabilistic compressive strengths at ULS [54] and SLS [57] for stiffened plates simply supported along the longitudinal edges with two equidistant flat plate longitudinal stiffeners, hereinafter named as Model-2. This kind of stiffened plate configuration is most relevant to the current Japanese design specification, JSHB. In this study, relative stiffness of the longitudinal stiffeners satisfies the relative stiffness requirement of JSHB ($\gamma_1/\gamma_{1,req} = 1$). Aspect ratio of the stiffened plates are taken $\alpha = 1.0$ to produce column-like behavior. The compressive strengths were obtained by employing numerical and probabilistic approaches. A total of 1152 FEA was carried out for 96 stiffened plate models with varying parameters. Monte Carlo simulation was applied in association with the response surface method to obtain the probabilistic ULS and SLS strengths.

The effect of thick plates and SHBS steels was investigated in the domain of ULS. The effect of variation of plate thickness does not significantly affect the ultimate strengths but the effect of SBHS steels are significant. Compared to the conventional steels, SBHS steels have higher mean value of σ_{ULS}/σ_y for $R_R \geq 0.7$. For example, at $R_R = 1.2$, SBHS500 shows 10.67% higher mean strength than SM490Y. However, for $R_R < 0.7$, mean strengths of SBHS steels are lower than that of conventional steels.

The MCS results for ULS strengths were compared with different design codes, study of Nara et al. [27] as well as experimental results of Kanai et al. [38]. Furthermore, MCS results for SLS strengths were compared with that of ULS strengths and JSHB code. The ULS strength with a $p_f = 5\%$ showed very good agreement with those of Nara et al. and Eurocode interpolated strength. Moreover, the SLS strength with a $p_f = 5\%$ showed good agreement with the ULS strength curve of JSHB.

The uniqueness of this Chapter is that probabilistic strengths are provided for stiffened plates exhibiting column-like behavior, yet considering the actual condition of the bottom flange of a box girder bridge, i.e. simply supported along the two longitudinal edges as well as continuous along the longitudinal direction. The results of the present study can be used as an important baseline for deriving a reliability-based ultimate strength curve.

Probabilistic compressive strength of stiffened plates exhibiting plate-like behavior: ULS and SLS

4.1 Introduction

Longitudinally stiffened plates with an aspect ratio more than one ($\alpha > 1.0$; length is higher than the width) and simply supported along their longitudinal edges, can sustain a compressive load far in excess of their buckling load, until reaching the ultimate load carrying capacity. The margin between the buckling load and the ultimate load in plates is known as the post-buckling strength [62]. Stiffened plates with above configuration, possesses a significant post-buckling strength due to a strong catenary action, generated in the transverse direction by the longitudinal edge supports. Figure 4.1 illustrates the catenary action in a stiffened plate, used as a bottom flange of a narrow steel box girder, as an example.

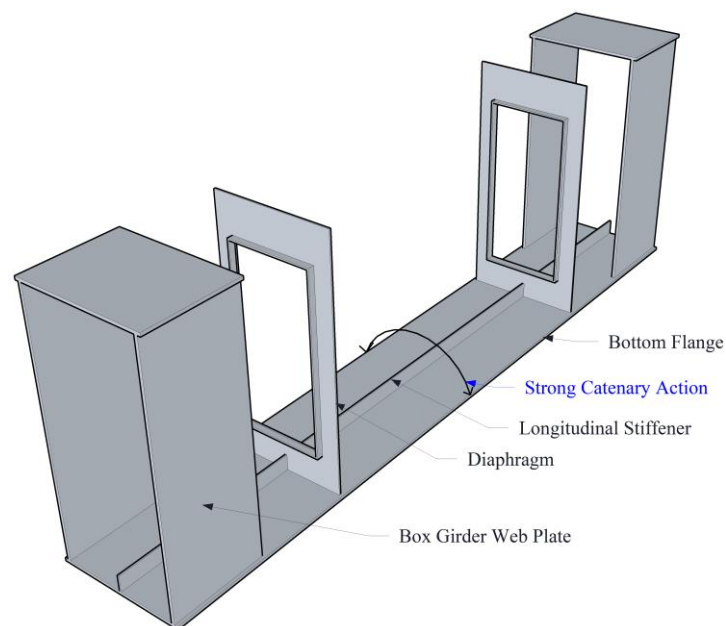


Fig. 4.1 Stiffened plates used in the bottom flange of a narrow box girder.

The compressive resistance of long stiffened plates with significant post-buckling strength reserve is discussed in the Eurocode under the concept of “*plate-like behavior*”. Plate-like buckling refers to the overall buckling or whole-plate buckling of the entire panel along with the longitudinal stiffeners, which is also known as stiffener buckling [43]. Assessment of the plate-like buckling strength, following the Eurocode, is a complex procedure. Especially the determination procedure of *elastic critical plate-like buckling strength* ($\sigma_{cr,p}$) is cumbersome.

According to the effective width method of Eurocode, while determining the ultimate buckling strength for any stiffened plates, the buckling strength corresponding to two extreme behaviors, i.e. the plate-like behavior and the column-like behavior are evaluated first. There are two parameters, i.e. the aspect ratio, and the level of stiffening of the longitudinal stiffener, that governs which behavior will be prominent. The final buckling strength is determined by interpolating between the strengths corresponding to the two extreme behaviors.

The interpolated final strength will be very close to the plate-like buckling strength if the *elastic critical plate-like buckling strength* ($\sigma_{cr,p}$) becomes much higher than the *elastic critical column-like buckling strength* ($\sigma_{cr,c}$). Determination of the reduction factor due to plate-like buckling (ρ) also requires assessment of the *elastic critical plate-like buckling strength* ($\sigma_{cr,p}$). It is important to note that, the *elastic critical plate-like buckling* state, calculated according to the simplified equations from Annex A to EN 1993-1-5 or using the Klöppel et al. chart [63, 64] corresponds to an elastic buckling mode of whole-plate buckling [65].

In this study, the plate-like buckling strength for stiffened plates with a whole-plate elastic buckling mode is investigated with respect to varying reduced slenderness parameters. Hence, the obtained plate-like buckling strengths can be used directly without requiring the complex calculation of $\sigma_{cr,p}$. Furthermore, in order to ensure a level 1 reliability based design, instead of evaluating a deterministic strength, probabilistic information of the strengths, such as a mean value and a standard deviation, is also provided.

This study also takes into account one scope of improvement in the Eurocode, reported by Johansson and Veljkovic [46]. In the effective width method, an isolated panel is considered. However, in reality, the stiffened plates are continuous along the longitudinal direction. Neglecting the effect of continuity may result in a sharp drop in resistance after applying the maximum load. But if the continuity is considered, the drop in the resistance will be small and controlled by adjacent panels that have not reached the yield strength. This study, therefore, considers a continuous boundary condition along the longitudinal direction of the stiffened plates.

In association with the general problems identified in Section 1.5 of Chapter 1, this Chapter investigates the probabilistic information of compressive strengths at ULS as well as SLS for longitudinally continuous long stiffened steel plates, exhibiting plate-like behavior, hereinafter referred as the Model-3. Compressive strengths were determined from nonlinear elasto-plastic FEA, where both material and geometric nonlinearity were taken into account. In order to account for the variability of the compressive strengths in the same stiffened plate, three different initial imperfections, i.e. the residual stress (x_1), the initial whole-plate out-of-plane deflection (x_2), and the initial local out-of-plane deflection (x_3) were considered simultaneously in the nonlinear FEA. Finally, an approximate solution procedure was employed to obtain the first order probabilistic information, i.e. a mean value and a variance.

4.2 Selection of stiffened plate models

This study focuses on the stiffened plates used as the bottom flange of a narrow steel box girder bridge. Narrow box girder bridges are quite common in Japan. Usually, the width varies between 1000 mm to 1800 mm, and one longitudinal stiffener is used. Accordingly, for this study, width of the Model-3 stiffened plates was considered in the range of 1000 mm to 1800 mm. The relative stiffness of the longitudinal stiffener was selected in such a way that it satisfies the relative stiffness requirement of JSHB ($\gamma_1/\gamma_{1,req} = 1$). From the actual bridge data on the steel box girder bottom flanges constructed in Japan [66], the aspect ratio (α) of narrow box girder bottom flanges was found to vary from 3 to 5, as shown in Fig. 4.2.

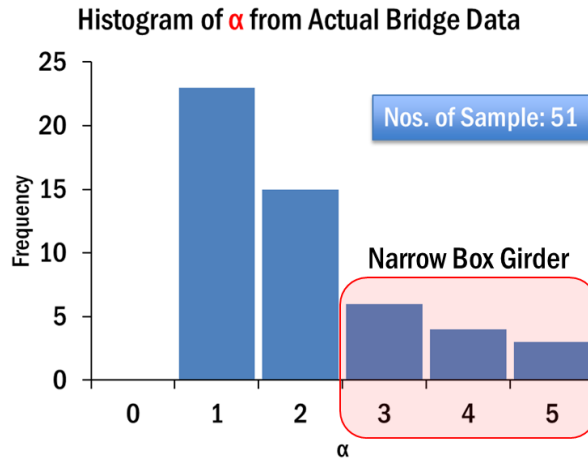


Fig. 4.2 Actual steel box girder bridge data for the aspect ratio of bottom flanges.

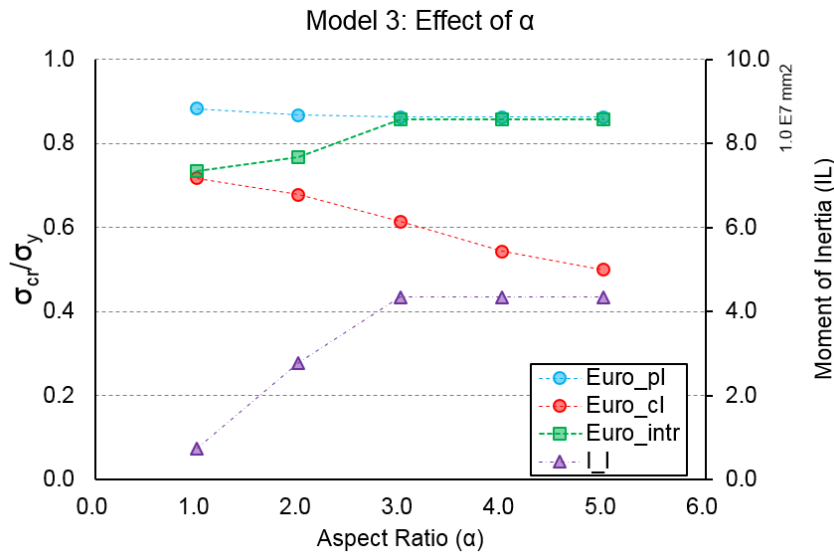


Fig. 4.3 Effect of aspect ratio on the plate-like behavior.

However, in order to determine the minimum aspect ratio to produce plate-like buckling for Model-3 stiffened plates, the effect of aspect ratio was investigated and presented in Fig. 4.3. Five stiffened plates with varying aspect ratio from 1 to 5, and with one longitudinal stiffener, was considered for the investigation. Longitudinal stiffener for each of the stiffened plates satisfies the relative stiffness requirement of JSHB ($\gamma_1/\gamma_{1,req} = 1$). The plate-like buckling strength, the column-like buckling strength, and the interpolated final strength, calculated according to the Eurocode, are plotted in Fig. 4.3 for the five stiffened plates. It was found that the interpolated strength starts to shift from the column-like strength to the plate-like

strength with the increase of aspect ratio. When the aspect ratio becomes 3 or more, the interpolated strength turn out to be very close to the plate-like buckling strength. Furthermore, for an aspect ratio of $\alpha \geq 3$, the second moment of inertia of the longitudinal stiffener to fulfill the required relative stiffness of JSHB, becomes constant. Hence, the aspect ratio of Model-3 stiffened plates was taken as 3 in this study.

In summary, Model-3 stiffened plates has the following characteristics

- i. Width of the panel plate (b) varies from 1000 mm to 1800 mm,
- ii. Aspect ratio $\alpha = 3$,
- iii. Number of subpanels divided by longitudinal stiffener $n = 2$,
- iv. Size of the longitudinal stiffener determined by the JSHB requirement ($\gamma_l / \gamma_{l,req} = 1$)

4.3 Numerical analysis

4.3.1 Model geometry, boundary conditions, and material model

The geometric configuration of the Model-3 stiffened plates is presented through a schematic diagram in Fig. 4.4. Full width of the model (the shaded rectangular area in Fig. 4.4) is taken into account for the numerical analysis. However, in order to simulate the continuous behavior in the longitudinal direction, keeping the transverse stiffener in the middle, half-lengths from two adjacent panels were taken. The commercial software ABAQUS was used for the modeling, FEA, and post processing. The modeling procedure in ABAQUS is similar to that of Model-1 and Model-2 as described earlier in Chapter-2 and Chapter-3, respectively.

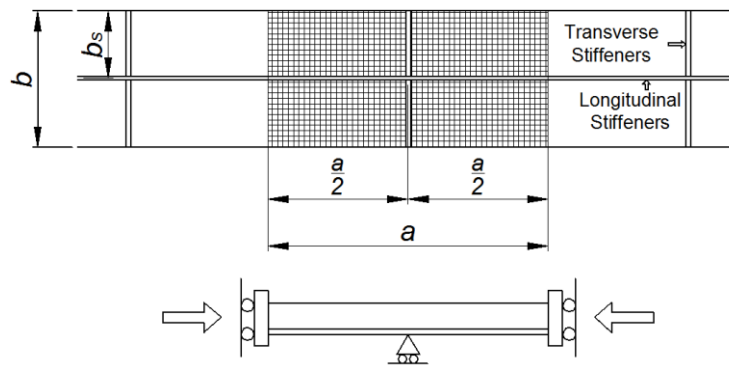


Fig. 4.4 Geometric configuration of Model-3.

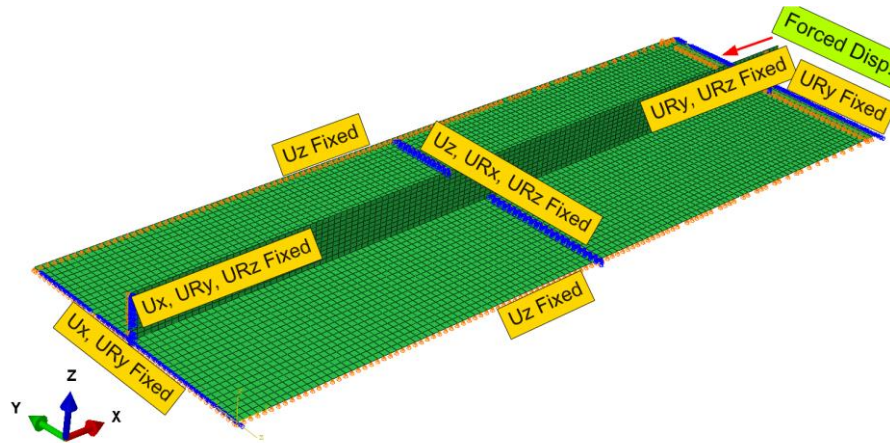


Fig. 4.5 Boundary conditions for Model-3.

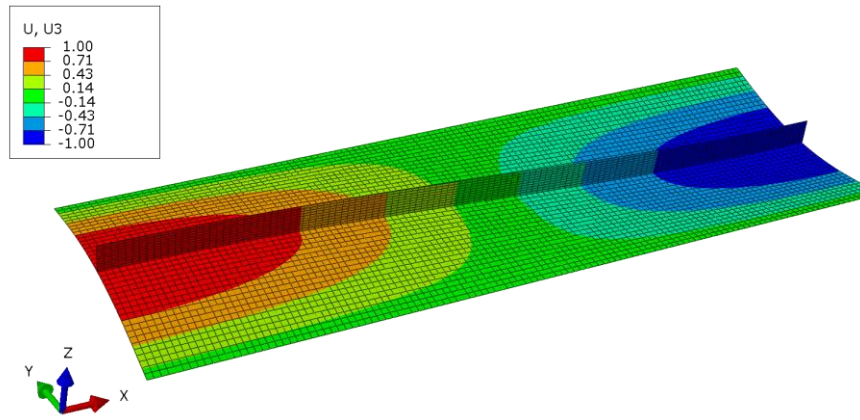
Fig. 4.5 illustrates the boundary conditions of Model-3. In this figure U_x , U_y , and U_z denote translation along the X, Y, and Z axes, respectively, and UR_x , UR_y , and UR_z denote the rotational degrees of freedom around the X, Y, and Z axes, respectively. A simply supported boundary conditions were applied along the both longitudinal edges of Model-3. However, boundary conditions for the continuity in longitudinal direction, for the transverse stiffener (assuming sufficient rigidity), and for the application of forced displacement were similar to that of Model-1 and Model-2.

Four different material grades, i.e. SM490Y, SM570, SBHS500, and SBHS700 were considered for this study. The elastic and inelastic characteristics of the four material grades were same as that of Model-1 and Model-2, as described in Subsection 2.2.3 of Chapter 2.

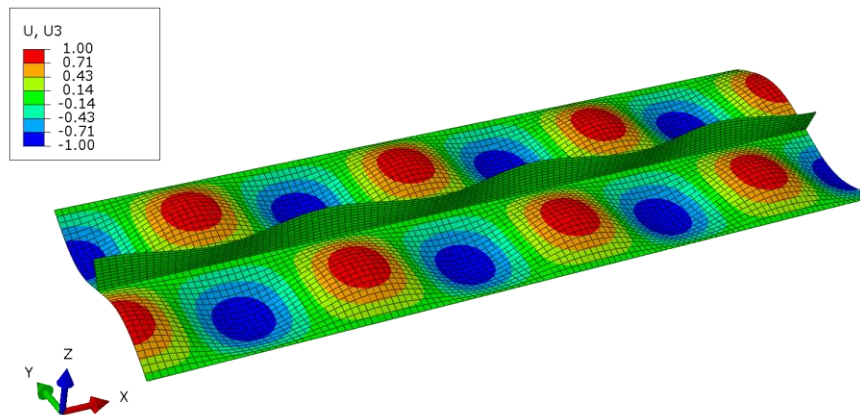
4.3.2 Elastic buckling analysis

Eigenvalue buckling analyses were carried out for Model-3 stiffened plates in order to investigate the elastic buckling modes and elastic buckling strengths (σ_e). In the analysis, a compressive load was applied through a forced displacement. It is interesting to note that, even though the relative stiffness of longitudinal stiffener conforms to the required relative stiffness of JSHB to avoid whole-plate buckling, for most of the Model-3 stiffened plates, the first elastic buckling mode obtained from the eigenvalue buckling analyses was the whole-plate mode. The second elastic buckling mode was a local buckling mode. The first

two buckling modes and the normalized elastic buckling strength (σ_e/σ_y) for a particular Model-3 stiffened plate is presented in Fig. 4.6 as an example.



(a) 1st buckling mode ($\sigma_e/\sigma_y = 0.96$).



(b) 2nd buckling mode ($\sigma_e/\sigma_y = 1.07$).

Fig. 4.6 Buckling modes and σ_e/σ_y values for Model-2 stiffened plate with $R_R = 1.0$, $t = 15$ mm and steel grade SM490Y.

4.3.3 Nonlinear elasto-plastic FEA

The nonlinear elasto-plastic FEA procedure that has been followed for Model-3 stiffened plates is similar to that of Model-1 and Model-2, as described earlier in Chapter-2 and Chapter-3. Nonlinearity for both material and geometric properties were taken into account.

Mises plasticity, isotropic strain hardening theory and associated flow rule were applied to model the material nonlinearity.

Before applying the forced displacement, initial imperfections were simulated to represent the initial condition. Three different initial imperfections, i.e. the normalized residual stress (x_1), the normalized initial whole-plate out-of-plane deflection (x_2), and the normalized initial local out-of-plane deflection (x_3) were considered simultaneously in the nonlinear FEA. Detail description of the imperfection types, their statistical information, and simulation procedure is discussed earlier in Subsection 2.3.2 of Chapter-2.

4.3.4 Nonlinear FEA result for ULS

Figure 4.7 demonstrates the normalized axial stress-strain curves for Model-3 stiffened plates, obtained from the nonlinear elasto-plastic FEA analysis. The peak value of the curves represents the ultimate strength, corresponding to the ULS. In this figure, the normalized stress-strain curves are plotted for SBHS700 stiffened plates with different reduced slenderness parameter R_r for a combination of initial imperfections corresponding to the mean value of x_1 , x_2 , and x_3 , as an example. It was found that, Model-3 stiffened plates exhibit yielding for $R_r \leq 0.6$, whereas inelastic buckling for $R_r \geq 0.8$. With the increase of R_r values, the ultimate buckling strength decreased, as expected.

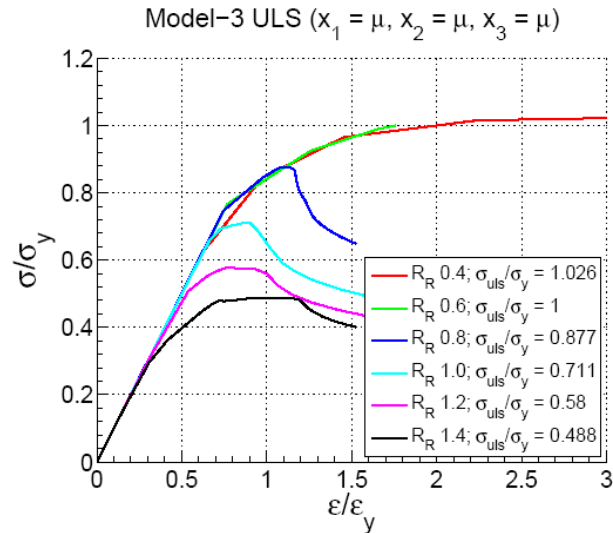


Fig. 4.7 Effect of R_R on normalized stress-strain curves for Model-3 stiffened plates with SBHS700 steel grade and for mean values of the x_1 , x_2 , and x_3 .

4.3.5 Nonlinear FEA result for SLS

The definition as well as the determination procedure of the compressive strengths at SLS for Model-3 is the same as of Model-1, as described earlier in Subsection 2.5.1 of Chapter-2. Figure 4.8 presents the normalized compressive stress versus normalized out-of-plane deflection (after loading) curves, where the vertical solid red line represents the fabrication tolerance. Here, b_s is the subpanel width and Δ represents the magnitude of local out-of-plane deflection after loading. The intersection points between the vertical line and the normalized stress versus out-of-plane deflection curves correspond to the compressive strength at SLS (σ_{SLS}). Comparing Fig. 4.7 and Fig. 4.8, it was observed that the ratio of SLS strength to the ULS strength ($\sigma_{SLS}/\sigma_{ULS}$) decreased with the increase of R_R value. For example, at $R_R = 1.0$, $\sigma_{SLS}/\sigma_{ULS} = 96.55\%$ while at $R_R = 1.4$, $\sigma_{SLS}/\sigma_{ULS} = 77.93\%$. From this result, it is also evident that the consideration of SLS is not important for Model-3 stiffened plates with $R_R < 1.0$.

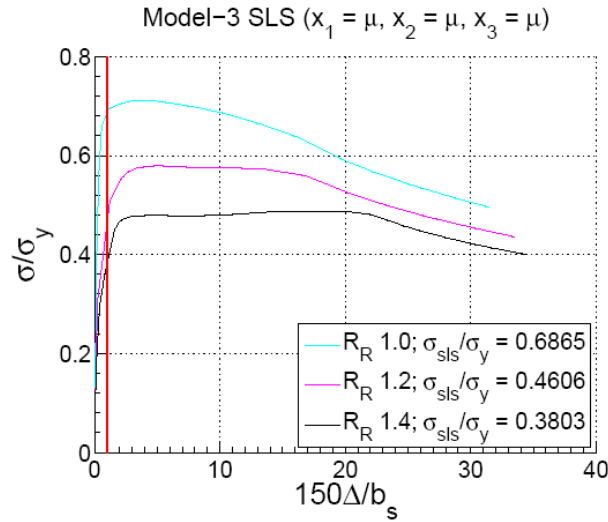


Fig. 4.8 Effect of R_R on the SLS strengths of Model-3 stiffened plates with SBHS700 steel grade and for mean values of the x_1 , x_2 , and x_3 .

4.3.6 Effect of local initial out-of-plane deflection

Earlier, in Chapter-2 and Chapter-3, the effect of addition of local initial out-of-plane deflection (x_3) was investigated for Model-1 and Model-2 respectively, where it was found that the effect was significant for Model-1 and negligible for Model-2. This section describes the effect of x_3 on Model-3. To investigate the effect, a Model-3 stiffened plate with $R_R = 1.0$ was selected, because in previous two models, it was found that the effect of imperfection was highest at $R_R = 1.0$. Material grade of the selected plate was SM490Y and plate thickness was 15 mm.

Three different imperfection scenario were considered as Case-1, Case-2, and Case-3. The imperfection combinations for the three cases are described in Table 4.1. Case-1 signifies a whole-plate mode initial deflection, Case-2 represents a local mode initial deflection, and Case-3 is a combination of whole-plate and local mode initial out-of-plane deflection. All of the three cases includes a constant level of residual stress ($x_1 = \mu$).

Table 4.1 Effect of initial out-of-plane deflection modes on Model-3.

[SM490Y_ $R_R = 1.0$ _t = 30mm]

Imperfection Cases	Residual Stress x_1	Initial out-of-plane deflection modes		σ_{ULS}/σ_y	σ_{ULS} reduction w.r.to Case-1
		Whole-plate x_2	Local Mode x_3		
Case-1	μ	μ	0	0.770	0.0%
Case-2	μ	0	μ	0.725	5.8%
Case-3	μ	μ	μ	0.718	6.8%

After carrying out the nonlinear elasto-plastic FEA for the three cases, it was found that the Case-3 yields most conservative result in terms of normalized ultimate buckling strength (σ_{ULS}/σ_y). Comparing to Case-1, the σ_{ULS}/σ_y value for Case-2 and Case-3 is 5.8% and 6.8% lower, respectively. Hence, the effect of local initial out-of-plane deflection could not be neglected for Model-3. Consequently, all of the three imperfections, x_1 , x_2 , and x_3 were considered simultaneously in the subsequent FEAs.

4.3.7 Parametric analysis

Parametric study was carried out in order to account for the variability of the compressive strengths at ULS and SLS in the probabilistic analysis. A total of 24 stiffened plate models with 4 different material grades i.e. SM490Y, SM570, SBHS500 and SBHS700 were selected. For each material grade, a variation of the reduced slenderness parameter (R_R) was considered in the range of 0.4 to 1.4, with an increment of 0.2. For Model-1 and Model-2, the effect of variation of plate thickness under a certain R_R value was not significant. Accordingly, the variation of the plate thickness for a single R_R value was not considered for Model-3.

Each of the 24 stiffened plates was analyzed for 7 combinations of initial imperfections, consisting of x_1 , x_2 , and x_3 . The combinations were based on the respective mean values (μ) and standard deviations (σ) of x_1 , x_2 , and x_3 . Selection procedure of the 7 imperfection combinations is described in Subsection 4.5.1. In total, 168 number of FEAs were carried out for Model-3. Details of the dimensions of the Model-3 stiffened plates and FEA results are presented in Appendix C and Appendix F, respectively.

4.4 Experimental verification

The numerical investigations can be an alternative to the experiments, provided the numerical model is validated. It is important to verify whether the plate-like behavior with large post buckling strength, obtained from the nonlinear FEA results, are consistent with that of the experimental results or not. Furthermore, verifying the FEA results at ULS and SLS for the SBHS stiffened plates is also necessary due to the different inelastic behavior as well as possibility of a lower normalized (normalized with respect to the yield stress) compressive residual stress in the SBHS steels. Hence, the validation of the numerical model will be carried out against the experimental result of SBHS stiffened plate exhibiting plate-like behavior. To be mentioned here, the experiments were carried out by the members of the same research group from Nagaoka National College of Technology (NNCT) and reported elsewhere [67].

4.4.1 Experimental model

The compression tests were carried out for four different specimens of stiffened box columns with a general configuration as shown in Fig. 4.9. Among these four specimen, one specimen with SBHS500 material grade and $R_r = 1.2$ was chosen for the verification. Furthermore, as the study focuses on a single stiffened plate (not the box column), therefore, only the right web was selected for the numerical modeling and analysis considering a simple assumption that the four stiffened plates on the four sides of the box column goes under simultaneous buckling. Details of the dimensions and material properties of the selected right web are given in Table 4.2.

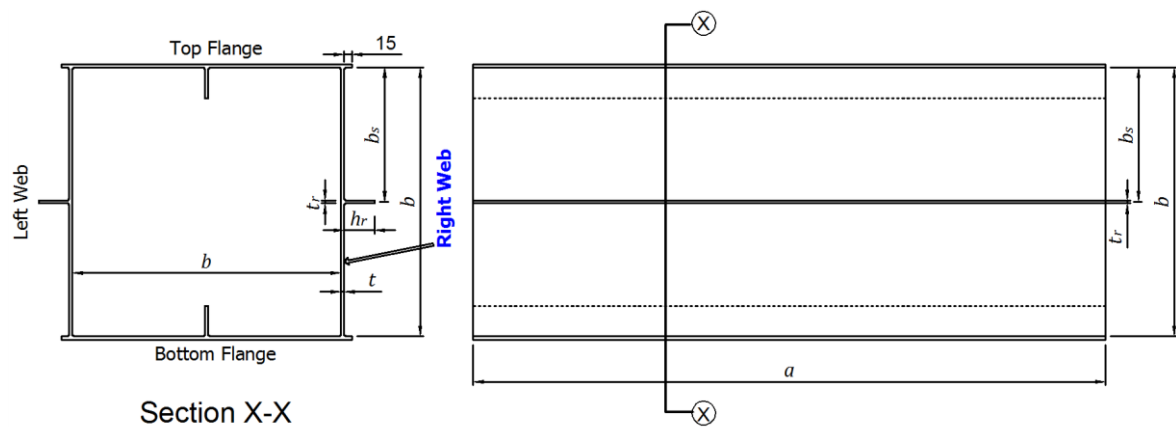


Fig. 4.9 General configuration of experimental model (units in mm).

Table 4.2 Geometric and material properties of the right web of the box column.

(a) Geometric dimensions

a (mm)	b (mm)	b_s (mm)	t (mm)	h_r (mm)	t_r (mm)	α	R_R	$\gamma/\gamma_{l,req}$
1685	520	260	6	59	6	3.24	1.2	1.01

(b) Material properties for panel plate and longitudinal stiffeners

σ_y (MPa)	σ_T (MPa)	E (GPa)	ν	% of elongation
543	620	213	0.276	29.7

4.4.2 Initial out-of-plane deflection measurement

The initial out-of-plane deflection was measured at the intersecting points of the gridlines as depicted in Fig. 4.10 (a), by using a deformation dial gauge. Fig. 4.10 (b) shows the arrangement for the measurement. The measured values of the initial out-of-plane deflection for the right web is presented as a contour diagram in Fig. 4.11. It was found that the deflection shape was irregular and did not represent any prominent elastic buckling modes. Highest deformation (around 0.8 mm) was observed at the upper left side and bottom right side of the plate.

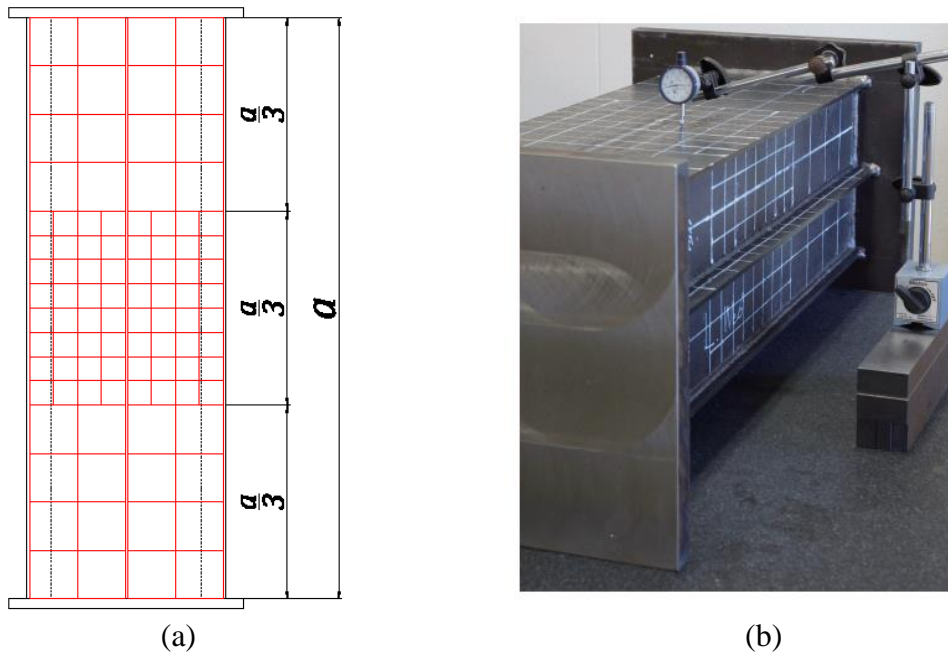


Fig. 4.10 Initial out-of-plane deflection measurement: (a) Gridlines, (b) Measurement arrangement (Picture ref: [67]).

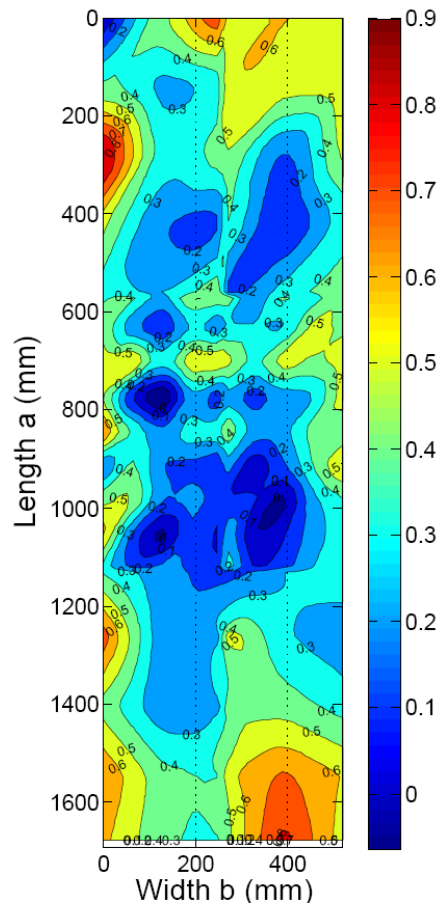


Fig. 4.11 Contour plot of measured Initial out-of-plane deflection (units in mm).

4.4.3 Measurement of residual stress

Residual stresses were measured for the panel plate and longitudinal stiffener by mechanical cutting using the concept of stress release method. Details of the measurement procedure is explained in the JSSC report [67]. Fig. 4.12 illustrates the measured residual stress (denoted by the red line) and the idealized residual stress distribution (represented by the blue line) along the longitudinal direction of the panel plate. The average compressive residual stress (σ_{rc}) in the panel plate was $0.28\sigma_y$, which is greater than the mean value of the compressive residual stress ($\sigma_{rc}=0.23\sigma_y$), reported by Fukumoto et al. [51]. The compressive residual stress in the stiffener was found as $0.21\sigma_y$, wherein σ_y is the yield stress of the SBHS test specimen.

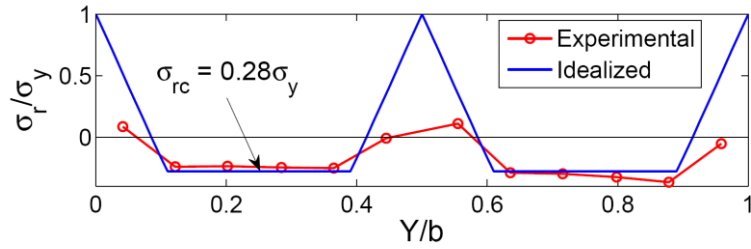


Fig. 4.12 Measured and idealized residual stress distribution in the panel plate.

4.4.4 Test setup

The experiment was carried out in the Japan Construction Method and Machinery Research Institute. A fatigue testing machine as shown in Fig. 4.13 with a static load capacity of 6,000kN was used for the compression test. In order to evenly apply the compression as well as to ensure the same axial deformation in the four sides of the stiffened box column, two 25mm thick end plates were attached at the two ends of the column. The applied load was measured from the load cell attached to the machine. To obtain the axial deformation and out-of-plane deformation, 3-directional and unidirectional elastic strain gauges as well as displacement dial gauges were installed at different locations of the specimen (as shown in Fig. 4.14).



Fig. 4.13 Test setup in the fatigue testing machine with a static load capacity of 6,000kN.

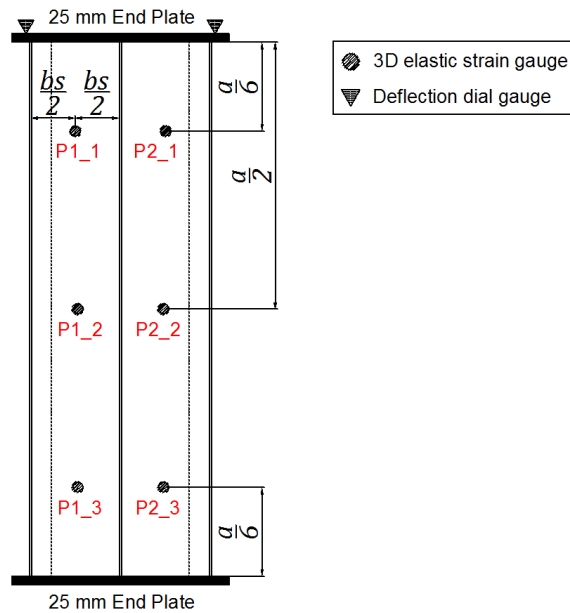


Fig. 4.14 Position of displacement dial gauges and elastic strain gauges.

4.4.5 Numerical simulation of the experimental model

As mentioned earlier, only the right web of the stiffened box column was modeled and analyzed in the commercial FE software ABAQUS. The modeling procedure, selection of element type and size are the same as that of Model-3 stiffened plates. Boundary conditions of the numerical model represents the experimental condition, i.e. a four side simply supported condition. Elastic and plastic properties of the SBHS steel in the FEA was modeled from the actual test data.

The initial out-of-plane deflection was simulated in the numerical model according to the shape and magnitude obtained from the experiment. A nonlinear interpolation between the experimental values provided the out-of-plane deflection magnitude at each node of the elements. Fig. 4.15 illustrates the simulated initial out-of-plane deflection in the panel plate, where the mesh grid represents the elements of the panel plate and the black dots indicate the experimental observations for out-of-plane deflections.

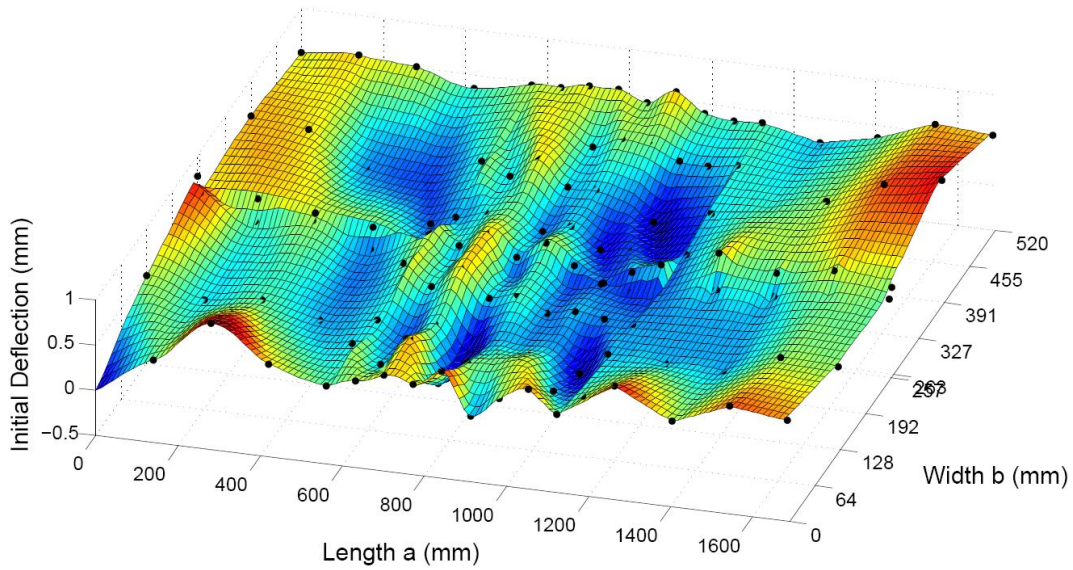


Fig. 4.15 Simulation of initial out-of-plane deflection in the panel plate.

The residual stresses along the longitudinal direction in the panel plate were simulated in the FE model following the idealized stress distribution pattern as presented earlier in Fig. 4.12. For the longitudinal stiffener, the idealized stress distribution of Fig. 2.7(b) was followed with a σ_{rc} value of $0.21\sigma_y$.

The application of loading through a forced displacement and the nonlinear elasto-plastic FEA procedure with a “Modified Riks” method is the same as that of Model-3 stiffened plates.

4.4.6 Result verification

The normalized average stress σ/σ_y versus normalized average strain $\varepsilon/\varepsilon_y$ curves, obtained from the experiment and FEA for the right web of the stiffened box column are plotted in Fig. 4.16. It was found that the ultimate buckling strength, obtained from FEA, was only 0.85% lower than that of the test result, confirming very good agreement in the ULS between the test result and the FEA result.

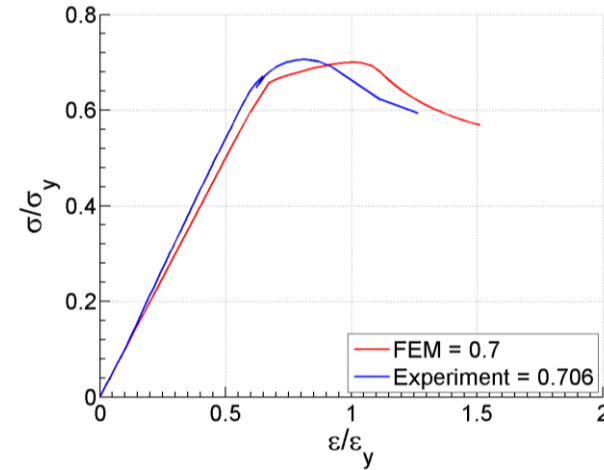
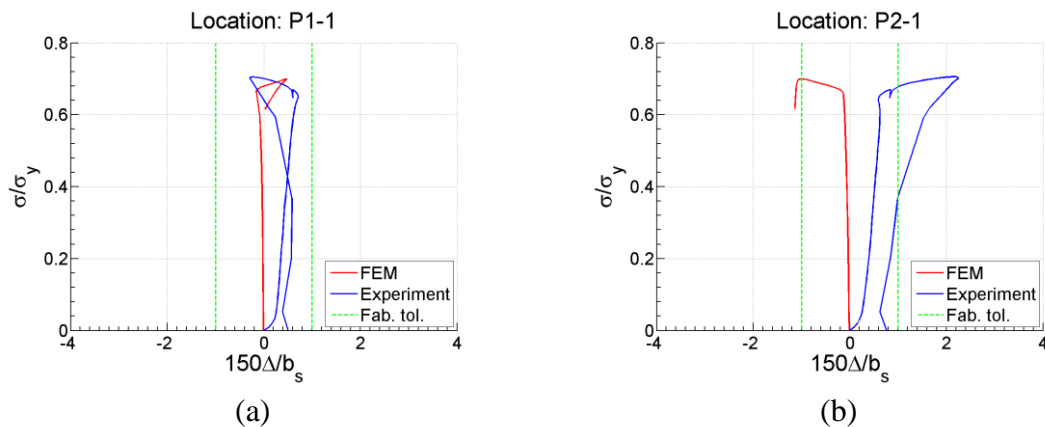


Fig. 4.16 Comparison of FEA and Test result at the ULS.

Furthermore, the normalized average stress σ/σ_y versus normalized out-of-plane deflection (after loading) $150\Delta/b_s$ curves, obtained from the experiment and FEA in six different locations of the right web are plotted in Figs. 4.17. In these figures, the fabrication tolerance, which has been taken as the limit for out-of-plane deflection, is indicated by green dotted vertical lines. The intersecting points of the fabrication tolerance and the $\sigma/\sigma_y - 150\Delta/b_s$ curves represents the compressive strengths at SLS. It was observed from the figures that even though the experimental results show higher early deformation, the stress levels at the SLS indicates fair agreement between the experimental and FEA results.

Based on the verification, it can be concluded that the FEA results can be recognized as an alternative to the test results, not only for the ULS but also for the SLS.



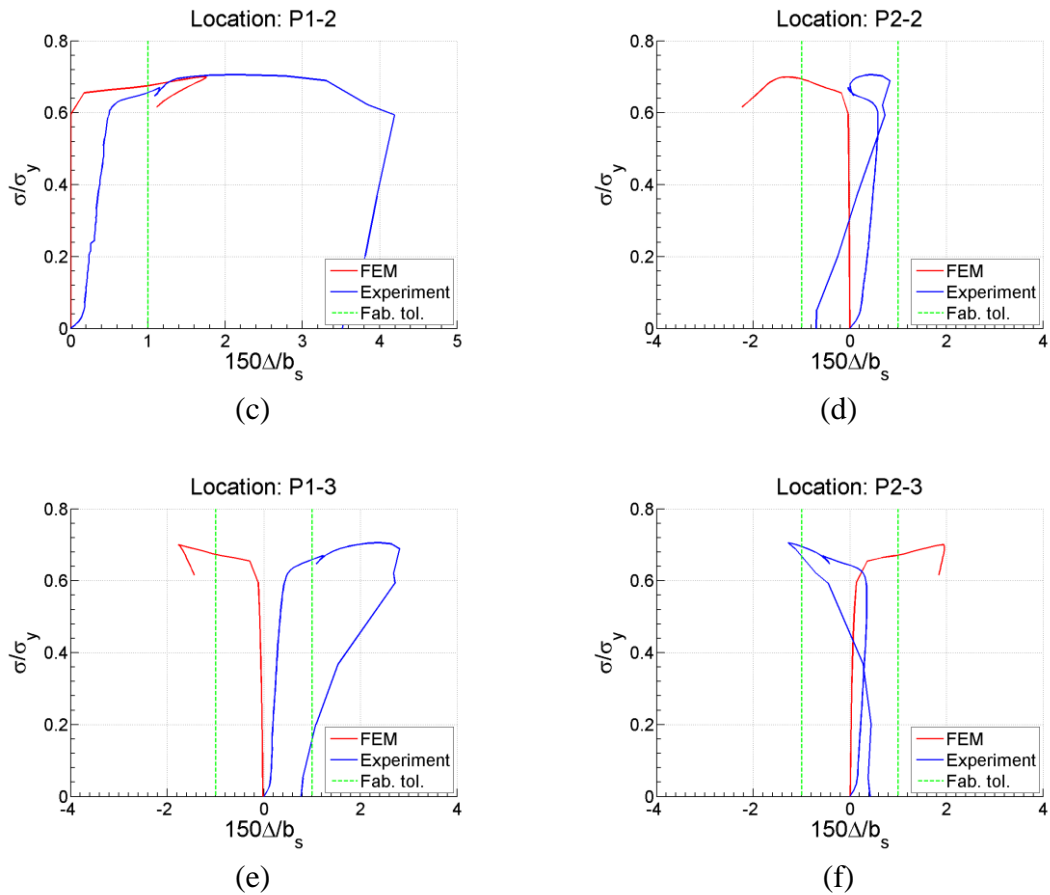


Fig. 4.17 Comparison of FEA and Test result at the SLS.

4.5 Approximate solution for probabilistic strengths: ULS and SLS

Earlier, in case of Model-1 and Model-2, the probabilistic analyses were carried out through Monte Carlo simulation (MCS) in association with the response surface method. The response surface was a polynomial function of the basic variables up to second order. Hence, the estimated mean value and the standard deviation was also of second order. However, the probabilistic strengths obtained through this process was numerically expensive. In order to reduce the number of numerical analysis, an approximate solution to determine the probabilistic strengths was employed for Model-3, which gives the estimation of first order mean value and standard deviation.

4.5.1 Estimation of first order mean and first order variance

If a response variable is a function of multiple random variables, the mean and variance of the response variable can be estimated approximately, even if the response function is unknown. However, in such estimation, at least the mean and variance of the random variables should be known [68]. The response variable can be expressed as follows:

$$Y = g(x_1, x_2, x_3) \quad (4.1)$$

where,

$$Y = \frac{\sigma_{ULS}}{\sigma_Y} \quad \text{and/or} \quad \frac{\sigma_{SLS}}{\sigma_Y};$$

$$x_1 = \frac{\sigma_{rc}}{\sigma_y}; \quad x_2 = \frac{1000\delta_{01}}{a}; \quad x_3 = \frac{150\Delta_{ini}}{b_s};$$

and g is the response surface.

In Eq. 4.1, the response surface g is unknown. Therefore, the approximate first order mean value can be estimated by

$$\mu_{Y'} \approx Y[\mu_{x_1}, \mu_{x_2}, \mu_{x_3}] \quad (4.2)$$

where, $\mu_{Y'}$ is the first order mean value of Y , and $Y[\mu_{x_1}, \mu_{x_2}, \mu_{x_3}]$ represents the

$\frac{\sigma_{ULS}}{\sigma_Y}$ and/or $\frac{\sigma_{SLS}}{\sigma_Y}$ value, obtained for a combination of initial imperfections

$$x_1 = \mu; \quad x_2 = \mu; \quad \text{and} \quad x_3 = \mu.$$

Furthermore, the first order variance can be obtained by Taylor series finite difference (central difference) TSFD estimation procedure [68]. The first order variance is given by

$$\text{Var}_{Y'} \approx \sum_{i=1}^3 \left(\frac{Y_i^+ - Y_i^-}{2} \right)^2 \quad (4.3)$$

where, the Y_i^+ and Y_i^- can be expanded as follows

$$Y_1^\pm = Y[(\mu_{x_1} \pm \sigma_{x_1}), \mu_{x_2}, \mu_{x_3}] \quad (4.4.1)$$

$$Y_2^\pm = Y[\mu_{x_1}, (\mu_{x_2} \pm \sigma_{x_2}), \mu_{x_3}] \quad (4.4.2)$$

$$Y_3^\pm = Y[\mu_{x_1}, \mu_{x_2}, (\mu_{x_3} \pm \sigma_{x_3})] \quad (4.4.3)$$

In Eq. 4.4, the expression $Y[]$ has the similar meaning as of Eq. 4.2, which refers to the $\frac{\sigma_{ULS}}{\sigma_Y}$ and/or $\frac{\sigma_{SLS}}{\sigma_Y}$ values obtained from the numerical analysis with respect to different combinations of initial imperfections. Here, the μ and σ represents the mean and standard deviation of respective imperfections.

Therefore, in order to estimate the first order mean and first order variance, altogether 7 cases of numerical analysis are needed for a single stiffened plate model, with respect to 7 different initial imperfection combinations. The initial imperfection combinations are presented in detail in Table 4.3.

Table 4.3 Initial imperfection combinations for Model-3.

Imperfection Cases	$x_1 = \sigma_{rc}/\sigma_Y$	$x_2 = 1000\delta_{01}/a$	$x_3 = 150 \Delta_{ini} /b_s$
C1	μ	μ	μ
C2	$\mu+\sigma$	μ	μ
C3	μ	$\mu+\sigma$	μ
C4	μ	μ	$\mu+\sigma$
C5	$\mu+\sigma$	μ	μ
C6	μ	$\mu+\sigma$	μ
C7	μ	μ	$\mu+\sigma$

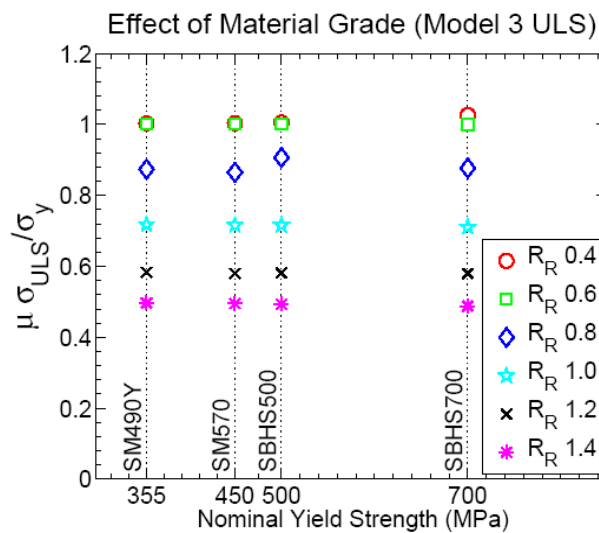
4.5.2 Probabilistic compressive strengths: ULS and SLS

Following the approximate estimation procedure as stated above, the first order mean values and first order variances of the compressive strengths at ULS and SLS were determined for different R_R values and different material grades. Table 4.4 presents the calculated mean values and standard deviations.

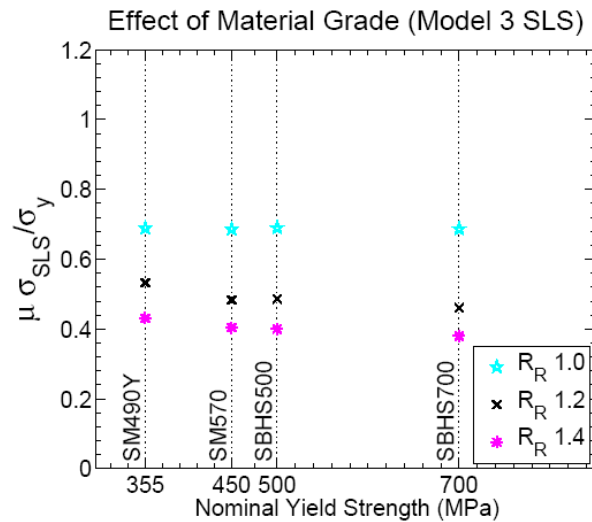
Table 4.4 Mean values and standard deviations of σ_{ULS}/σ_y and σ_{SLS}/σ_y for Model-3.

Steel grades	Statistical parameter	σ_{ULS}/σ_y						σ_{SLS}/σ_y		
		R_R								
		0.4	0.6	0.8	1.0	1.2	1.4	1.0	1.2	1.4
SM490Y	μ	1.003	1.001	0.874	0.718	0.583	0.497	0.689	0.533	0.431
	σ	0.001	0.007	0.036	0.065	0.046	0.032	0.107	0.076	0.088
SM570	μ	1.004	1.001	0.865	0.716	0.580	0.495	0.686	0.483	0.404
	σ	0.002	0.035	0.037	0.066	0.050	0.032	0.056	0.075	0.104
SBHS500	μ	1.005	1.002	0.907	0.716	0.581	0.494	0.690	0.486	0.400
	σ	0.001	0.023	0.034	0.070	0.048	0.033	0.107	0.073	0.096
SBHS700	μ	1.026	1.000	0.877	0.711	0.580	0.488	0.687	0.461	0.380
	σ	0.002	0.008	0.027	0.074	0.051	0.034	0.079	0.082	0.093
Combined all steel	μ	1.009	1.001	0.881	0.715	0.581	0.493	0.688	0.491	0.404
	σ	0.002	0.018	0.033	0.069	0.049	0.033	0.087	0.076	0.095

The mean value strengths at ULS and SLS for four different material grades are plotted in Fig. 4.18(a) and 4.18(b), respectively. From these figures, the influence of the material grade on the mean value strengths can be identified.



(a)



(b)

Fig. 4.18 Effect of material grades on the mean value strengths at (a) ULS and (b) SLS

From Fig. 4.18(a), at the ULS, it was observed that the $\mu_{\sigma_{ULS}/\sigma_y}$ values for SBHS steels are higher than that of normal steels, when $R_R \leq 0.8$. However, for $R_R \geq 1.0$, the effect of material grade is not significant.

Furthermore, at the SLS (Fig. 4.18(b)), it was found that for $R_R \geq 1.2$, the $\mu_{\sigma_{SLS}/\sigma_y}$ values decreased with the increase in the nominal strength of the material grades. Nonetheless, at $R_R = 1.0$, the effect of material grade is insignificant.

4.5.3 Partial safety factors: ULS and SLS

If the first order mean values and standard deviations (as presented in Table 4.4) are assumed to be normally distributed, the PSFs for Model-3 can be obtained for several non-exceedance probability ($p_f = 5\%$, 3% , and 1%) using the reliability indexing method, as described earlier in Subsection 2.6.2 of Chapter-2. Table 4.5 presents the calculated PSFs for both ULS and SLS of Model-3 stiffened plates, considering the nominal strengths (f_N) equal to the mean value strengths, as an example.

Table 4.5 PSFs for Model-3 ULS and SLS strengths assuming that the nominal strength is equal to the mean value strength.

Limit States	R_R	μ	σ	f_N	PSFs (γ)		
					$p_f = 1\%$	$p_f = 3\%$	$p_f = 5\%$
ULS	0.4	1.009	0.002	1.009	1.003	1.003	1.004
	0.6	1.001	0.018	1.001	1.031	1.036	1.044
	0.8	0.881	0.033	0.881	1.066	1.077	1.097
	1.0	0.715	0.069	0.715	1.187	1.221	1.289
	1.2	0.581	0.049	0.581	1.160	1.188	1.244
	1.4	0.493	0.033	0.493	1.123	1.144	1.185
SLS	1.0	0.688	0.087	0.688	1.263	1.313	1.420
	1.2	0.491	0.076	0.491	1.343	1.414	1.569
	1.4	0.404	0.095	0.404	1.630	1.795	2.217

For the ULS, it was observed that the PSF's with any non-exceedance probability (p_f) at $R_R = 1.0$, is the highest than that of other R_R values, which means that the variation due to imperfection is also highest at $R_R = 1.0$ for the ULS. On the other hand, for the SLS, with the increase of R_R values, the PSFs for any non-exceedance probability also increased. At $R_R = 1.4$, the PSF for SLS corresponding to $p_f = 5\%$ reached the highest value of 2.217.

4.6 Discussion

The probabilistic ULS strengths for Model-3, obtained from the approximate estimation procedure, were compared with the ULS strengths of different design codes in Fig. 4.19. In this figure, all of the strengths, predicted from different sources, corresponds to the ULS strength of a stiffened plate with same configuration as of Model-3. The red error bar plots represent the ULS strengths obtained from the approximate estimation procedure, where the midpoints represent the mean value (μ) strengths, top and bottom error bars represent the strengths corresponding to $(\mu+\sigma)$ and $(\mu-\sigma)$, respectively. Moreover, predictions from different design codes i.e. JSHB, AASHTO, Canadian Code, and Eurocode are also presented. The predictions from Eurocode are presented separately for plate-like, column-like, and interpolated buckling strength.

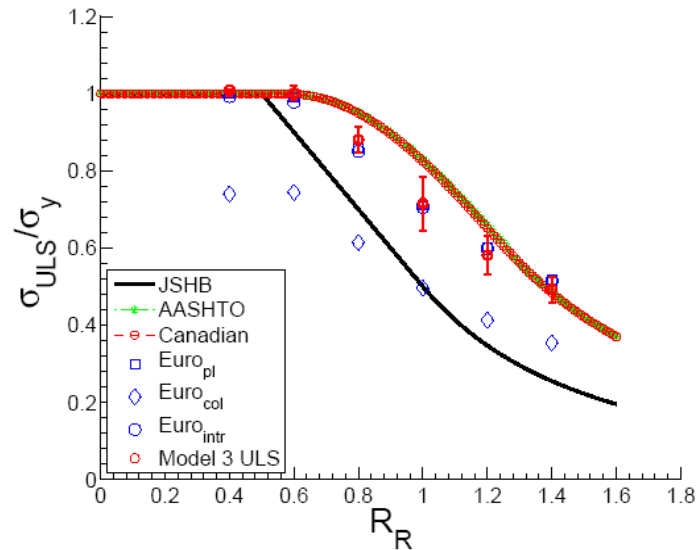


Fig. 4.19 Comparison of probabilistic ULS strengths with different design codes.

From Fig. 4.19, it is observed that the Eurocode interpolated buckling strengths are very close to the Eurocode plate-like buckling strengths, for the entire range of R_R values, considered for the study. Hence, it is evident that the behavior of Model-3 stiffened plates corresponds to the plate-like behavior. The mean value (μ) strengths, obtained from the approximate estimation procedure showed very good agreement with the Eurocode plate-like buckling. Similar to Model-1 and Model-2, for Model-3 as well, the ULS strength prediction from the AASHTO and Canadian code are the same. It is well documented that, for stiffened plates with one longitudinal stiffener, AASHTO does not predict conservative results [23, 61]. However, while comparing to the mean value (μ) strengths of this study as well as the Eurocode plate-like buckling strengths, it is found that the AASHTO and Canadian code actually overestimate the strength in the range of $0.6 < R_R < 1.4$. On the contrary, the JSHB strength curve is significantly conservative comparing to the mean value (μ) strengths as well as the predictions from Eurocode, AASHTO, and Canadian code.

Fig. 4.20 presents the comparison of probabilistic ULS strength to the probabilistic SLS strengths. With the increase of the R_R values, the difference between the mean value (μ) strengths of ULS and SLS also increased. The coefficient of variance (CoV) of the SLS strengths are found to be higher than that of the ULS strengths. Furthermore, it is evident

that the consideration of SLS is not essential for $R_R < 1.0$ because the mean SLS strength at $R_R = 1.0$ becomes very close to the mean ULS strength.

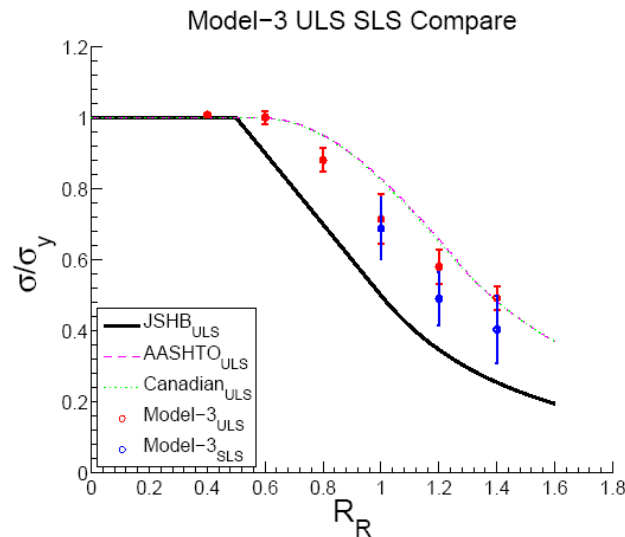


Fig. 4.20 Comparison of probabilistic ULS and SLS strengths of Model-3 stiffened plates.

4.7 Conclusion

Chapter 4 focused on the plate-like behavior of longitudinally continuous stiffened steel plates, simply supported along the two longitudinal edges. Long stiffened plates with an aspect ratio of $a = 3.0$ and one flat plate longitudinal stiffener, satisfying the relative stiffness requirement of JSHB was selected to produce plate-like buckling. This kind of stiffened plates are generally used in the bottom flange of narrow steel box girder bridges that are very common in Japan. The probabilistic compressive strengths at ULS and SLS were obtained through approximate estimation procedure of the first order mean values. The first order variances were also estimated approximately, employing Taylor series finite difference (TSFD) method. As a source of the variability of the strengths at ULS and SLS, the FEAs were carried out for a single stiffened plate with seven different combinations of residual stress, initial whole-plate out-of-plane deflections, and initial local out-of-plane deflections. A total of 168 FEAs were carried out in order to investigate the probabilistic strengths.

The effect of SHBS steels was investigated in the domain of ULS and SLS. Compared to the conventional steels, SBHS steels have higher mean value of σ_{ULS}/σ_y for $R_R \leq 0.8$, while lower mean value of σ_{SLS}/σ_y for $R_R > 1.0$. Comparing to the mean value strength, it was found that the predictions from AASHTO and Canadian code overestimates the ULS strengths in the range of $0.6 < R_R < 1.4$, while JSMB underestimates the ULS strengths in the range of $R_R > 0.5$. However, Eurocode plate-like buckling strength or interpolated final strength showed very good agreement with the mean value strength.

The uniqueness of this Chapter is that the plate-like behavior of stiffened plates with a whole-plate elastic buckling mode is investigated. Probabilistic strengths for plate-like buckling is obtained not only for the ULS but also for the SLS. Continuity in the longitudinal direction has been taken into account which is considered to be a scope of improvement in the further development of Eurocode plate buckling strength. The results of the present study can be used for developing a reliability-based design strength curve, with the *Level I* reliability.

[This page is left intentionally blank]

Summary and recommendations for future study

5.1 Summary

The compressive strengths of stiffened steel plates at ULS and SLS were investigated in this research by employing a combination of numerical and probabilistic approaches. Two distinct behavior of stiffened plates under compression, i.e. the column-like behavior and the plate-like behavior were addressed. Three stiffened plate models with three, two, and one flat plate longitudinal stiffeners, corresponding to Model-1, Model-2, and Model-3 were considered for the study, where Model-1 and Model-2 shows column-like behavior and Model-3 exhibits plate-like behavior. Relative stiffness of the longitudinal stiffener for all of the three models conforms to the required relative stiffness of JSHB ($\gamma_1/\gamma_{1,req} = 1$).

In case of Model-1, to achieve the column behavior, aspect ratio was set to one and an unconnected strut consisting of a longitudinal stiffener and the associated subpanel width was considered, neglecting the effect of longitudinal edge supports. After carrying out the numerical and probabilistic analysis, major findings are as follows:

- Comparing to the Model-1 ULS strength with a 5% non-exceedance probability ($p_f = 5\%$), the JSHB, AASHTO, and Canadian Code overestimates the strengths for $R_R < 0.8$ and is significantly conservative for $R_R > 0.8$.
- Eurocode column-like buckling strengths shows good agreement with the ULS strengths corresponding to $p_f = 5\%$.
- The mean values of the SLS strengths at $R_R = 1.0, 1.2$, and 1.4 are 18%, 29%, and 34% lower than those of the ULS strengths, respectively.

- The SLS strengths with $p_f = 5\%$ are lower than the current ULS strengths of the JSHB.

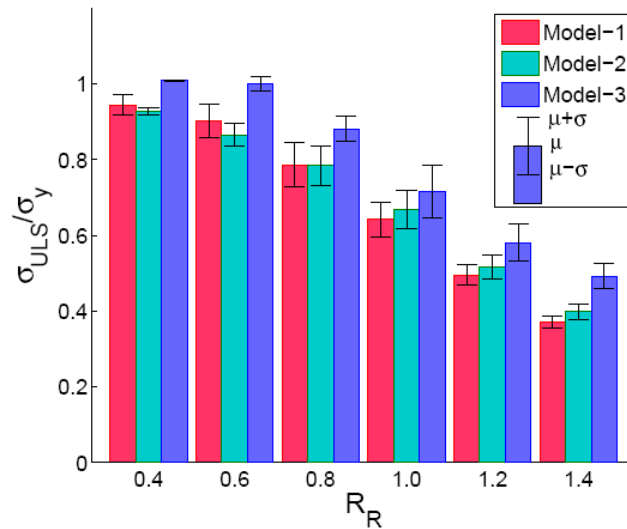
Model-2 investigates the effect of longitudinal edge support on column-like behavior. A simply supported boundary conditions along the longitudinal edges were considered for Model-2 stiffened plates. After carrying out the probabilistic analysis, results were compared with different design codes and the key observations are the followings:

- Compared to the Model-2 ULS strength with a $p_f = 5\%$, the JSHB, AASHTO and Canadian Code overestimates the strength for $R_R \leq 0.6$, and underestimate it for $R_R \geq 0.6$.
- The ULS strengths with a $p_f = 5\%$ agree well with those of Nara et al. [27] and those of Eurocode, except for R_R values in the range of 0.8-1.2.
- The mean SLS strength at $R_R = 1.0$ is 92.6% of mean ULS strength, while the same at $R_R = 1.4$ is 80.4%.
- The JSHB strength curve for ULS remarkably matches well with the SLS strengths for a $p_f = 5\%$.

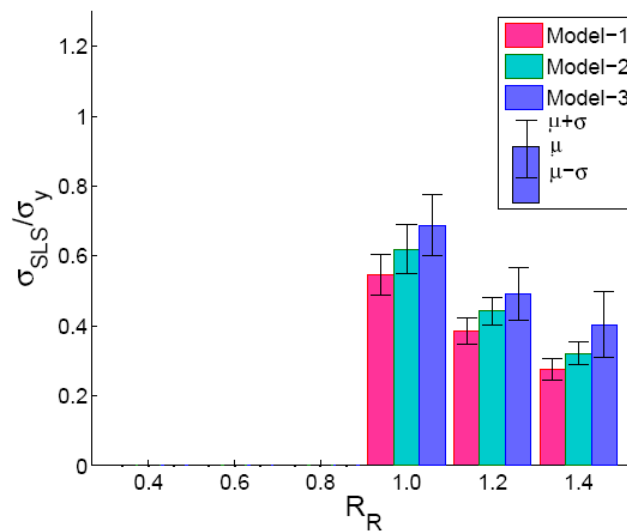
Model-3 stiffened plates are selected so as to exhibit plate-like behavior, where the plates possess a large post-buckling strength reserve. To achieve the plate behavior, aspect ratio was set to three and simply supported boundary conditions were considered along the two longitudinal edges. Employing an approximate estimation procedure, first-order mean values and first-order variances were obtained for the ULS and SLS strengths. Important remarks on Model-3 stiffened plates are presented below:

- The mean value (μ) ULS strengths of Model-3 are in good agreement with the Eurocode plate-like buckling strength or interpolated final strength.
- Comparing to the mean value (μ) ULS strengths, the AASHTO and Canadian code overestimates the strength in the range of $0.6 < R_R < 1.4$.
- JSHB strength curve is significantly conservative for Model-3 stiffened plates.
- With the increase of the R_R values, the difference between the mean value (μ) strengths of ULS and SLS also increased. The coefficient of variance (CoV) of the SLS strengths are found to be higher than that of the ULS strengths.

A comparison of the probabilistic information of the three stiffened plate models are presented for the ULS and the SLS in Figs 5.1(a) and 5.1(b), respectively. In these figures, the mean value (μ) strengths are presented in the form of a group bar chart of three models, with respect to different reduced slenderness parameter (R_r). The top and bottom error bars represents the strengths corresponding to $(\mu+\sigma)$ and $(\mu-\sigma)$, respectively, where σ is the standard deviation.



(a)



(b)

Fig. 5.1 Comparison of the probabilistic compressive strengths for three different stiffened plate models at (a) ULS and (b) SLS.

It is expected that the column-like buckling strength will be smaller than the plate-like buckling strength, due to the difference in the post-buckling strength reserve. Reflecting to the expectation, mean value strength of Model-1 and Model-2 was found to be smaller than that of Model-3, for the both ULS and SLS. Furthermore, due to consideration of simply supported boundary conditions along the longitudinal support edge, it is also desired that the Model-2 strengths will be slightly higher strength than that of Model-1. For the both ULS and SLS, this phenomenon was observed for $R_R \geq 1.0$.

5.2 Recommendations for future study

The ultimate strength of a stiffened plate in JSHB is predicted with respect to the reduced slenderness parameter R_R , which is used in this research as well. The reduced slenderness parameter R_R includes only the subpanel width b_s and the panel plate thickness t as the geometric parameters (see Fig. 5.2). However, the effect of variation of size/stiffness of a longitudinal stiffener, satisfying the JSHB requirement, as presented in Eq. (1.3 and 1.4), cannot be estimated by the current strength curve. For example, a stiffened plate with a certain R_R value can have different $\gamma_1/\gamma_{1,req}$ value, e.g. 1, 2, 3 etc. According to the current strength curve, the plates with $\gamma_1/\gamma_{1,req} = 1.0$ and $\gamma_1/\gamma_{1,req} = 3.0$ will have the same ultimate strength. This cannot be true because the increased stiffness of the longitudinal stiffener will contribute to resist more compressive stress, resulting higher ultimate strength.

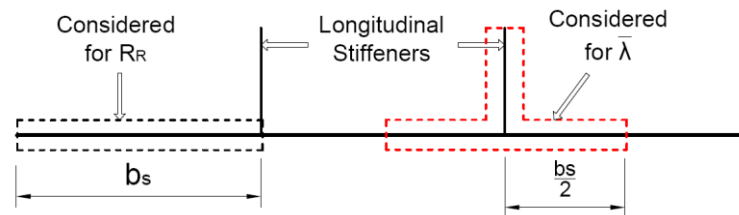


Fig. 5.2 Considered sections for R_R and $\bar{\lambda}$.

This limitation can be addressed by modifying the reduced slenderness parameter, which includes the effect of size/stiffness variation of a longitudinal stiffener. Nara [29] proposed

a reduced slenderness parameter $\bar{\lambda}^*$ that includes the effect of size variation, given by

$$\bar{\lambda}^* = \left(\frac{235.44}{\sigma_y} \right)^{0.2} \bar{\lambda} \quad (5.1)$$

where,

$$\bar{\lambda} = \frac{\eta a}{\pi r} \sqrt{\frac{\sigma_y}{E}} \quad (5.2)$$

In Eq. 5.2, $\eta = 1/\sqrt{(\sigma_{cr}/\sigma_y)}$ and r is the radius of gyration of the section marked by red dotted line in Fig. 5.2. The parameter r , therefore, includes the effect of size/stiffness variation of longitudinal stiffener.

In this research, we restricted our attention to the stiffened steel plates used in the bottom flange of steel box girder bridges with $\gamma_1/\gamma_{1,req} = 1.0$. However, stiffened plates used in the box column sections usually have $\gamma_1/\gamma_{1,req} > 1.0$. In order to address the effect of size/stiffness variation of the longitudinal stiffeners, a probabilistic study considering the reduced slenderness parameter $\bar{\lambda}^*$ can be of future research interest.

References

- [1] K. Le, L. Davaine, C. Douthe, K. Sab, Stability of curved panels under uniform axial compression, *J. Constr. Steel Res.* 69 (2012) 30–38. doi:10.1016/j.jcsr.2011.07.015.
- [2] G. Grondin, A. Elwi, J.J. Cheng, Buckling of stiffened steel plates—a parametric study, *J. Constr. Steel Res.* 50 (1999) 151–175. doi:10.1016/S0143-974X(98)00242-9.
- [3] Y.B. Kwon, H.S. Park, Compression tests of longitudinally stiffened plates undergoing distortional buckling, *J. Constr. Steel Res.* 67 (2011) 1212–1224. doi:10.1016/j.jcsr.2011.02.015.
- [4] C. Guedes Soares, Design equation for the compressive strength of unstiffened plate elements with initial imperfections, *J. Constr. Steel Res.* 9 (1988) 287–310. doi:10.1016/0143-974X(88)90065-X.
- [5] N.E. Shanmugam, M. Arockiasamy, Local Buckling of Stiffened Plates in Offshore Structures, *J. Constr. Steel Res.* 38 (1996) 41–59. doi:10.1016/0143-974X(96)00005-3.
- [6] N.E. Shanmugam, Z. Dongqi, Y.S. Choo, M. Arockiaswamy, Experimental studies on stiffened plates under in-plane load and lateral pressure, *Thin-Walled Struct.* 80 (2014) 22–31. doi:10.1016/j.tws.2014.02.026.
- [7] M.R. Khedmati, M. Rastani, K. Ghavami, Ultimate strength and ductility characteristics of intermittently welded stiffened plates, *J. Constr. Steel Res.* 65 (2009) 599–610. doi:10.1016/j.jcsr.2008.07.029.
- [8] J.G.M. Wood, Merrison Revolutionised Design after 1970 UK Box Girder Collapses, *Proc. of 40th IABSE Symposium, Nantes, (2018) S25-17-24.*
- [9] BS 153, Specification for steel girder bridges, British Standard Institute, 1954.
- [10] S. Brady, West Gate Bridge collapse – the story of the box girders, *The Structural Engineer* 94 (2016) 26–28.

- [11] M. Fahey, Presentation Slides on Engineering Structures 101, accessed 28 November 2018, <<https://slideplayer.com/slide/4420543/>>.
- [12] Great Britain, A. W. Merrison, Inquiry into the basis of design and method of erection of steel box-girder bridges: report of the Committee, H.M.S.O, London, 1975.
- [13] JSHB, Specifications for Highway Bridges: Part-II Steel bridges, Japan Road Association, 2017.
- [14] AASHTO, AASHTO LRFD Bridge design specifications, 4th Ed., American Association of State Highway and Transportation Officials, 2007.
- [15] Canadian Highway Bridge Design Code: S6-14, Canadian Standard Association (CSA) Group, 2016.
- [16] EN 1993-1-5, Eurocode 3: Design of steel structures - Part 1-5: Plated structural elements, European Committee for Standardization, Brussels, 2006.
- [17] ISO 2394:1998(E), General principles on reliability for structures, International Organization for Standardization, Geneva, Switzerland, 1998.
- [18] H. Gulvanessian, J.A. Calgaro, M. Holciky, Designers' Guide to Eurocode: Basis of Structural Design EN 1990, second ed., ICE Publishing, London, 2012.
- [19] D. Beghin, Reliability-based structural design, Technical and research bulletin 2-32, The Society of Naval Architects and Marine Engineers, New Jersey, 2007.
- [20] Y. Fukumoto, K. Yamaguchi, T. Usami, Inelastic buckling strength of stiffened plates in compression, IABSE Proc. P-8 (1977) 1–15.
- [21] K. Sadao, U. Masayuki, K. Toshiyuki, An experimental study on residual stress and initial deformations of stiffened plates, Proc. JSCE. 265 (1977) 25–35.
- [22] C.C. Chou, C.M. Uang, F. Seible, Experimental Evaluation of Compressive Behavior of Orthotropic Steel Plates for the New San Francisco–Oakland Bay Bridge, J. Bridg. Eng. 11 (2006) 140–150. doi:10.1061/(ASCE)1084-0702(2006)11:2(140).
- [23] B.H. Choi, M. oh Hwang, T. yang Yoon, C.H. Yoo, Experimental study of inelastic buckling strength and stiffness requirements for longitudinally stiffened panels, Eng. Struct. 31 (2009) 1141–1153. doi:10.1016/j.engstruct.2009.01.010.

- [24] M.C. Xu, C. Guedes Soares, Numerical assessment of experiments on the ultimate strength of stiffened panels, *Eng. Struct.* 45 (2012) 460–471. doi:10.1016/j.engstruct.2012.06.045.
- [25] S. Komatsu, T. Kitada, Statistical Study on Compression Flange Plates, *J. Struct. Eng.* 109 (1983) 404–417. doi:10.1061/(ASCE)0733-9445(1983)109:2(404).
- [26] S. Komatsu, S. Nara, Statistical study on steel plate members, *J. Struct. Eng.* 109 (1983) 977–992. doi:10.1061/(ASCE)0733-9445(1983)109:4(977).
- [27] S. Nara, S. Komatsu, Statistical study on ultimate strength curves of longitudinally stiffened plates under uniaxial compression, *JSCE Struct. Eng. Earthquake Eng.*, 392 (1988) 289–296. (In Japanese). doi:10.2208/jscej.1988.392_289.
- [28] S. Nara, S. Komatsu, T. Kitada, A study on ultimate compressive strength properties of longitudinally stiffened continuous plates under uniaxial compression, *JSCE Struct. Eng. Earthquake Eng.*, 392 (1988) 273–280. (In Japanese)
- [29] S. Nara, Evaluation of ultimate strength of longitudinally stiffened continuous plates under uniaxial compression, *Proc. of JSCE*, 38A (1992) 289–296. (In Japanese)
- [30] D.K. Shin, V.A. Le, K. Kim, In-plane ultimate compressive strengths of HPS deck panel system stiffened with U-shaped ribs, *Thin-Walled Struct.* 63 (2013) 70–81. doi:10.1016/j.tws.2012.10.001.
- [31] D.K. Shin, B. Van Dat, K. Kim, Compressive strength of HPS box girder flanges stiffened with open ribs, *J. Constr. Steel Res.* 95 (2014) 230–241. doi:10.1016/j.jcsr.2013.12.014.
- [32] M. Tekgoz, Y. Garbatov, C. Guedes Soares, Ultimate strength assessment of welded stiffened plates, *Eng. Struct.* 84 (2015) 325–339. doi:10.1016/j.engstruct.2014.12.001.
- [33] JSHB, Specifications for Highway Bridges: Part-II Steel bridges, Japan Road Association, 1980.
- [34] JSHB, Specifications for Highway Bridges: Part-II Steel bridges, Japan Road Association, 2012.
- [35] Research Group on Steel Products for Bridges, High performance steels (for bridge construction), The Japan Iron and Steel Federation, Tokyo, Japan. 2015.

- [36] T. Yoneyama, T. Fujii, Fabrication and erection of Tokyo Gate Bridge, Proc. of IABSE-JSCE Joint Conference on Advances in Bridge Engineering-III, Dhaka, (2015) 268-277.
- [37] D.K. Shin, E.Y. Cho, K. Kim, Ultimate flexural strengths of plate girders subjected to web local buckling, *Int. J. Steel Struct.* 13 (2013) 291–303. doi:10.1007/s13296-013-2008-3.
- [38] M. Kanai, K. Otsuka, Design method of stiffened plate, *J. JSCE.* 19 (1977) 498-503. (In Japanese)
- [39] E. DiPasquale, A. S. Cakmak, Identification of the serviceability limit state and detection of seismic structural damage, Technical Report NCEER-88-0022, National Center for Earthquake Engineering Research, New Jersey, 1988.
- [40] J.K. Paik, Ultimate strength of perforated steel plates under edge shear loading, *Thin-Walled Struct.* 45 (2007) 301–306. doi:10.1016/j.tws.2007.02.013.
- [41] J.K. Paik, A.K. Thayamballi, Ultimate limit state design of steel plated structures, first ed., J. Wiley, Chichester, 2003.
- [42] B. Johansson, R. Maquoi, G. Sedlacek, C. Müller, D. Beg, Commentary and worked examples to EN 1993-1-5 “Plated Structural Elements”, JRC – ECCS, Luxembourg, 2007.
- [43] D. Beg, U. Kuhlmann, L. Davaine, B. Braun, Design of Plated Structures: Eurocode 3: Design of Steel Structures, Part 1-5 - Design of Plated Structures: First Edition, 2012. doi:10.1002/9783433601143.
- [44] K.L. Tran, C. Douthe, K. Sab, J. Dallot, L. Davaine, Buckling of stiffened curved panels under uniform axial compression, *J. Constr. Steel Res.* 103 (2014) 140–147. doi:10.1016/j.jcsr.2014.07.004.
- [45] Vayas, A. Iliopoulos, Design of Steel-Concrete Composite Bridges to Eurocodes, CRC Press, Florida, 2013.
- [46] B. Johansson, M. Veljkovic, Review of plate buckling rules in EN 1993-1-5, *Steel Constr.* 2 (2009) 228–234. doi:10.1002/stco.200910031.
- [47] B.T. Braun, Stability of steel plates under combined loading, Institut für Konstruktion und Entwurf; Stuttgart 2010.

- [48] JIS G 3140, Higher yield strength steel plates for bridges, Japanese Industrial Standard, 2008.
- [49] Research committee for rational structure and design for steel bridges, Rationalization of strength design for steel bridges, Japan Society of Steel Construction, JSSC technical report No. 98, 2013. (In Japanese)
- [50] ABAQUS 6.14 documentation, Dassault Systèmes Simulia Corp., 2014.
- [51] Y. Fukumoto, Y. Itoh, Basic compressive strength of steel plates from test data, JSCE Struct. Eng. Earthquake Eng., 344 (1984) 129-139.
- [52] S. Komatsu, T. Kitada, E. Watanabe, M. Akiraumi, K. Nara, Statistical study of the initial deformation and the ultimate strengths of steel bridge members, JSSC, 16 (1980) 10-43. (In Japanese)
- [53] S. Komatsu, M. Ushio, T. Kitada, S. Nara, An experimental study on the ultimate strength of orthogonally stiffened plates under uniaxial compression, Proc. of JSCE 288 (1979) 13-27. (In Japanese)
- [54] M. Rahman, Y. Okui, T. Shoji, M. Komuro, Probabilistic ultimate buckling strength of stiffened plates, considering thick and high-performance steel, J. Constr. Steel Res. 138 (2017) 184–195. doi:10.1016/j.jcsr.2017.07.004.
- [55] B. Gaspar, A. Naess, B.J. Leira, C. Guedes Soares, System reliability analysis of a stiffened panel under combined uniaxial compression and lateral pressure loads, Struct. Saf. 39 (2012) 30–43. doi:10.1016/J.STRUSAFE.2012.06.002.
- [56] D.V. Duc, Y. Okui, K. Hagiwara, M. Nagai, Probabilistic distributions of plate buckling strength for normal and bridge high-performance steels, Int. J. Steel Struct. 13 (2013) 557–567. doi:10.1007/s13296-013-3014-1.
- [57] M. Rahman, Y. Okui, M.A. Anwer, Probabilistic strength at serviceability limit state for normal and SBHS slender stiffened plates under uniaxial compression. Int. J. Steel Struct. 18 (2018) 1397–1409, doi:10.1007/s13296-018-0147-2.
- [58] DNV-RP-C201, Buckling strength of plated structures, Det Norske Veritas Recommended Practice, Norway, 2002.
- [59] K. Niwa, Studies on method of predicting ultimate strength of stiffened steel plates, Doctoral dissertation, Kansai University, 1999. (In Japanese)

- [60] M. Rahman, D. Miyazaki, Y. Okui, H. Honma, Numerical study on ultimate buckling strength of stiffened steel plate considering initial deflection and residual stress, Proc. of IABSE-JSCE Joint Conference on Advances in Bridge Engineering-III, Dhaka, (2015) 278-285.
- [61] D.D. Thang, M.S. Koo, A. Hameed, Y.D. Jeong, Stiffness requirement for flat-bar longitudinal stiffener of box-girder compression flanges, *Int. J. Steel Struct.* 9 (2009) 115–122. doi:10.1007/BF03249486.
- [62] R.D. Ziemian, *Guide to stability design criteria for metal structures*, sixth ed., John Wiley & Sons Inc., New Jersey, 2010.
- [63] E. Klöppel, J. Sheer, *Beulwerte ausgesteifter Rechteckplatten. Kurventaffeln zum direkten Nachweis der Beulsicherheit für verschiedene Steifenanordnungen und Belastungen*. Berlin: Verlag; 1960. (In German)
- [64] E. Klöppel, K. Möller, *Beulwerte. Ausgesteifter Rechteckplatten. II. Band*. Berlin: Verlag; 1968. (In German)
- [65] Y. Galéa, P.-O. Martin, Longitudinally stiffened plates in Eurocode 3: Calculation of the global critical buckling stress, *J. Constr. Steel Res.* 66 (2010) 1345-1353. doi.10.1016/j.jcsr.2010.05.001.
- [66] JSSC report, Performance evaluation of steel bridges and rationalization of strength design, Technical report No. 105, Research committee for rational structure and design for steel bridges, Japan Society of Steel Construction (JSSC), 2015. (In Japanese)
- [67] JSSC report, Design of steel bridges-advancement of evaluation technology, Technical report No. 114, Research committee for rational structure and design for steel bridges, Japan Society of Steel Construction (JSSC), 2018. (In Japanese)
- [68] A. Haldar, S. Mahadevan, *Probability, Reliability, and Statistical Methods in Engineering Design*. First ed., John Wiley and Sons, New York, 1999.

APPENDIX A

Detailed dimensions of the Model-1 stiffened plates

R_R	t	b	α	n	h_r	t_r	γ_i/γ_{ireq}	R_R	t	b	α	n	h_r	t_r	γ_i/γ_{ireq}
SM490Y								SM570							
0.4	30	2166	1	4	210	23	1.03	0.4	30	1924	1	4	190	21	1.03
	50	3717	1	4	360	38	1.02		50	3280	1	4	320	36	1.01
	70	5203	1	4	510	50	1.00		70	4593	1	4	450	49	1.01
	90	6792	1	4	660	67	1.01		90	5975	1	4	590	61	1.00
0.6	10	1068	1	4	85	10	1.05	0.6	10	952	1	4	80	11	1.04
	30	3249	1	4	260	27	1.01		30	2886	1	4	250	28	1.02
	50	5575	1	4	440	44	1.01		50	4921	1	4	420	46	1.01
	70	7805	1	4	610	63	1.00		70	6889	1	4	590	63	1.01
									90	8962	1	4	770	79	1.02
0.8	10	1424	1	4	90	11	1.06	0.8	10	1269	1	4	80	14	1.00
	30	4333	1	4	280	28	1.02		30	3848	1	4	270	29	1.04
	50	7433	1	4	470	46	1.01		50	6561	1	4	450	47	1.00
									70	9185	1	4	630	66	1.00
1.0	10	1780	1	4	95	11	1.04	1.0	10	1586	1	4	85	14	1.04
	30	5416	1	4	290	31	1.02		30	4810	1	4	280	31	1.02
	50	9292	1	4	490	50	1.01		50	8201	1	4	470	51	1.01
1.2	10	2136	1	4	100	11	1.03	1.2	10	1903	1	4	90	14	1.02
	30	6499	1	4	310	30	1.03		30	5772	1	4	290	33	1.02
									50	9841	1	4	490	53	1.01
1.4	10	2492	1	4	105	11	1.04	1.4	10	2220	1	4	95	14	1.07
	30	7582	1	4	320	31	1.02		30	6734	1	4	300	34	1.02
SBHS500								SBHS700							
0.4	30	1825	1	4	200	23	1.08	0.4	30	1543	1	4	190	26	1.14
	50	3042	1	4	330	38	1.04		50	2571	1	4	310	42	1.06
	70	4259	1	4	460	53	1.03		70	3600	1	4	430	58	1.02
	90	5476	1	4	590	68	1.02		90	4628	1	4	550	74	1.00
0.6	10	913	1	4	80	11	1.07	0.6	30	2314	1	4	230	31	1.03
	30	2738	1	4	250	29	1.09		50	3857	1	4	380	52	1.01
	50	4563	1	4	410	47	1.02		70	5399	1	4	540	72	1.04
	70	6389	1	4	580	66	1.05		90	6942	1	4	690	92	1.02
	90	8214	1	4	740	86	1.04								
0.8	10	1217	1	4	85	11	1.02	0.8	10	1028	1	4	80	12	1.04
	30	3651	1	4	260	30	1.00		30	3085	1	4	250	34	1.12
	50	6084	1	4	440	50	1.05		50	5142	1	4	410	55	1.05
	70	8518	1	4	610	70	1.02		70	7199	1	4	570	76	1.02
									90	9256	1	4	730	98	1.01
1.0	10	1521	1	4	90	11	1.01	1.0	10	1286	1	4	90	12	1.22
	30	4563	1	4	280	32	1.09		30	3857	1	4	260	35	1.08
	50	7606	1	4	460	53	1.04		50	6428	1	4	430	58	1.05
									70	8999	1	4	600	80	1.03
1.2	10	1825	1	4	90	14	1.06	1.2	10	1543	1	4	90	12	1.07
	30	5476	1	4	290	33	1.07		30	4628	1	4	270	36	1.07
	50	9127	1	4	480	55	1.05		50	7713	1	4	440	60	1.03
1.4	10	2130	1	4	90	16	1.04	1.4	10	1800	1	4	90	13	1.01
	30	6389	1	4	280	41	1.09		30	5399	1	4	280	38	1.09
									50	8999	1	4	460	62	1.03

* all dimensions are in mm

APPENDIX B

Detailed dimensions of the Model-2 stiffened plates

R_R	t	b	α	n	h_r	t_r	γ/γ_{req}	R_R	t	b	α	n	h_r	t_r	γ/γ_{req}
SM490Y								SM570							
0.4	20	1079	1	3	120	12	1.06	0.4	20	959	1	3	105	12	1.06
	30	1635	1	3	180	18	1.03		30	1443	1	3	160	17	1.05
	50	2788	1	3	310	30	1.05		50	2460	1	3	270	29	1.03
	70	3903	1	3	430	41	1.00		70	3445	1	3	380	40	1.03
	90	5094	1	3	560	54	1.01		90	4481	1	3	490	52	1.01
0.6	10	801	1	3	70	9	1.05	0.6	10	714	1	3	70	9	1.15
	20	1618	1	3	150	15	1.09		20	1439	1	3	140	16	1.04
	30	2437	1	3	220	22	1.00		30	2165	1	3	210	23	1.00
	50	4181	1	3	370	37	1.01		50	3691	1	3	360	38	1.06
	70	5854	1	3	520	51	1.01		70	5167	1	3	500	52	1.01
0.8	10	1068	1	3	75	9	1.01	0.8	10	952	1	3	75	9	1.11
	20	2158	1	3	160	16	1.09		20	1918	1	3	150	17	1.05
	30	3249	1	3	240	23	1.05		30	2886	1	3	230	25	1.10
	50	5575	1	3	400	39	1.04		50	4921	1	3	380	40	1.02
1.0	10	1335	1	3	80	9	1.00	1.0	10	1189	1	3	80	9	1.11
	20	2697	1	3	170	17	1.13		20	2398	1	3	160	17	1.05
	30	4062	1	3	250	24	1.01		30	3608	1	3	240	26	1.06
1.2	10	1602	1	3	85	9	1.02	1.2	10	1427	1	3	80	10	1.17
	20	3237	1	3	170	18	1.01		20	2877	1	3	170	18	1.12
	30	4874	1	3	260	26	1.03		30	4329	1	3	250	27	1.06
1.4	10	1869	1	3	90	9	1.05	1.4	10	1665	1	3	85	10	1.08
	20	3776	1	3	180	18	1.04		20	3357	1	3	170	19	1.03
	30	5686	1	3	270	26	1.01		30	5051	1	3	260	28	1.07
SBHS500								SBHS700							
0.4	20	913	1	3	100	11	1.01	0.4	20	771	1	3	85	11	1.15
	30	1369	1	3	150	17	1.04		30	1157	1	3	125	16	1.06
	50	2282	1	3	250	28	1.03		50	1928	1	3	210	26	1.06
	70	3194	1	3	350	38	1.01		70	2706	1	3	290	36	1.00
	90	4107	1	3	460	49	1.07		90	3471	1	3	380	46	1.06
0.6	10	684	1	3	70	9	1.18	0.6	20	1157	1	3	120	15	1.02
	20	1369	1	3	140	15	1.03		30	1736	1	3	180	23	1.04
	30	2053	1	3	210	23	1.04		50	2893	1	3	300	37	1.01
	50	3422	1	3	350	37	1.02		70	4050	1	3	420	52	1.01
	70	4791	1	3	490	51	1.00		90	5207	1	3	540	66	1.00
0.8	10	913	1	3	75	9	1.14	0.8	10	771	1	3	70	9	1.08
	20	1825	1	3	150	16	1.04		20	1543	1	3	140	17	1.03
	30	2738	1	3	220	25	1.01		30	2314	1	3	210	26	1.05
	50	4563	1	3	370	40	1.00		50	3857	1	3	350	43	1.04
									70	5399	1	3	490	60	1.04
1.0	10	1141	1	3	80	9	1.14	1.0	10	964	1	3	75	10	1.19
	20	2282	1	3	160	17	1.09		20	1928	1	3	150	19	1.14
	30	3422	1	3	240	26	1.11		30	2893	1	3	220	27	1.03
	50	5704	1	3	390	42	1.01		50	4821	1	3	370	45	1.05
1.2	10	1369	1	3	80	10	1.07	1.2	10	1157	1	3	75	10	1.03
	20	2738	1	3	180	17	1.31		20	2314	1	3	150	20	1.03
	30	4107	1	3	250	27	1.10		30	3471	1	3	230	28	1.03
									50	5785	1	3	380	47	1.01
1.4	10	1597	1	3	85	9	1.02	1.4	10	1350	1	3	80	10	1.09
	20	3194	1	3	170	18	1.02		20	2700	1	3	160	20	1.09
	30	4791	1	3	260	28	1.12		30	4050	1	3	240	29	1.06

* all dimensions are in mm

APPENDIX C

Detailed dimensions of the Model-3 stiffened plates

R_R	t	b	α	n	h_r	t_r	γ_l/γ_{lreq}
SM490Y							
0.4	40	1444	3	2	240	30	1.03
0.6	30	1625	3	2	270	27	1.02
0.8	20	1444	3	2	190	19	1.03
1.0	15	1335	3	2	145	16	1.03
1.2	15	1602	3	2	150	16	1.00
1.4	10	1246	3	2	100	13	1.03
SBHS500							
0.4	50	1521	3	2	220	27	1.04
0.6	30	1369	3	2	260	27	1.01
0.8	20	1217	3	2	180	20	1.01
1.0	20	1521	3	2	190	20	1.03
1.2	15	1369	3	2	145	16	1.01
1.4	15	1597	3	2	150	16	1.01
SM570							
0.4	40	1283	3	2	195	24	1.05
0.6	30	1443	3	2	260	28	1.00
0.8	20	1283	3	2	185	19	1.03
1.0	20	1603	3	2	190	20	1.00
1.2	15	1427	3	2	150	15	1.04
1.4	15	1665	3	2	155	15	1.03
SBHS700							
0.4	50	1286	3	2	150	19	1.01
0.6	30	1157	3	2	205	22	1.00
0.8	20	1028	3	2	175	19	1.00
1.0	20	1286	3	2	185	19	1.03
1.2	15	1157	3	2	140	16	1.02
1.4	15	1350	3	2	145	16	1.02

* all dimensions are in mm

APPENDIX D

FEA Results for Model-1

Note: This appendix should be read in conjunction with Table-2.5 in order to interpret the imperfection index.

R_R = 0.4				
Imperfection Index	σ_{ULS}/σ_y	σ_{ULS}/σ_y	σ_{ULS}/σ_y	σ_{ULS}/σ_y
Model ID →	SM490Y R _R = 0.4 T = 30	SM490Y R _R = 0.4 T = 50	SM490Y R _R = 0.4 T = 70	SM490Y R _R = 0.4 T = 90
C130	1.014	1.041	1.014	1.027
C131	1.013	1.038	1.016	1.026
C132	0.991	1.022	1.003	1.010
C160	0.917	0.953	0.924	0.941
C161	0.916	0.951	0.922	0.940
C162	0.908	0.940	0.913	0.930
C220	0.919	0.950	0.921	0.941
C221	0.915	0.949	0.921	0.941
C222	0.916	0.946	0.922	0.938
C230	0.955	0.987	0.960	0.965
C231	0.954	0.986	0.953	0.978
C232	0.947	0.978	0.955	0.974
C240	0.903	0.933	0.908	0.924
C241	0.902	0.932	0.905	0.924
C242	0.898	0.927	0.904	0.919
C250	0.877	0.905	0.883	0.898
C251	0.876	0.905	0.881	0.898
C252	0.872	0.900	0.878	0.894
C310	0.871	0.904	0.875	0.899
C311	0.869	0.900	0.874	0.898
C312	0.868	0.899	0.869	0.893
C330	0.941	0.987	0.960	0.976
C331	0.954	0.986	0.956	0.972
C332	0.952	0.981	0.952	0.966
C430	0.955	0.991	0.957	0.979
C431	0.954	0.989	0.954	0.979
C432	0.952	0.986	0.951	0.973
C460	0.833	0.865	0.842	0.862
C461	0.831	0.864	0.842	0.862
C462	0.829	0.860	0.837	0.858
C540	0.892	0.929	0.902	0.923
C541	0.892	0.925	0.897	0.921
C542	0.875	0.909	0.896	0.919
C560	0.833	0.866	0.844	0.865
C561	0.833	0.866	0.843	0.864
C562	0.828	0.861	0.838	0.861
Model ID →	SM570 R _R = 0.4 T = 30	SM570 R _R = 0.4 T = 50	SM570 R _R = 0.4 T = 70	SM570 R _R = 0.4 T = 90
C130	1.008	1.027	1.009	1.018
C131	1.006	1.025	1.006	1.017
C132	0.994	1.012	0.995	1.005
C160	0.875	0.908	0.879	0.895

Imperfection Index	σ_{ULS}/σ_y	σ_{ULS}/σ_y	σ_{ULS}/σ_y	σ_{ULS}/σ_y
C161	0.874	0.907	0.878	0.894
C162	0.870	0.903	0.873	0.889
C220	0.897	0.918	0.899	0.910
C221	0.897	0.917	0.899	0.910
C222	0.894	0.913	0.896	0.907
C230	0.925	0.946	0.928	0.940
C231	0.924	0.945	0.927	0.938
C232	0.920	0.942	0.923	0.936
C240	0.883	0.904	0.885	0.895
C241	0.882	0.903	0.884	0.895
C242	0.878	0.899	0.880	0.891
C250	0.855	0.876	0.856	0.867
C251	0.854	0.875	0.855	0.866
C252	0.849	0.870	0.850	0.862
C310	0.829	0.853	0.831	0.843
C311	0.828	0.852	0.831	0.843
C312	0.827	0.851	0.830	0.843
C330	0.931	0.955	0.928	0.946
C331	0.928	0.953	0.931	0.945
C332	0.922	0.946	0.925	0.938
C430	0.927	0.958	0.930	0.945
C431	0.928	0.955	0.930	0.944
C432	0.923	0.947	0.926	0.939
C460	0.782	0.805	0.788	0.801
C461	0.782	0.805	0.787	0.800
C462	0.780	0.802	0.785	0.797
C540	0.849	0.878	0.852	0.866
C541	0.849	0.877	0.852	0.866
C542	0.849	0.875	0.851	0.866
C560	0.783	0.806	0.788	0.802
C561	0.783	0.806	0.788	0.801
C562	0.780	0.803	0.786	0.798
Model ID →	SBHS500 R _R = 0.4 T = 30	SBHS500 R _R = 0.4 T = 50	SBHS500 R _R = 0.4 T = 70	SBHS500 R _R = 0.4 T = 90
C230	0.955	0.934	0.948	0.945
C231	0.930	0.951	0.948	0.946
C232	0.953	0.952	0.948	0.946
C250	0.883	0.881	0.877	0.876
C251	0.882	0.881	0.877	0.876
C252	0.881	0.879	0.876	0.875
C240	0.908	0.906	0.902	0.902
C241	0.906	0.904	0.903	0.901
C242	0.906	0.905	0.902	0.901
C220	0.923	0.921	0.918	0.918
C221	0.922	0.919	0.918	0.917
C222	0.922	0.920	0.917	0.916
C430	0.958	0.956	0.952	0.953
C431	0.956	0.952	0.951	0.935
C432	0.956	0.952	0.950	0.948
C460	0.848	0.845	0.837	0.834
C461	0.847	0.844	0.836	0.834
C462	0.843	0.841	0.832	0.830
C560	0.849	0.846	0.838	0.835
C561	0.848	0.846	0.837	0.834
C562	0.843	0.842	0.833	0.830

Imperfection Index	σ_{ULS}/σ_y	σ_{ULS}/σ_y	σ_{ULS}/σ_y	σ_{ULS}/σ_y
C540	0.901	0.900	0.892	0.891
C541	0.901	0.897	0.891	0.889
C542	0.897	0.896	0.889	0.887
C330	0.951	0.956	0.954	0.952
C331	0.956	0.956	0.951	0.949
C332	0.952	0.953	0.950	0.948
C310	0.873	0.878	0.870	0.868
C311	0.876	0.877	0.870	0.868
C312	0.877	0.875	0.868	0.866
C130	1.013	1.012	1.012	1.012
C131	1.013	1.013	1.012	1.012
C132	1.001	1.005	1.002	1.003
C160	0.929	0.926	0.921	0.919
C161	0.928	0.925	0.920	0.918
C162	0.922	0.919	0.914	0.913
Model ID →	SBHS700 R _R = 0.4 T = 30	SBHS500 R _R = 0.4 T = 50	SBHS500 R _R = 0.4 T = 70	SBHS500 R _R = 0.4 T = 90
C230	0.953	0.956	0.951	0.945
C231	0.952	0.954	0.948	0.946
C232	0.954	0.955	0.949	0.947
C250	0.886	0.889	0.885	0.883
C251	0.886	0.889	0.885	0.883
C252	0.886	0.889	0.885	0.883
C240	0.909	0.911	0.909	0.907
C241	0.900	0.911	0.907	0.906
C242	0.908	0.912	0.908	0.906
C220	0.922	0.925	0.923	0.919
C221	0.924	0.925	0.920	0.920
C222	0.923	0.927	0.922	0.920
C430	0.953	0.954	0.944	0.952
C431	0.957	0.959	0.954	0.946
C432	0.956	0.956	0.949	0.951
C460	0.847	0.854	0.845	0.840
C461	0.846	0.853	0.844	0.840
C462	0.845	0.850	0.842	0.838
C560	0.847	0.853	0.846	0.841
C561	0.847	0.853	0.845	0.840
C562	0.845	0.850	0.842	0.838
C540	0.900	0.908	0.903	0.900
C541	0.898	0.907	0.901	0.899
C542	0.899	0.906	0.900	0.898
C330	0.956	0.959	0.952	0.951
C331	0.940	0.956	0.955	0.953
C332	0.955	0.956	0.952	0.950
C310	0.885	0.888	0.883	0.877
C311	0.883	0.888	0.881	0.878
C312	0.882	0.887	0.880	0.877
C130	1.011	1.012	1.011	1.009
C131	1.012	1.005	1.011	1.020
C132	1.004	1.005	1.004	0.992
C160	0.948	0.952	0.947	0.943
C161	0.932	0.939	0.935	0.932
C162	0.931	0.934	0.930	0.927

R_R = 0.6

Imperfection Index	σ_{ULS}/σ_y	σ_{ULS}/σ_y	σ_{ULS}/σ_y	σ_{ULS}/σ_y	σ_{ULS}/σ_y
Model ID →	SM490Y R _R = 0.6 T = 10	SM490Y R _R = 0.6 T = 30	SM490Y R _R = 0.6 T = 50	SM490Y R _R = 0.6 T = 70	
C130	0.999	0.990	0.999	0.995	
C131	0.980	0.972	0.976	1.002	
C132	0.939	0.931	0.932	0.931	
C160	0.829	0.823	0.811	0.810	
C161	0.827	0.822	0.810	0.809	
C162	0.816	0.811	0.798	0.798	
C220	0.876	0.874	0.874	0.874	
C221	0.870	0.865	0.835	0.866	
C222	0.846	0.839	0.836	0.837	
C230	0.898	0.897	0.898	0.896	
C231	0.894	0.892	0.890	0.890	
C232	0.871	0.867	0.863	0.862	
C240	0.861	0.841	0.858	0.856	
C241	0.855	0.850	0.849	0.847	
C242	0.831	0.825	0.820	0.821	
C250	0.827	0.825	0.818	0.816	
C251	0.820	0.817	0.810	0.809	
C252	0.798	0.795	0.786	0.785	
C310	0.794	0.794	0.783	0.782	
C311	0.791	0.788	0.780	0.779	
C312	0.778	0.776	0.767	0.765	
C330	0.899	0.900	0.896	0.889	
C331	0.892	0.889	0.880	0.882	
C332	0.862	0.858	0.852	0.852	
C430	0.902	0.902	0.899	0.892	
C431	0.891	0.887	0.884	0.881	
C432	0.860	0.849	0.850	0.850	
C460	0.727	0.728	0.714	0.713	
C461	0.725	0.726	0.712	0.710	
C462	0.717	0.718	0.703	0.701	
C540	0.814	0.812	0.802	0.801	
C541	0.810	0.808	0.798	0.798	
C542	0.795	0.793	0.782	0.781	
C560	0.703	0.726	0.710	0.708	
C561	0.702	0.724	0.708	0.706	
C562	0.696	0.715	0.700	0.698	
Model ID →	SM570 R _R = 0.6 T = 10	SM570 R _R = 0.6 T = 30	SM570 R _R = 0.6 T = 50	SM570 R _R = 0.6 T = 70	SM570 R _R = 0.6 T = 90
C130	1.051	1.013	1.014	0.996	1.015
C131	1.002	0.972	1.022	1.025	1.023
C132	0.946	0.959	0.958	0.950	0.939
C160	0.846	0.838	0.833	0.831	0.831
C161	0.844	0.837	0.832	0.830	0.830
C162	0.834	0.827	0.822	0.821	0.821
C220	0.876	0.875	0.874	0.875	0.876
C221	0.871	0.870	0.869	0.868	0.870
C222	0.852	0.847	0.845	0.844	0.845
C230	0.898	0.899	0.896	0.896	0.898
C231	0.893	0.893	0.892	0.891	0.893

Imperfection Index	σ_{ULS}/σ_y	σ_{ULS}/σ_y	σ_{ULS}/σ_y	σ_{ULS}/σ_y	σ_{ULS}/σ_y
C232	0.874	0.871	0.869	0.868	0.869
C240	0.863	0.862	0.861	0.860	0.862
C241	0.856	0.855	0.854	0.853	0.855
C242	0.838	0.833	0.831	0.830	0.831
C250	0.832	0.829	0.828	0.827	0.828
C251	0.827	0.824	0.821	0.819	0.820
C252	0.808	0.804	0.801	0.799	0.800
C310	0.800	0.796	0.793	0.792	0.794
C311	0.797	0.793	0.790	0.789	0.790
C312	0.786	0.781	0.779	0.777	0.778
C330	0.898	0.897	0.894	0.893	0.896
C331	0.892	0.888	0.887	0.885	0.887
C332	0.865	0.860	0.858	0.857	0.858
C430	0.884	0.898	0.898	0.897	0.893
C431	0.890	0.888	0.887	0.885	0.887
C432	0.864	0.858	0.857	0.856	0.857
C460	0.739	0.733	0.729	0.727	0.729
C461	0.737	0.731	0.727	0.725	0.727
C462	0.730	0.724	0.719	0.718	0.719
C540	0.818	0.815	0.813	0.811	0.813
C541	0.816	0.811	0.809	0.807	0.809
C542	0.803	0.797	0.794	0.793	0.794
C560	0.737	0.731	0.726	0.724	0.726
C561	0.735	0.729	0.725	0.723	0.724
C562	0.728	0.721	0.717	0.715	0.716
Model ID →	SBHS500 R _R = 0.6 T = 10	SBHS500 R _R = 0.6 T = 30	SBHS500 R _R = 0.6 T = 50	SBHS500 R _R = 0.6 T = 70	SBHS500 R _R = 0.6 T = 90
C230	0.899	0.904	0.898	0.901	0.900
C231	0.897	0.898	0.893	0.897	0.895
C232	0.879	0.880	0.872	0.876	0.874
C250	0.839	0.841	0.833	0.839	0.838
C251	0.835	0.837	0.828	0.833	0.831
C252	0.815	0.817	0.809	0.813	0.811
C240	0.866	0.871	0.864	0.867	0.864
C241	0.862	0.864	0.858	0.861	0.861
C242	0.841	0.844	0.836	0.839	0.838
C220	0.880	0.884	0.876	0.869	0.879
C221	0.876	0.877	0.871	0.874	0.874
C222	0.857	0.857	0.849	0.853	0.851
C430	0.905	0.910	0.901	0.907	0.896
C431	0.895	0.876	0.888	0.892	0.892
C432	0.868	0.867	0.860	0.863	0.863
C460	0.748	0.753	0.738	0.746	0.743
C461	0.747	0.751	0.737	0.744	0.741
C462	0.740	0.753	0.730	0.737	0.734
C560	0.748	0.751	0.737	0.744	0.742
C561	0.746	0.749	0.735	0.742	0.740
C562	0.738	0.741	0.728	0.734	0.732
C540	0.826	0.828	0.817	0.823	0.822
C541	0.819	0.826	0.815	0.821	0.819
C542	0.809	0.812	0.801	0.806	0.805
C330	0.907	0.906	0.898	0.902	0.901
C331	0.930	0.898	0.889	0.893	0.893

Imperfection Index	σ_{ULS}/σ_y	σ_{ULS}/σ_y	σ_{ULS}/σ_y	σ_{ULS}/σ_y	σ_{ULS}/σ_y
C332	0.865	0.868	0.861	0.865	0.864
C310	0.807	0.812	0.797	0.805	0.803
C311	0.805	0.808	0.797	0.802	0.800
C312	0.794	0.798	0.786	0.792	0.790
C130	0.996	1.013	0.998	0.999	1.013
C131	0.997	0.999	1.007	1.008	0.982
C132	0.949	0.946	0.944	0.945	0.945
C160	0.854	0.856	0.846	0.851	0.849
C161	0.856	0.856	0.845	0.851	0.848
C162	0.846	0.845	0.835	0.840	0.839
Model ID →	SBHS700 R _R = 0.6 T = 30	SBHS700 R _R = 0.6 T = 50	SBHS700 R _R = 0.6 T = 70	SBHS700 R _R = 0.6 T = 90	
C230	0.892	0.892	0.895	0.897	
C231	0.893	0.891	0.895	0.893	
C232	0.876	0.876	0.879	0.877	
C250	0.841	0.842	0.843	0.843	
C251	0.839	0.837	0.840	0.839	
C252	0.822	0.821	0.824	0.822	
C240	0.868	0.864	0.869	0.865	
C241	0.863	0.861	0.865	0.863	
C242	0.846	0.845	0.848	0.846	
C220	0.851	0.875	0.878	0.877	
C221	0.873	0.873	0.877	0.874	
C222	0.858	0.856	0.860	0.858	
C430	0.898	0.896	0.908	0.899	
C431	0.894	0.891	0.896	0.892	
C432	0.866	0.865	0.868	0.865	
C460	0.759	0.756	0.763	0.759	
C461	0.758	0.754	0.761	0.758	
C462	0.752	0.748	0.754	0.751	
C560	0.759	0.755	0.762	0.759	
C561	0.757	0.754	0.760	0.757	
C562	0.751	0.746	0.753	0.749	
C540	0.828	0.826	0.833	0.829	
C541	0.826	0.823	0.830	0.826	
C542	0.750	0.812	0.817	0.814	
C330	0.848	0.900	0.904	0.894	
C331	0.887	0.890	0.896	0.893	
C332	0.865	0.865	0.869	0.865	
C310	0.812	0.808	0.815	0.811	
C311	0.808	0.806	0.812	0.809	
C312	0.800	0.796	0.802	0.799	
C130	0.995	1.007	1.135	0.993	
C131	1.001	0.982	1.004	0.983	
C132	0.970	0.951	0.952	0.952	
C160	0.877	0.876	0.881	0.878	
C161	0.869	0.866	0.873	0.869	
C162	0.750	0.857	0.862	0.859	

R_R = 0.8				
Imperfection Index	σ_{ULS}/σ_y	σ_{ULS}/σ_y	σ_{ULS}/σ_y	σ_{ULS}/σ_y
Model ID →	SM490Y R _R = 0.8 T = 10	SM490Y R _R = 0.8 T = 30	SM490Y R _R = 0.8 T = 50	
C130	0.919	0.912	0.913	
C131	0.883	0.873	0.868	
C132	0.837	0.829	0.825	
C160	0.682	0.664	0.656	
C161	0.679	0.661	0.653	
C162	0.667	0.650	0.642	
C220	0.781	0.771	0.766	
C221	0.757	0.746	0.741	
C222	0.724	0.716	0.711	
C230	0.827	0.823	0.820	
C231	0.787	0.778	0.775	
C232	0.780	0.744	0.740	
C240	0.752	0.737	0.733	
C241	0.731	0.722	0.716	
C242	0.703	0.695	0.689	
C250	0.672	0.679	0.673	
C251	0.686	0.669	0.665	
C252	0.665	0.651	0.645	
C310	0.681	0.673	0.665	
C311	0.666	0.654	0.649	
C312	0.643	0.631	0.626	
C330	0.749	0.744	0.768	
C331	0.730	0.720	0.717	
C332	0.689	0.698	0.694	
C430	0.747	0.741	0.737	
C431	0.719	0.710	0.707	
C432	0.702	0.692	0.688	
C460	0.599	0.585	0.579	
C461	0.592	0.579	0.571	
C462	0.576	0.565	0.556	
C540	0.669	0.655	0.651	
C541	0.655	0.643	0.638	
C542	0.639	0.627	0.622	
C560	0.581	0.573	0.564	
C561	0.579	0.565	0.559	
C562	0.567	0.555	0.547	
Model ID →	SM570 R _R = 0.8 T = 10	SM570 R _R = 0.8 T = 30	SM570 R _R = 0.8 T = 50	SM570 R _R = 0.8 T = 70
C130	0.920	0.929	0.922	0.922
C131	0.891	0.810	0.872	0.872
C132	0.842	0.835	0.829	0.829
C160	0.687	0.693	0.676	0.677
C161	0.684	0.690	0.673	0.674
C162	0.674	0.677	0.662	0.663
C220	0.769	0.781	0.770	0.770
C221	0.757	0.756	0.747	0.747
C222	0.725	0.726	0.717	0.718
C230	0.817	0.827	0.821	0.821

Imperfection Index	σ_{ULS}/σ_y	σ_{ULS}/σ_y	σ_{ULS}/σ_y	σ_{ULS}/σ_y	σ_{ULS}/σ_y
C231	0.790	0.785	0.779	0.779	
C232	0.754	0.752	0.745	0.746	
C240	0.742	0.753	0.740	0.741	
C241	0.733	0.735	0.725	0.725	
C242	0.706	0.708	0.698	0.699	
C250	0.693	0.702	0.687	0.688	
C251	0.688	0.692	0.678	0.679	
C252	0.669	0.671	0.659	0.659	
C310	0.673	0.684	0.674	0.674	
C311	0.664	0.667	0.657	0.658	
C312	0.643	0.646	0.636	0.636	
C330	0.730	0.746	0.738	0.739	
C331	0.723	0.726	0.718	0.719	
C332	0.701	0.706	0.697	0.698	
C430	0.728	0.746	0.735	0.736	
C431	0.714	0.718	0.708	0.708	
C432	0.693	0.700	0.690	0.691	
C460	0.597	0.603	0.592	0.592	
C461	0.593	0.597	0.586	0.586	
C462	0.581	0.582	0.571	0.571	
C540	0.658	0.670	0.659	0.659	
C541	0.652	0.657	0.645	0.646	
C542	0.636	0.641	0.629	0.630	
C560	0.586	0.593	0.580	0.580	
C561	0.583	0.586	0.573	0.574	
C562	0.571	0.573	0.561	0.561	
Model ID →	SBHS500 R _R = 0.8 T = 10	SBHS500 R _R = 0.8 T = 30	SBHS500 R _R = 0.8 T = 50	SBHS500 R _R = 0.8 T = 70	
C230	0.823	0.821	0.828	0.824	
C231	0.771	0.783	0.788	0.785	
C232	0.752	0.749	0.788	0.751	
C250	0.697	0.695	0.708	0.699	
C251	0.694	0.687	0.699	0.692	
C252	0.673	0.667	0.677	0.671	
C240	0.749	0.745	0.758	0.750	
C241	0.736	0.731	0.740	0.735	
C242	0.708	0.704	0.712	0.707	
C220	0.777	0.773	0.784	0.777	
C221	0.757	0.752	0.760	0.755	
C222	0.727	0.722	0.730	0.725	
C430	0.737	0.651	0.747	0.739	
C431	0.715	0.709	0.720	0.713	
C432	0.694	0.691	0.702	0.696	
C460	0.605	0.600	0.609	0.602	
C461	0.598	0.593	0.603	0.597	
C462	0.582	0.579	0.589	0.583	
C560	0.586	0.589	0.599	0.592	
C561	0.579	0.581	0.593	0.587	
C562	0.573	0.571	0.581	0.574	
C540	0.665	0.662	0.676	0.667	
C541	0.656	0.651	0.662	0.655	
C542	0.641	0.635	0.646	0.639	
C330	0.738	0.773	0.746	0.740	

Imperfection Index	σ_{ULS}/σ_y	σ_{ULS}/σ_y	σ_{ULS}/σ_y	σ_{ULS}/σ_y	σ_{ULS}/σ_y
C331	0.725	0.720	0.728	0.723	
C332	0.704	0.699	0.709	0.703	
C310	0.682	0.678	0.688	0.681	
C311	0.669	0.663	0.672	0.667	
C312	0.647	0.642	0.651	0.645	
C130	0.929	0.909	0.934	0.929	
C131	0.885	0.875	0.884	0.881	
C132	0.818	0.834	0.840	0.836	
C160	0.693	0.690	0.703	0.695	
C161	0.686	0.686	0.700	0.692	
C162	0.676	0.674	0.687	0.679	
Model ID →	SBHS700 R _R = 0.8 T = 10	SBHS700 R _R = 0.8 T = 30	SBHS700 R _R = 0.8 T = 50	SBHS700 R _R = 0.8 T = 70	SBHS700 R _R = 0.8 T = 90
C230	0.820	0.802	0.826	0.824	0.822
C231	0.799	0.792	0.796	0.792	0.792
C232	0.757	0.757	0.763	0.758	0.757
C250	0.720	0.710	0.724	0.716	0.714
C251	0.715	0.704	0.672	0.709	0.706
C252	0.692	0.685	0.694	0.687	0.685
C240	0.764	0.753	0.766	0.758	0.756
C241	0.715	0.743	0.752	0.746	0.744
C242	0.706	0.716	0.724	0.719	0.717
C220	0.786	0.780	0.789	0.783	0.782
C221	0.771	0.764	0.770	0.765	0.764
C222	0.740	0.733	0.740	0.734	0.733
C430	0.740	0.731	0.745	0.738	0.735
C431	0.761	0.714	0.725	0.717	0.715
C432	0.704	0.695	0.706	0.699	0.697
C460	0.624	0.613	0.625	0.618	0.616
C461	0.619	0.609	0.620	0.613	0.611
C462	0.606	0.597	0.606	0.600	0.598
C560	0.613	0.604	0.618	0.609	0.607
C561	0.610	0.600	0.612	0.604	0.602
C562	0.597	0.588	0.599	0.592	0.589
C540	0.681	0.671	0.686	0.676	0.674
C541	0.672	0.661	0.674	0.666	0.664
C542	0.654	0.646	0.657	0.650	0.647
C330	0.775	0.732	0.743	0.737	0.735
C331	0.728	0.724	0.732	0.726	0.725
C332	0.712	0.704	0.714	0.707	0.705
C310	0.691	0.683	0.693	0.688	0.686
C311	0.680	0.674	0.683	0.677	0.676
C312	0.663	0.654	0.663	0.657	0.655
C130	0.926	0.907	0.912	0.916	0.916
C131	0.865	0.890	0.892	0.890	0.889
C132	0.874	0.842	0.847	0.844	0.843
C160	0.734	0.720	0.735	0.726	0.719
C161	0.726	0.710	0.726	0.717	0.715
C162	0.712	0.701	0.713	0.705	0.703

R_R = 1.0								
Imperfection Index	σ_{ULS}/σ_y	σ_{SLS}/σ_y	σ_{ULS}/σ_y	σ_{SLS}/σ_y	σ_{ULS}/σ_y	σ_{SLS}/σ_y	σ_{ULS}/σ_y	σ_{SLS}/σ_y
Model ID →	SM490Y_R _R 1.0_T10		SM490Y_R _R 1.0_T30		SM490Y_R _R 1.0_T50			
C130	0.732	0.724	0.735	0.724	0.730	0.721		
C131	0.704	0.578	0.709	0.573	0.707	0.572		
C132	0.699	0.472	0.698	0.476	0.694	0.483		
C160	0.527	0.434	0.518	0.329	0.512	0.331		
C161	0.523	0.360	0.514	0.344	0.508	0.345		
C162	0.514	0.303	0.510	0.288	0.501	0.303		
C220	0.634	0.624	0.631	0.589	0.625	0.588		
C221	0.613	0.459	0.608	0.460	0.602	0.460		
C222	0.590	0.380	0.591	0.366	0.587	0.372		
C230	0.692	0.687	0.702	0.701	0.697	0.697		
C231	0.661	0.524	0.658	0.521	0.655	0.521		
C232	0.640	0.416	0.637	0.417	0.634	0.422		
C240	0.599	0.574	0.593	0.515	0.587	0.512		
C241	0.584	0.438	0.578	0.426	0.572	0.426		
C242	0.567	0.354	0.564	0.337	0.558	0.353		
C250	0.543	0.491	0.538	0.401	0.531	0.398		
C251	0.534	0.381	0.529	0.366	0.523	0.380		
C252	0.525	0.304	0.519	0.291	0.513	0.305		
C310	0.537	0.432	0.534	0.438	0.528	0.438		
C311	0.522	0.381	0.520	0.366	0.514	0.366		
C312	0.513	0.162	0.509	0.292	0.504	0.164		
C330	0.640	0.639	0.637	0.637	0.634	0.633		
C331	0.595	0.478	0.592	0.477	0.589	0.480		
C332	0.579	0.214	0.577	0.372	0.574	0.378		
C430	0.589	0.574	0.587	0.532	0.584	0.572		
C431	0.560	0.339	0.558	0.439	0.554	0.334		
C432	0.552	0.190	0.550	0.339	0.547	0.184		
C460	0.470	0.318	0.468	0.313	0.461	0.316		
C461	0.462	0.206	0.456	0.290	0.450	0.202		
C462	0.453	0.120	0.449	0.227	0.443	0.116		
C540	0.522	0.489	0.519	0.441	0.515	0.441		
C541	0.505	0.366	0.501	0.352	0.497	0.353		
C542	0.494	0.271	0.494	0.278	0.490	0.271		
C560	0.459	0.379	0.452	0.305	0.447	0.381		
C561	0.442	0.295	0.443	0.291	0.438	0.292		
C562	0.439	0.214	0.437	0.215	0.432	0.216		
Model ID →	SM570_R _R 1.0_T10		SM570_R _R 1.0_T30		SM570_R _R 1.0_T50			
C130	0.713	0.690	0.732	0.713	0.728	0.711		
C131	0.698	0.597	0.710	0.559	0.707	0.559		
C132	0.685	0.482	0.697	0.449	0.694	0.452		
C160	0.532	0.315	0.534	0.327	0.529	0.325		
C161	0.529	0.343	0.531	0.341	0.525	0.340		
C162	0.522	0.284	0.524	0.278	0.518	0.278		
C220	0.627	0.559	0.637	0.580	0.632	0.578		
C221	0.612	0.480	0.613	0.452	0.610	0.451		
C222	0.594	0.372	0.598	0.348	0.595	0.350		
C230	0.687	0.679	0.702	0.699	0.698	0.696		

Imperfection Index	σ_{ULS}/σ_y	σ_{SLS}/σ_y	σ_{ULS}/σ_y	σ_{SLS}/σ_y	σ_{ULS}/σ_y	σ_{SLS}/σ_y	σ_{ULS}/σ_y	σ_{SLS}/σ_y
C231	0.657	0.554	0.659	0.506	0.657	0.507		
C232	0.635	0.427	0.640	0.389	0.637	0.392		
C240	0.595	0.487	0.601	0.506	0.596	0.505		
C241	0.584	0.441	0.586	0.419	0.582	0.419		
C242	0.569	0.343	0.572	0.322	0.568	0.324		
C250	0.545	0.378	0.548	0.393	0.543	0.392		
C251	0.538	0.372	0.540	0.361	0.535	0.360		
C252	0.528	0.291	0.530	0.277	0.525	0.278		
C310	0.538	0.418	0.542	0.433	0.538	0.431		
C311	0.528	0.379	0.527	0.360	0.524	0.359		
C312	0.515	0.283	0.517	0.275	0.513	0.276		
C330	0.631	0.631	0.638	0.638	0.636	0.636		
C331	0.594	0.515	0.592	0.465	0.590	0.465		
C332	0.576	0.385	0.578	0.346	0.576	0.349		
C430	0.572	0.554	0.584	0.536	0.582	0.536		
C431	0.553	0.473	0.557	0.431	0.555	0.431		
C432	0.544	0.356	0.551	0.318	0.548	0.321		
C460	0.476	0.302	0.478	0.314	0.474	0.312		
C461	0.467	0.300	0.466	0.287	0.462	0.286		
C462	0.458	0.230	0.459	0.216	0.455	0.216		
C540	0.515	0.426	0.522	0.437	0.519	0.436		
C541	0.502	0.372	0.505	0.348	0.502	0.347		
C542	0.495	0.272	0.499	0.249	0.496	0.250		
C560	0.460	0.296	0.463	0.307	0.458	0.306		
C561	0.453	0.303	0.453	0.277	0.449	0.276		
C562	0.446	0.210	0.446	0.206	0.443	0.206		
Model ID →	SBHS500_R _R 1.0_T10	SBHS500_R _R 1.0_T30	SBHS500_R _R 1.0_T50					
C230	0.693	0.678	0.728	0.727	0.710	0.709		
C231	0.653	0.502	0.674	0.509	0.665	0.506		
C232	0.638	0.386	0.655	0.384	0.646	0.382		
C250	0.549	0.386	0.575	0.413	0.560	0.399		
C251	0.542	0.365	0.564	0.374	0.551	0.366		
C252	0.531	0.168	0.553	0.283	0.540	0.277		
C240	0.597	0.493	0.628	0.532	0.612	0.513		
C241	0.585	0.419	0.609	0.428	0.596	0.423		
C242	0.570	0.318	0.593	0.322	0.582	0.319		
C220	0.631	0.566	0.662	0.612	0.647	0.588		
C221	0.610	0.448	0.634	0.459	0.622	0.454		
C222	0.597	0.350	0.617	0.346	0.606	0.344		
C430	0.578	0.562	0.602	0.580	0.589	0.568		
C431	0.553	0.427	0.575	0.435	0.562	0.433		
C432	0.547	0.315	0.569	0.311	0.557	0.311		
C460	0.479	0.305	0.502	0.328	0.489	0.317		
C461	0.466	0.284	0.487	0.297	0.476	0.292		
C462	0.460	0.203	0.478	0.208	0.468	0.204		
C560	0.461	0.297	0.485	0.319	0.473	0.309		
C561	0.453	0.274	0.473	0.288	0.462	0.283		
C562	0.445	0.194	0.467	0.198	0.456	0.194		
C540	0.520	0.434	0.544	0.455	0.530	0.442		
C541	0.504	0.348	0.524	0.354	0.512	0.352		
C542	0.496	0.252	0.518	0.251	0.507	0.249		
C330	0.635	0.635	0.654	0.654	0.644	0.643		

Imperfection Index	σ_{ULS}/σ_y	σ_{SLS}/σ_y	σ_{ULS}/σ_y	σ_{SLS}/σ_y	σ_{ULS}/σ_y	σ_{SLS}/σ_y	σ_{ULS}/σ_y	σ_{SLS}/σ_y
C331	0.598	0.463	0.607	0.469	0.598	0.467		
C332	0.583	0.340	0.593	0.340	0.584	0.339		
C310	0.533	0.446	0.696	0.455	0.552	0.437		
C311	0.527	0.362	0.672	0.371	0.536	0.365		
C312	0.518	0.260	0.659	0.268	0.526	0.264		
C130	0.719	0.692	0.768	0.750	0.743	0.722		
C131	0.703	0.554	0.734	0.563	0.718	0.559		
C132	0.687	0.436	0.718	0.442	0.705	0.441		
C160	0.534	0.317	0.564	0.343	0.548	0.331		
C161	0.531	0.340	0.559	0.355	0.544	0.346		
C162	0.522	0.274	0.552	0.286	0.538	0.279		
Model ID →	SBHS700_RR 1.0_T10	SBHS700_RR 1.0_T30	SBHS700_RR 1.0_T50	SBHS700_RR 1.0_T70				
C230	0.707	0.666	0.722	0.715	0.711	0.703	0.703	0.691
C231	0.667	0.505	0.675	0.508	0.669	0.507	0.667	0.588
C232	0.647	0.363	0.657	0.366	0.651	0.363	0.649	0.497
C250	0.575	0.377	0.586	0.398	0.577	0.392	0.570	0.386
C251	0.567	0.358	0.576	0.370	0.569	0.366	0.565	0.432
C252	0.556	0.265	0.565	0.272	0.558	0.270	0.555	0.369
C240	0.621	0.489	0.635	0.513	0.625	0.504	0.618	0.495
C241	0.608	0.412	0.617	0.426	0.609	0.423	0.607	0.500
C242	0.593	0.305	0.601	0.309	0.595	0.308	0.594	0.423
C220	0.647	0.557	0.665	0.590	0.656	0.579	0.648	0.568
C221	0.630	0.445	0.639	0.460	0.632	0.456	0.630	0.536
C222	0.613	0.330	0.622	0.332	0.616	0.331	0.615	0.453
C430	0.584	0.550	0.594	0.566	0.587	0.560	0.581	0.556
C431	0.562	0.426	0.572	0.439	0.565	0.437	0.558	0.485
C432	0.554	0.295	0.566	0.297	0.559	0.296	0.553	0.397
C460	0.500	0.303	0.510	0.317	0.503	0.311	0.498	0.306
C461	0.488	0.287	0.497	0.294	0.491	0.291	0.487	0.341
C462	0.481	0.197	0.489	0.200	0.483	0.198	0.479	0.271
C560	0.485	0.297	0.494	0.309	0.487	0.306	0.482	0.302
C561	0.475	0.277	0.483	0.285	0.477	0.283	0.472	0.326
C562	0.469	0.187	0.476	0.190	0.470	0.188	0.465	0.257
C540	0.534	0.430	0.545	0.446	0.537	0.440	0.531	0.434
C541	0.518	0.351	0.527	0.357	0.520	0.354	0.515	0.397
C542	0.512	0.239	0.521	0.242	0.515	0.240	0.509	0.322
C330	0.644	0.635	0.652	0.651	0.646	0.646	0.642	0.642
C331	0.571	0.463	0.607	0.469	0.602	0.467	0.600	0.534
C332	0.611	0.355	0.594	0.324	0.588	0.324	0.587	0.440
C310	0.561	0.414	0.574	0.440	0.566	0.431	0.559	0.423
C311	0.548	0.359	0.555	0.370	0.549	0.366	0.546	0.431
C312	0.536	0.253	0.544	0.259	0.538	0.256	0.535	0.350
C130	0.731	0.672	0.754	0.724	0.740	0.710	0.729	0.697
C131	0.715	0.549	0.728	0.562	0.718	0.558	0.713	0.655
C132	0.701	0.416	0.713	0.422	0.704	0.421	0.701	0.578
C160	0.566	0.317	0.582	0.331	0.573	0.327	0.566	0.319
C161	0.558	0.336	0.575	0.349	0.566	0.344	0.560	0.401
C162	0.554	0.267	0.568	0.275	0.559	0.273	0.554	0.367

R_R = 1.2						
Imperfection Index	σ_{ULS}/σ_y	σ_{SLS}/σ_y	σ_{ULS}/σ_y	σ_{SLS}/σ_y	σ_{ULS}/σ_y	σ_{SLS}/σ_y
Model ID →	SM490Y_R _R 1.2_T10		SM490Y_R _R 1.2_T30			
C130	0.540	0.512	0.544	0.517		
C131	0.535	0.402	0.539	0.406		
C132	0.536	0.354	0.541	0.359		
C160	0.406	0.231	0.404	0.235		
C161	0.403	0.251	0.401	0.252		
C162	0.398	0.218	0.401	0.218		
C220	0.484	0.413	0.487	0.418		
C221	0.475	0.314	0.478	0.311		
C222	0.470	0.266	0.476	0.256		
C230	0.528	0.505	0.531	0.509		
C231	0.518	0.357	0.521	0.352		
C232	0.511	0.296	0.520	0.295		
C240	0.460	0.362	0.461	0.365		
C241	0.453	0.288	0.454	0.286		
C242	0.450	0.246	0.452	0.235		
C250	0.422	0.280	0.420	0.282		
C251	0.417	0.247	0.414	0.245		
C252	0.414	0.212	0.412	0.211		
C310	0.420	0.311	0.419	0.309		
C311	0.411	0.240	0.410	0.235		
C312	0.409	0.194	0.407	0.190		
C330	0.506	0.500	0.513	0.503		
C331	0.480	0.318	0.486	0.310		
C332	0.479	0.253	0.479	0.250		
C430	0.477	0.474	0.478	0.474		
C431	0.445	0.289	0.446	0.282		
C432	0.441	0.222	0.442	0.219		
C460	0.368	0.223	0.365	0.218		
C461	0.362	0.198	0.358	0.194		
C462	0.360	0.142	0.356	0.141		
C540	0.411	0.343	0.410	0.342		
C541	0.395	0.086	0.393	0.222		
C542	0.393	0.173	0.392	0.170		
C560	0.361	0.221	0.357	0.216		
C561	0.351	0.188	0.348	0.172		
C562	0.350	0.132	0.347	0.131		
Model ID →	SM570_R _R 1.2_T10		SM570_R _R 1.2_T30		SM570_R _R 1.2_T50	
C130	0.525	0.494	0.533	0.503	0.530	0.500
C131	0.519	0.420	0.528	0.399	0.525	0.397
C132	0.520	0.352	0.530	0.335	0.527	0.337
C160	0.414	0.225	0.413	0.229	0.407	0.228
C161	0.411	0.242	0.410	0.239	0.404	0.237
C162	0.409	0.202	0.409	0.199	0.403	0.199
C220	0.482	0.399	0.485	0.406	0.482	0.404
C221	0.473	0.326	0.476	0.307	0.473	0.305
C222	0.471	0.256	0.475	0.242	0.472	0.243
C230	0.514	0.487	0.522	0.496	0.519	0.493
C231	0.505	0.373	0.513	0.346	0.510	0.344
C232	0.505	0.296	0.513	0.276	0.511	0.278

Imperfection Index	σ_{ULS}/σ_y	σ_{SLS}/σ_y	σ_{ULS}/σ_y	σ_{SLS}/σ_y	σ_{ULS}/σ_y	σ_{SLS}/σ_y
C240	0.460	0.347	0.462	0.353	0.458	0.354
C241	0.453	0.298	0.455	0.283	0.451	0.281
C242	0.450	0.233	0.453	0.222	0.449	0.223
C250	0.425	0.270	0.425	0.274	0.420	0.273
C251	0.419	0.254	0.419	0.244	0.415	0.243
C252	0.417	0.199	0.417	0.191	0.413	0.191
C310	0.422	0.296	0.422	0.302	0.418	0.301
C311	0.413	0.250	0.413	0.235	0.409	0.233
C312	0.410	0.184	0.410	0.172	0.407	0.173
C330	0.501	0.481	0.506	0.490	0.503	0.488
C331	0.479	0.335	0.482	0.305	0.480	0.304
C332	0.474	0.252	0.477	0.231	0.475	0.232
C430	0.468	0.466	0.472	0.469	0.469	0.467
C431	0.441	0.308	0.442	0.277	0.440	0.276
C432	0.438	0.223	0.439	0.202	0.437	0.203
C460	0.373	0.211	0.371	0.214	0.367	0.213
C461	0.365	0.192	0.364	0.182	0.360	0.180
C462	0.363	0.133	0.362	0.125	0.359	0.125
C540	0.407	0.331	0.409	0.335	0.406	0.334
C541	0.391	0.242	0.393	0.221	0.390	0.219
C542	0.391	0.166	0.392	0.151	0.389	0.152
C560	0.364	0.208	0.363	0.212	0.359	0.211
C561	0.354	0.184	0.353	0.172	0.349	0.170
C562	0.353	0.124	0.352	0.115	0.348	0.115
Model ID →	SBHS500_R _R 1.2_T10	SBHS500_R _R 1.2_T30	SBHS500_R _R 1.2_T50	SBHS500_R _R 1.2_T50	SBHS500_R _R 1.2_T50	SBHS500_R _R 1.2_T50
C230	0.612	0.576	0.539	0.512	0.530	0.503
C231	0.579	0.355	0.528	0.343	0.520	0.343
C232	0.574	0.276	0.527	0.267	0.520	0.267
C250	0.493	0.320	0.441	0.283	0.435	0.277
C251	0.482	0.267	0.435	0.246	0.429	0.245
C252	0.478	0.203	0.432	0.188	0.427	0.188
C240	0.536	0.417	0.479	0.365	0.472	0.359
C241	0.521	0.302	0.470	0.286	0.464	0.283
C242	0.516	0.231	0.468	0.220	0.462	0.218
C220	0.561	0.473	0.502	0.419	0.495	0.413
C221	0.543	0.322	0.492	0.307	0.485	0.306
C222	0.538	0.248	0.490	0.238	0.483	0.237
C430	0.530	0.516	0.485	0.481	0.479	0.476
C431	0.487	0.284	0.452	0.273	0.448	0.273
C432	0.487	0.201	0.449	0.193	0.444	0.193
C460	0.430	0.251	0.386	0.222	0.380	0.219
C461	0.414	0.199	0.374	0.180	0.372	0.183
C462	0.412	0.135	0.375	0.123	0.371	0.123
C560	0.418	0.248	0.377	0.220	0.372	0.223
C561	0.400	0.190	0.365	0.173	0.361	0.173
C562	0.401	0.123	0.364	0.113	0.360	0.112
C540	0.463	0.377	0.422	0.346	0.416	0.341
C541	0.442	0.234	0.404	0.220	0.399	0.220
C542	0.443	0.157	0.403	0.148	0.399	0.147
C330	0.582	0.564	0.521	0.504	0.515	0.497
C331	0.505	0.312	0.492	0.300	0.488	0.301
C332	0.524	0.230	0.487	0.222	0.483	0.222
C310	0.488	0.350	0.437	0.310	0.520	0.507

Imperfection Index	σ_{ULS}/σ_y	σ_{SLS}/σ_y	σ_{ULS}/σ_y	σ_{SLS}/σ_y	σ_{ULS}/σ_y	σ_{SLS}/σ_y
C311	0.468	0.252	0.426	0.236	0.492	0.304
C312	0.464	0.182	0.423	0.170	0.487	0.225
C130	0.628	0.585	0.551	0.519	0.542	0.510
C131	0.615	0.414	0.545	0.397	0.536	0.396
C132	0.614	0.336	0.546	0.328	0.538	0.327
C160	0.480	0.270	0.430	0.234	0.424	0.232
C161	0.475	0.266	0.427	0.242	0.420	0.241
C162	0.472	0.216	0.425	0.200	0.419	0.198
Model ID →	SBHS700_R _R 1.2_T10	SBHS700_R _R 1.2_T30	SBHS700_R _R 1.2_T50	SBHS700_R _R 1.2_T50	SBHS700_R _R 1.2_T50	SBHS700_R _R 1.2_T50
C230	0.531	0.494	0.531	0.500	0.504	0.473
C231	0.521	0.337	0.521	0.340	0.497	0.338
C232	0.520	0.248	0.521	0.248	0.498	0.247
C250	0.449	0.273	0.450	0.275	0.430	0.261
C251	0.443	0.247	0.444	0.246	0.425	0.240
C252	0.442	0.181	0.442	0.180	0.423	0.176
C240	0.482	0.353	0.483	0.356	0.460	0.338
C241	0.474	0.282	0.474	0.284	0.453	0.278
C242	0.472	0.207	0.472	0.208	0.452	0.204
C220	0.500	0.408	0.502	0.410	0.478	0.388
C221	0.491	0.303	0.492	0.305	0.470	0.301
C222	0.490	0.222	0.490	0.223	0.469	0.221
C430	0.481	0.473	0.481	0.478	0.464	0.461
C431	0.450	0.270	0.451	0.271	0.436	0.270
C432	0.459	0.194	0.448	0.178	0.434	0.178
C460	0.396	0.215	0.396	0.216	0.379	0.206
C461	0.385	0.183	0.385	0.184	0.371	0.179
C462	0.383	0.118	0.384	0.117	0.370	0.114
C560	0.385	0.213	0.385	0.213	0.369	0.204
C561	0.372	0.175	0.373	0.174	0.359	0.170
C562	0.372	0.107	0.372	0.106	0.358	0.104
C540	0.423	0.334	0.423	0.340	0.406	0.325
C541	0.405	0.220	0.405	0.220	0.390	0.218
C542	0.405	0.138	0.406	0.138	0.390	0.136
C330	0.517	0.489	0.517	0.494	0.493	0.467
C331	0.491	0.297	0.492	0.299	0.474	0.297
C332	0.485	0.205	0.487	0.206	0.471	0.205
C310	0.444	0.300	0.444	0.303	0.424	0.287
C311	0.433	0.235	0.433	0.235	0.416	0.001
C312	0.430	0.161	0.430	0.160	0.413	0.158
C130	0.542	0.501	0.542	0.507	0.514	0.480
C131	0.535	0.393	0.535	0.392	0.508	0.388
C132	0.537	0.305	0.537	0.306	0.510	0.305
C160	0.442	0.230	0.443	0.230	0.423	0.219
C161	0.437	0.242	0.477	0.296	0.419	0.233
C162	0.434	0.192	0.436	0.193	0.417	0.187

R_R = 1.4

Imperfection Index	σ_{ULS}/σ_y	σ_{SLS}/σ_y	σ_{ULS}/σ_y	σ_{SLS}/σ_y
Model ID →	SM490Y_R _R 1.4_T10		SM490Y_R _R 1.4_T30	
C130	0.409	0.384	0.404	0.379
C131	0.408	0.307	0.403	0.304
C132	0.415	0.282	0.407	0.279
C160	0.321	0.172	0.313	0.171
C161	0.319	0.178	0.313	0.174
C162	0.321	0.156	0.315	0.154
C220	0.375	0.308	0.369	0.302
C221	0.373	0.222	0.368	0.219
C222	0.375	0.190	0.370	0.188
C230	0.399	0.376	0.394	0.370
C231	0.399	0.255	0.394	0.251
C232	0.403	0.224	0.398	0.222
C240	0.359	0.268	0.353	0.262
C241	0.357	0.204	0.351	0.202
C242	0.358	0.172	0.353	0.171
C250	0.331	0.205	0.324	0.205
C251	0.328	0.174	0.323	0.171
C252	0.330	0.144	0.324	0.144
C310	0.329	0.224	0.324	0.221
C311	0.325	0.159	0.320	0.156
C312	0.326	0.125	0.321	0.044
C330	0.389	0.369	0.384	0.364
C331	0.385	0.212	0.380	0.209
C332	0.388	0.175	0.398	0.174
C430	0.374	0.364	0.369	0.359
C431	0.356	0.183	0.352	0.180
C432	0.359	0.143	0.355	0.142
C460	0.288	0.157	0.282	0.155
C461	0.285	0.116	0.280	0.114
C462	0.286	0.083	0.281	0.088
C540	0.322	0.253	0.317	0.251
C541	0.308	0.138	0.319	0.136
C542	0.313	0.099	0.309	0.098
C560	0.282	0.155	0.276	0.153
C561	0.275	0.106	0.271	0.104
C562	0.279	0.071	0.274	0.070
Model ID →	SM570_R _R 1.4_T10		SM570_R _R 1.4_T30	
C130	0.404	0.377	0.397	0.371
C131	0.401	0.313	0.395	0.297
C132	0.404	0.274	0.399	0.262
C160	0.330	0.170	0.320	0.167
C161	0.328	0.179	0.319	0.174
C162	0.328	0.152	0.320	0.147
C220	0.375	0.302	0.367	0.297
C221	0.371	0.230	0.365	0.215
C222	0.374	0.185	0.368	0.174
C230	0.395	0.369	0.387	0.363
C231	0.392	0.263	0.387	0.244
C232	0.396	0.215	0.391	0.203

Imperfection Index	σ_{ULS}/σ_y	σ_{SLS}/σ_y	σ_{ULS}/σ_y	σ_{SLS}/σ_y
C240	0.362	0.263	0.353	0.258
C241	0.358	0.210	0.351	0.197
C242	0.360	0.168	0.353	0.158
C250	0.337	0.201	0.328	0.198
C251	0.334	0.180	0.326	0.170
C252	0.335	0.141	0.328	0.134
C310	0.335	0.221	0.326	0.217
C311	0.330	0.167	0.322	0.154
C312	0.330	0.123	0.323	0.114
C330	0.386	0.363	0.378	0.356
C331	0.380	0.223	0.375	0.202
C332	0.383	0.169	0.378	0.155
C430	0.373	0.358	0.366	0.352
C431	0.355	0.194	0.349	0.173
C432	0.357	0.139	0.352	0.125
C460	0.297	0.155	0.288	0.152
C461	0.291	0.123	0.284	0.113
C462	0.293	0.081	0.286	0.074
C540	0.317	0.247	0.318	0.247
C541	0.309	0.148	0.304	0.132
C542	0.314	0.097	0.308	0.087
C560	0.290	0.152	0.282	0.147
C561	0.281	0.114	0.275	0.103
C562	0.284	0.071	0.278	0.063
Model ID →	SBHS700_R _R 1.4_T10		SBHS700_R _R 1.4_T50	
C230	0.376	0.346	0.385	0.358
C231	0.373	0.238	0.383	0.236
C232	0.377	0.177	0.386	0.175
C250	0.331	0.192	0.339	0.196
C251	0.329	0.167	0.336	0.169
C252	0.330	0.123	0.338	0.123
C240	0.351	0.246	0.359	0.255
C241	0.348	0.197	0.356	0.196
C242	0.349	0.145	0.358	0.144
C220	0.361	0.286	0.370	0.294
C221	0.358	0.212	0.367	0.211
C222	0.361	0.158	0.369	0.156
C430	0.358	0.336	0.366	0.347
C431	0.343	0.170	0.350	0.166
C432	0.346	0.107	0.353	0.104
C460	0.295	0.145	0.300	0.149
C461	0.289	0.113	0.294	0.113
C462	0.291	0.066	0.296	0.065
C560	0.289	0.143	0.294	0.146
C561	0.278	0.104	0.284	0.103
C562	0.282	0.056	0.287	0.054
C540	0.317	0.238	0.324	0.237
C541	0.302	0.132	0.307	0.129
C542	0.306	0.075	0.312	0.073
C330	0.368	0.341	0.377	0.352
C331	0.363	0.198	0.372	0.194
C332	0.367	0.135	0.376	0.132
C310	0.328	0.207	0.335	0.214

Imperfection Index	σ_{ULS}/σ_y	σ_{SLS}/σ_y	σ_{ULS}/σ_y	σ_{SLS}/σ_y
C311	0.324	0.153	0.330	0.153
C312	0.325	0.102	0.332	0.101
C130	0.384	0.354	0.394	0.366
C131	0.381	0.288	0.391	0.288
C132	0.384	0.235	0.394	0.234
C160	0.329	0.161	0.336	0.167
C161	0.326	0.170	0.332	0.173
C162	0.325	0.139	0.333	0.140

APPENDIX E

FEA Results for Model-2

$R_R = 0.4$

$x_1 = \sigma_{rc}/\sigma_y$	$x_2 = 1000\delta_{0l}/a$	σ_{ULS}/σ_y	$x_1 = \sigma_{rc}/\sigma_y$	$x_2 = 1000\delta_{0l}/a$	σ_{ULS}/σ_y
SM490Y_Rr04_T20			SBHS500_Rr04_T20		
0.085	-0.330	0.9537	0.375	-0.757	0.898
0.085	0.096	0.9634	0.375	0.096	0.889
0.085	0.522	0.9495	0.520	1.375	0.879
0.230	-0.330	0.9480	0.520	0.096	0.892
0.230	0.096	0.9652	0.665	0.522	0.910
0.230	0.522	0.9405	0.665	1.375	0.881
0.230	0.949	0.9286	0.085	1.375	0.908
0.375	-0.330	0.9508	0.085	0.096	0.938
0.375	0.096	0.9947	0.230	0.522	0.903
0.375	0.522	0.9431	0.230	0.949	0.890
0.520	0.096	0.9672	0.230	-0.330	0.912
0.520	0.949	0.9322	0.230	0.096	0.932
SM490Y_Rr04_T30			SBHS500_Rr04_T30		
0.085	-0.330	0.9466	0.375	-0.757	0.900
0.085	0.096	0.9520	0.375	0.096	0.935
0.085	0.522	0.9425	0.520	1.375	0.882
0.230	-0.330	0.9400	0.520	0.096	0.936
0.230	0.096	0.9569	0.665	0.522	0.912
0.230	0.522	0.9326	0.665	1.375	0.883
0.230	0.949	0.9211	0.085	1.375	0.909
0.375	-0.330	0.9426	0.085	0.096	0.939
0.375	0.096	0.9595	0.230	0.522	0.905
0.375	0.522	0.9353	0.230	0.949	0.892
0.520	0.096	0.9594	0.230	-0.330	0.914
0.520	0.949	0.9244	0.230	0.096	0.934
SM490Y_Rr04_T50			SBHS500_Rr04_T50		
0.085	-0.330	0.9707	0.375	-0.757	0.898
0.085	0.096	0.9706	0.375	0.096	0.932
0.085	0.522	0.9573	0.520	1.375	0.881
0.230	-0.330	0.9566	0.520	0.096	0.937
0.230	0.096	0.9696	0.665	0.522	0.911
0.230	0.522	0.9491	0.665	1.375	0.882
0.230	0.949	0.9371	0.085	1.375	0.909
0.375	-0.330	0.9429	0.085	0.096	0.936
0.375	0.096	0.9497	0.230	0.522	0.904
0.375	0.522	0.9377	0.230	0.949	0.891
0.520	0.096	0.9735	0.230	-0.330	0.913
0.520	0.949	0.9407	0.230	0.096	0.933
SM490Y_Rr04_T70			SBHS500_Rr04_T70		
0.085	-0.330	0.9498	0.375	-0.757	0.897
0.085	0.096	0.9569	0.375	0.096	0.933
0.085	0.522	0.9458	0.520	1.375	0.879
0.230	-0.330	0.9444	0.520	0.096	0.935

$x_1 = \sigma_{rc}/\sigma_y$	$x_2 = 1000\delta_{01}/a$	σ_{ULS}/σ_y	$x_1 = \sigma_{rc}/\sigma_y$	$x_2 = 1000\delta_{01}/a$	σ_{ULS}/σ_y
0.230	0.096	0.9606	0.665	0.522	0.909
0.230	0.522	0.9372	0.665	1.375	0.880
0.230	0.949	0.9258	0.085	1.375	0.908
0.375	-0.330	0.9471	0.085	0.096	0.938
0.375	0.096	0.9625	0.230	0.522	0.903
0.375	0.522	0.9398	0.230	0.949	0.889
0.520	0.096	0.9626	0.230	-0.330	0.912
0.520	0.949	0.9292	0.230	0.096	0.932
SM490Y_Rr04_T90			SBHS500_Rr04_T90		
0.085	-0.330	0.9554	0.375	-0.757	0.904
0.085	0.096	0.9660	0.375	0.096	0.941
0.085	0.522	0.9512	0.520	1.375	0.886
0.230	-0.330	0.9519	0.520	0.096	0.942
0.230	0.096	0.9683	0.665	0.522	0.916
0.230	0.522	0.9446	0.665	1.375	0.888
0.230	0.949	0.9330	0.085	1.375	0.911
0.375	-0.330	0.9530	0.085	0.096	0.940
0.375	0.096	0.9933	0.230	0.522	0.909
0.375	0.522	0.9456	0.230	0.949	0.896
0.520	0.096	0.9684	0.230	-0.330	0.918
0.520	0.949	0.9351	0.230	0.096	0.938
SM570_Rr04_T20			SBHS700_Rr04_T20		
0.375	-0.757	0.920	0.085	0.096	0.931
0.375	0.096	0.955	0.085	1.375	0.895
0.520	1.375	0.903	0.230	-0.330	0.880
0.520	0.096	0.963	0.230	0.096	0.899
0.665	0.522	0.931	0.230	0.522	0.871
0.665	1.375	0.904	0.230	0.949	0.859
0.085	1.375	0.920	0.375	-0.757	0.864
0.085	0.096	0.950	0.375	0.096	0.902
0.230	0.522	0.924	0.520	0.096	0.905
0.230	0.949	0.911	0.520	1.375	0.845
0.230	-0.330	0.932	0.665	0.522	0.877
0.230	0.096	0.952	0.665	1.375	0.846
SM570_Rr04_T30			SBHS700_Rr04_T30		
0.375	-0.757	0.916	0.085	0.096	0.914
0.375	0.096	0.950	0.085	1.375	0.890
0.520	1.375	0.899	0.230	-0.330	0.872
0.520	0.096	0.951	0.230	0.096	0.891
0.665	0.522	0.927	0.230	0.522	0.863
0.665	1.375	0.900	0.230	0.949	0.850
0.085	1.375	0.917	0.375	-0.757	0.853
0.085	0.096	0.946	0.375	0.096	0.894
0.230	0.522	0.920	0.520	0.096	0.896
0.230	0.949	0.908	0.520	1.375	0.834
0.230	-0.330	0.929	0.665	0.522	0.868
0.230	0.096	0.948	0.665	1.375	0.836
SM570_Rr04_T50			SBHS700_Rr04_T50		
0.375	-0.757	0.926	0.085	0.096	0.930
0.375	0.096	0.961	0.085	1.375	0.890
0.520	1.375	0.910	0.230	-0.330	0.873
0.520	0.096	0.962	0.230	0.096	0.891
0.665	0.522	0.937	0.230	0.522	0.864

Appendix E: FEA Results for Model-2

$x_1 = \sigma_{rc}/\sigma_y$	$x_2 = 1000\delta_{01}/a$	σ_{ULS}/σ_y	$x_1 = \sigma_{rc}/\sigma_y$	$x_2 = 1000\delta_{01}/a$	σ_{ULS}/σ_y
0.665	1.375	0.911	0.230	0.949	0.851
0.085	1.375	0.925	0.375	-0.757	0.854
0.085	0.096	0.955	0.375	0.096	0.894
0.230	0.522	0.930	0.520	0.096	0.897
0.230	0.949	0.917	0.520	1.375	0.835
0.230	-0.330	0.938	0.665	0.522	0.868
0.230	0.096	0.958	0.665	1.375	0.837
SM570_Rr04_T70			SBHS700_Rr04_T70		
0.375	-0.757	0.926	0.085	0.096	0.928
0.375	0.096	0.961	0.085	1.375	0.892
0.520	1.375	0.910	0.230	-0.330	0.868
0.520	0.096	0.962	0.230	0.096	0.886
0.665	0.522	0.938	0.230	0.522	0.859
0.665	1.375	0.911	0.230	0.949	0.846
0.085	1.375	0.926	0.375	-0.757	0.848
0.085	0.096	0.956	0.375	0.096	0.889
0.230	0.522	0.930	0.520	0.096	0.891
0.230	0.949	0.918	0.520	1.375	0.829
0.230	-0.330	0.939	0.665	0.522	0.862
0.230	0.096	0.958	0.665	1.375	0.831
SM570_Rr04_T90			SBHS700_Rr04_T90		
0.375	-0.757	0.923	0.085	0.096	0.931
0.375	0.096	0.957	0.085	1.375	0.890
0.520	1.375	0.907	0.230	-0.330	0.873
0.520	0.096	0.958	0.230	0.096	0.892
0.665	0.522	0.935	0.230	0.522	0.864
0.665	1.375	0.908	0.230	0.949	0.852
0.085	1.375	0.923	0.375	-0.757	0.855
0.085	0.096	0.950	0.375	0.096	0.895
0.230	0.522	0.928	0.520	0.096	0.897
0.230	0.949	0.915	0.520	1.375	0.836
0.230	-0.330	0.936	0.665	0.522	0.869
0.230	0.096	0.953	0.665	1.375	0.837

R_R = 0.6

$x_1 = \sigma_{rc}/\sigma_y$	$x_2 = 1000\delta_{01}/a$	σ_{ULS}/σ_y	$x_1 = \sigma_{rc}/\sigma_y$	$x_2 = 1000\delta_{01}/a$	σ_{ULS}/σ_y
SM490Y_Rr06_T10			SBHS500_Rr06_T10		
0.085	-0.330	1.0511	0.375	-0.757	0.840
0.085	0.096	1.0662	0.375	0.096	0.875
0.085	0.522	1.0369	0.520	1.375	0.821
0.230	-0.330	0.9605	0.520	0.096	0.877
0.230	0.096	0.9792	0.665	0.522	0.854
0.230	0.522	0.9508	0.665	1.375	0.823
0.230	0.949	0.9355	0.085	1.375	0.879
0.375	-0.330	0.9570	0.085	0.096	0.928
0.375	0.096	0.9816	0.230	0.522	0.848
0.375	0.522	0.9420	0.230	0.949	0.836
0.520	0.096	0.9788	0.230	-0.330	0.856
0.520	0.949	0.9185	0.230	0.096	0.876
SM490Y_Rr06_T20			SBHS500_Rr06_T20		
0.085	-0.330	0.9183	0.375	-0.757	0.814
0.085	0.096	0.9326	0.375	0.096	0.857
0.085	0.522	0.9088	0.520	1.375	0.794
0.230	-0.330	0.8472	0.520	0.096	0.857
0.230	0.096	0.8694	0.665	0.522	0.830
0.230	0.522	0.8392	0.665	1.375	0.796
0.230	0.949	0.8256	0.085	1.375	0.865
0.375	-0.330	0.8473	0.085	0.096	0.925
0.375	0.096	0.8695	0.230	0.522	0.829
0.375	0.522	0.8393	0.230	0.949	0.817
0.520	0.096	0.8660	0.230	-0.330	0.837
0.520	0.949	0.8130	0.230	0.096	0.859
SM490Y_Rr06_T30			SBHS500_Rr06_T30		
0.085	-0.330	0.9065	0.375	-0.757	0.818
0.085	0.096	0.9200	0.375	0.096	0.859
0.085	0.522	0.8911	0.520	1.375	0.798
0.230	-0.330	0.8265	0.520	0.096	0.859
0.230	0.096	0.8489	0.665	0.522	0.833
0.230	0.522	0.8185	0.665	1.375	0.799
0.230	0.949	0.8043	0.085	1.375	0.867
0.375	-0.330	0.8220	0.085	0.096	1.008
0.375	0.096	0.8444	0.230	0.522	0.832
0.375	0.522	0.8076	0.230	0.949	0.819
0.520	0.096	0.8444	0.230	-0.330	0.839
0.520	0.949	0.7877	0.230	0.096	0.861
SM490Y_Rr06_T50			SBHS500_Rr06_T50		
0.085	-0.330	0.9237	0.375	-0.757	0.812
0.085	0.096	0.9378	0.375	0.096	0.856
0.085	0.522	0.9137	0.520	1.375	0.792
0.230	-0.330	0.8427	0.520	0.096	0.856
0.230	0.096	0.8669	0.665	0.522	0.828
0.230	0.522	0.8320	0.665	1.375	0.794
0.230	0.949	0.8176	0.085	1.375	0.864
0.375	-0.330	0.8359	0.085	0.096	0.936
0.375	0.096	0.8625	0.230	0.522	0.828
0.375	0.522	0.8214	0.230	0.949	0.815
0.520	0.096	0.8630	0.230	-0.330	0.835

Appendix E: FEA Results for Model-2

$x_1 = \sigma_{rc}/\sigma_y$	$x_2 = 1000\delta_{01}/a$	σ_{ULS}/σ_y	$x_1 = \sigma_{rc}/\sigma_y$	$x_2 = 1000\delta_{01}/a$	σ_{ULS}/σ_y
0.520	0.949	0.8002	0.230	0.096	0.858
SM490Y_Rr06_T70			SBHS500_Rr06_T70		
0.085	-0.330	0.9060	0.375	-0.757	0.810
0.085	0.096	0.8281	0.375	0.096	0.855
0.085	0.522	0.8907	0.520	1.375	0.790
0.230	-0.330	0.8281	0.520	0.096	0.854
0.230	0.096	0.8497	0.665	0.522	0.826
0.230	0.522	0.8199	0.665	1.375	0.791
0.230	0.949	0.8052	0.085	1.375	0.863
0.375	-0.330	0.8235	0.085	0.096	0.934
0.375	0.096	0.8452	0.230	0.522	0.826
0.375	0.522	0.8088	0.230	0.949	0.813
0.520	0.096	0.8444	0.230	-0.330	0.833
0.520	0.949	0.7881	0.230	0.096	0.857
SM570_Rr06_T10			SBHS700_Rr06_T20		
0.375	-0.757	0.834	0.085	0.096	0.879
0.375	0.096	0.871	0.085	1.375	0.740
0.520	1.375	0.815	0.230	-0.330	0.764
0.520	0.096	0.873	0.230	0.096	0.778
0.665	0.522	0.849	0.230	0.522	0.753
0.665	1.375	0.816	0.230	0.949	0.731
0.085	1.375	0.875	0.375	-0.757	0.688
0.085	0.096	0.926	0.375	0.096	0.763
0.230	0.522	0.844	0.520	0.096	0.763
0.230	0.949	0.831	0.520	1.375	0.655
0.230	-0.330	0.851	0.665	0.522	0.694
0.230	0.096	0.871	0.665	1.375	0.655
SM570_Rr06_T20			SBHS700_Rr06_T30		
0.375	-0.757	0.823	0.085	0.096	0.919
0.375	0.096	0.866	0.085	1.375	0.827
0.520	1.375	0.802	0.230	-0.330	0.815
0.520	0.096	0.890	0.230	0.096	0.831
0.665	0.522	0.838	0.230	0.522	0.805
0.665	1.375	0.804	0.230	0.949	0.769
0.085	1.375	0.872	0.375	-0.757	0.761
0.085	0.096	0.943	0.375	0.096	0.832
0.230	0.522	0.837	0.520	0.096	0.830
0.230	0.949	0.824	0.520	1.375	0.739
0.230	-0.330	0.845	0.665	0.522	0.772
0.230	0.096	0.868	0.665	1.375	0.740
SM570_Rr06_T30			SBHS700_Rr06_T50		
3.000	-0.757	0.809	0.085	0.096	0.918
0.375	0.096	0.854	0.085	1.375	0.821
0.520	1.375	0.788	0.230	-0.330	0.812
0.520	0.096	0.854	0.230	0.096	0.828
0.665	0.522	0.825	0.230	0.522	0.802
0.665	1.375	0.790	0.230	0.949	0.783
0.085	1.375	0.860	0.375	-0.757	0.756
0.085	0.096	0.923	0.375	0.096	0.829
0.230	0.522	0.826	0.520	0.096	0.827
0.230	0.949	0.813	0.520	1.375	0.733
0.230	-0.330	0.833	0.665	0.522	0.767
0.230	0.096	0.856	0.665	1.375	0.735

Appendix E: FEA Results for Model-2

$x_1 = \sigma_{rc}/\sigma_y$	$x_2 = 1000\delta_{01}/a$	σ_{ULS}/σ_y	$x_1 = \sigma_{rc}/\sigma_y$	$x_2 = 1000\delta_{01}/a$	σ_{ULS}/σ_y
SM570_Rr06_T50			SBHS700_Rr06_T70		
0.375	-0.757	0.830	0.085	0.096	0.918
0.375	0.096	0.875	0.085	1.375	0.822
0.520	1.375	0.809	0.230	-0.330	0.813
0.520	0.096	0.876	0.230	0.096	0.829
0.665	0.522	0.846	0.230	0.522	0.803
0.665	1.375	0.811	0.230	0.949	0.784
0.085	1.375	0.879	0.375	-0.757	0.756
0.085	0.096	0.947	0.375	0.096	0.830
0.230	0.522	0.844	0.520	0.096	0.827
0.230	0.949	0.831	0.520	1.375	0.734
0.230	-0.330	0.853	0.665	0.522	0.767
0.230	0.096	0.877	0.665	1.375	0.735
SM570_Rr06_T70			SBHS700_Rr06_T90		
0.375	-0.757	0.812	0.085	0.096	0.918
0.375	0.096	0.855	0.085	1.375	0.820
0.520	1.375	0.791	0.230	-0.330	0.812
0.520	0.096	0.857	0.230	0.096	0.828
0.665	0.522	0.828	0.230	0.522	0.802
0.665	1.375	0.793	0.230	0.949	0.783
0.085	1.375	0.862	0.375	-0.757	0.754
0.085	0.096	0.923	0.375	0.096	0.827
0.230	0.522	0.829	0.520	0.096	0.826
0.230	0.949	0.816	0.520	1.375	0.732
0.230	-0.330	0.837	0.665	0.522	0.765
0.230	0.096	0.856	0.665	1.375	0.733

R_R = 0.8

$x_1 = \sigma_{rc}/\sigma_y$	$x_2 = 1000\delta_{01}/a$	σ_{ULS}/σ_y	$x_1 = \sigma_{rc}/\sigma_y$	$x_2 = 1000\delta_{01}/a$	σ_{ULS}/σ_y
SM490Y_Rr08_T10			SBHS500_Rr08_T10		
0.085	-0.330	0.8252	0.375	-0.757	0.690
0.085	0.096	0.8793	0.375	0.096	0.760
0.085	0.522	0.7888	0.520	1.375	0.630
0.230	-0.330	0.7471	0.520	0.096	0.760
0.230	0.096	0.7676	0.665	0.522	0.696
0.230	0.522	0.7260	0.665	1.375	0.627
0.230	0.949	0.6763	0.085	1.375	0.735
0.375	-0.330	0.6817	0.085	0.096	0.901
0.375	0.096	0.7127	0.230	0.522	0.766
0.375	0.522	0.6650	0.230	0.949	0.736
0.520	0.096	0.7135	0.230	-0.330	0.777
0.520	0.949	0.6083	0.230	0.096	0.793
0.665	0.096	0.7262			
SM490Y_Rr08_T20			SBHS500_Rr08_T20		
0.085	-0.330	0.8583	0.375	-0.757	0.674
0.085	0.096	0.9059	0.375	0.096	0.739
0.085	0.522	0.8205	0.520	1.375	0.611
0.230	-0.330	0.7654	0.520	0.096	0.734
0.230	0.096	0.7871	0.665	0.522	0.677
0.230	0.522	0.7494	0.665	1.375	0.604
0.230	0.949	0.7047	0.085	1.375	0.710
0.375	-0.330	0.7041	0.085	0.096	0.891
0.375	0.096	0.7396	0.230	0.522	0.755
0.375	0.522	0.6858	0.230	0.949	0.714
0.520	0.096	0.7451	0.230	-0.330	0.768
0.520	0.949	0.6304	0.230	0.096	0.784
0.665	0.096	0.7547			
SM490Y_Rr08_T30			SBHS500_Rr08_T30		
0.085	-0.330	0.8303	0.375	-0.757	0.670
0.085	0.096	0.8834	0.375	0.096	0.732
0.085	0.522	0.7931	0.520	1.375	0.606
0.230	-0.330	0.7510	0.520	0.096	0.727
0.230	0.096	0.7725	0.665	0.522	0.671
0.230	0.522	0.7309	0.665	1.375	0.597
0.230	0.949	0.6794	0.085	1.375	0.704
0.375	-0.330	0.6874	0.085	0.096	0.888
0.375	0.096	0.7215	0.230	0.522	0.751
0.375	0.522	0.6694	0.230	0.949	0.708
0.520	0.096	0.7248	0.230	-0.330	0.764
0.520	0.949	0.6118	0.230	0.096	0.780
0.665	0.096	0.7347			
SM490Y_Rr08_T50			SBHS500_Rr08_T50		
0.085	-0.330	0.8641	0.375	-0.757	0.668
0.085	0.096	0.9098	0.375	0.096	0.731
0.085	0.522	0.8231	0.520	1.375	0.604
0.230	-0.330	0.7666	0.520	0.096	0.726
0.230	0.096	0.7902	0.665	0.522	0.668
0.230	0.522	0.7495	0.665	1.375	0.595
0.230	0.949	0.7022	0.085	1.375	0.701
0.375	-0.330	0.7033	0.085	0.096	0.887

$x_1 = \sigma_{rc}/\sigma_y$	$x_2 = 1000\delta_{01}/a$	σ_{ULS}/σ_y	$x_1 = \sigma_{rc}/\sigma_y$	$x_2 = 1000\delta_{01}/a$	σ_{ULS}/σ_y
0.375	0.096	0.7354	0.230	0.522	0.749
0.375	0.522	0.6847	0.230	0.949	0.705
0.520	0.096	0.7366	0.230	-0.330	0.764
0.520	0.949	0.6266	0.230	0.096	0.780
0.665	0.096	0.7431			
SM570_Rr08_T10			SBHS700_Rr08_T20		
0.375	-0.757	0.683	0.085	0.096	0.963
0.375	0.096	0.752	0.085	1.375	0.870
0.520	1.375	0.621	0.230	-0.330	0.850
0.520	0.096	0.748	0.230	0.096	0.872
0.665	0.522	0.687	0.230	0.522	0.840
0.665	1.375	0.618	0.230	0.949	0.821
0.085	1.375	0.721	0.375	-0.757	0.800
0.085	0.096	0.898	0.375	0.096	0.875
0.230	0.522	0.761	0.520	0.096	0.871
0.230	0.949	0.725	0.520	1.375	0.773
0.230	-0.330	0.774	0.665	0.522	0.816
0.230	0.096	0.790	0.665	1.375	0.775
SM570_Rr08_T20			SBHS700_Rr08_T30		
0.375	-0.757	0.675	0.085	0.096	0.878
0.375	0.096	0.743	0.085	1.375	0.693
0.520	1.375	0.611	0.230	-0.330	0.754
0.520	0.096	0.738	0.230	0.096	0.783
0.665	0.522	0.678	0.230	0.522	0.738
0.665	1.375	0.607	0.230	0.949	0.696
0.085	1.375	0.708	0.375	-0.757	0.660
0.085	0.096	0.892	0.375	0.096	0.719
0.230	0.522	0.755	0.520	0.096	0.715
0.230	0.949	0.714	0.520	1.375	0.598
0.230	-0.330	0.769	0.665	0.522	0.660
0.230	0.096	0.785	0.665	1.375	0.589
SM570_Rr08_T30			SBHS700_Rr08_T50		
0.375	-0.757	0.680	0.085	0.096	0.895
0.375	0.096	0.750	0.085	1.375	0.737
0.520	1.375	0.618	0.230	-0.330	0.770
0.520	0.096	0.746	0.230	0.096	0.784
0.665	0.522	0.684	0.230	0.522	0.760
0.665	1.375	0.615	0.230	0.949	0.731
0.085	1.375	0.716	0.375	-0.757	0.684
0.085	0.096	0.897	0.375	0.096	0.741
0.230	0.522	0.760	0.520	0.096	0.737
0.230	0.949	0.721	0.520	1.375	0.629
0.230	-0.330	0.773	0.665	0.522	0.689
0.230	0.096	0.789	0.665	1.375	0.622
SM570_Rr08_T50			SBHS700_Rr08_T70		
0.375	-0.757	0.680	0.085	0.096	0.894
0.375	0.096	0.745	0.085	1.375	0.736
0.520	1.375	0.614	0.230	-0.330	0.770
0.520	0.096	0.742	0.230	0.096	0.729
0.665	0.522	0.681	0.230	0.522	0.759
0.665	1.375	0.605	0.230	0.949	0.729
0.085	1.375	0.715	0.375	-0.757	0.683
0.085	0.096	0.897	0.375	0.096	0.740

Appendix E: FEA Results for Model-2

$x_1 = \sigma_{rc}/\sigma_y$	$x_2 = 1000\delta_{01}/a$	σ_{ULS}/σ_y	$x_1 = \sigma_{rc}/\sigma_y$	$x_2 = 1000\delta_{01}/a$	σ_{ULS}/σ_y
0.230	0.522	0.762	0.520	0.096	0.736
0.230	0.949	0.723	0.520	1.375	0.627
0.230	-0.330	0.776	0.665	0.522	0.687
0.230	0.096	0.794	0.665	1.375	0.620
SBHS700_Rr08_T90					
			0.085	0.096	0.894
			0.085	1.375	0.735
			0.230	-0.330	0.769
			0.230	0.096	0.769
			0.230	0.522	0.759
			0.230	0.949	0.729
			0.375	-0.757	0.683
			0.375	0.096	0.740
			0.520	0.096	0.735
			0.520	1.375	0.627
			0.665	0.522	0.687
			0.665	1.375	0.620

R_R = 1.0							
$x_1 = \sigma_{rc}/\sigma_y$	$x_2 = 1000\delta_{0l}/a$	σ_{ULS}/σ_y	σ_{SLS}/σ_y	$x_1 = \sigma_{rc}/\sigma_y$	$x_2 = 1000\delta_{0l}/a$	σ_{ULS}/σ_y	σ_{SLS}/σ_y
SM490Y_Rr10_T10				SBHS500_Rr10_T20			
0.085	-0.330	0.675	0.619	0.085	0.096	0.787	0.787
0.085	0.096	0.748	0.748	0.085	1.375	0.585	0.364
0.085	0.522	0.640	0.540	0.230	-0.330	0.666	0.643
0.230	-0.330	0.621	0.603	0.230	0.096	0.721	0.721
0.230	0.096	0.687	0.687	0.230	0.522	0.635	0.561
0.230	0.522	0.588	0.524	0.230	0.949	0.590	0.433
0.230	0.949	0.543	0.403	0.375	-0.757	0.581	0.475
0.375	-0.330	0.581	0.554	0.375	0.096	0.637	0.631
0.375	0.096	0.614	0.610	0.520	0.096	0.611	0.587
0.375	0.522	0.559	0.510	0.520	1.375	0.513	0.336
0.520	0.096	0.571	0.549	0.665	0.522	0.555	0.454
0.520	0.949	0.500	0.391	0.665	1.375	0.498	0.322
0.665	0.096	0.586	0.566				
SM490Y_Rr10_T20				SBHS500_Rr10_T30			
0.085	-0.330	0.717	0.687	0.085	0.096	0.793	0.793
0.085	0.096	0.796	0.796	0.085	1.375	0.590	0.369
0.085	0.522	0.678	0.599	0.230	-0.330	0.670	0.650
0.230	-0.330	0.651	0.648	0.230	0.096	0.724	0.724
0.230	0.096	0.713	0.713	0.230	0.522	0.639	0.568
0.230	0.522	0.620	0.581	0.230	0.949	0.595	0.439
0.230	0.949	0.572	0.448	0.375	-0.757	0.586	0.481
0.375	-0.330	0.608	0.581	0.375	0.096	0.640	0.633
0.375	0.096	0.633	0.626	0.520	0.096	0.615	0.592
0.375	0.522	0.590	0.540	0.520	1.375	0.517	0.341
0.520	0.096	0.602	0.576	0.665	0.522	0.559	0.458
0.520	0.949	0.523	0.422	0.665	1.375	0.502	0.326
0.665	0.096	0.623	0.604				
SM490Y_Rr10_T30				SBHS500_Rr10_T50			
0.085	-0.330	0.675	0.624	0.085	0.096	0.755	0.747
0.085	0.096	0.750	0.750	0.085	1.375	0.562	0.341
0.085	0.522	0.638	0.545	0.230	-0.330	0.644	0.605
0.230	-0.330	0.620	0.606	0.230	0.096	0.702	0.702
0.230	0.096	0.687	0.688	0.230	0.522	0.613	0.526
0.230	0.522	0.586	0.528	0.230	0.949	0.568	0.407
0.230	0.949	0.540	0.406	0.375	-0.757	0.559	0.446
0.375	-0.330	0.580	0.554	0.375	0.096	0.625	0.622
0.375	0.096	0.616	0.611	0.520	0.096	0.585	0.559
0.375	0.522	0.558	0.511	0.520	1.375	0.497	0.315
0.520	0.096	0.572	0.551	0.665	0.522	0.536	0.436
0.520	0.949	0.498	0.392	0.665	1.375	0.480	0.305
0.665	0.096	0.587	0.568				
SM570_Rr10_T10				SBHS700_Rr10_T10			
0.085	0.096	0.794	0.793	0.085	0.096	0.820	0.820
0.085	1.375	0.585	0.370	0.085	1.375	0.633	0.376
0.230	-0.330	0.668	0.650	0.230	-0.330	0.697	0.671
0.230	0.096	0.724	0.723	0.230	0.096	0.740	0.740
0.230	0.522	0.636	0.569	0.230	0.522	0.669	0.585
0.230	0.949	0.592	0.440	0.230	0.949	0.630	0.453
0.375	-0.757	0.582	0.481	0.375	-0.757	0.610	0.496
0.375	0.096	0.640	0.633	0.375	0.096	0.650	0.639

Appendix E: FEA Results for Model-2

$x_1 = \sigma_{rc}/\sigma_y$	$x_2 = 1000\delta_{01}/a$	σ_{ULS}/σ_y	σ_{SLS}/σ_y	$x_1 = \sigma_{rc}/\sigma_y$	$x_2 = 1000\delta_{01}/a$	σ_{ULS}/σ_y	σ_{SLS}/σ_y
0.520	0.096	0.615	0.593	0.520	0.096	0.637	0.612
0.520	1.375	0.514	0.342	0.520	1.375	0.544	0.351
0.665	0.522	0.557	0.458	0.665	0.522	0.583	0.467
0.665	1.375	0.499	0.326	0.665	1.375	0.533	0.332
SM570_Rr10_T20				SBHS700_Rr10_T20			
0.085	0.096	0.773	0.773	0.085	0.096	0.805	0.805
0.085	1.375	0.569	0.357	0.085	1.375	0.620	0.365
0.230	-0.330	0.654	0.630	0.230	-0.330	0.687	0.653
0.230	0.096	0.712	0.711	0.230	0.096	0.733	0.733
0.230	0.522	0.622	0.549	0.230	0.522	0.659	0.569
0.230	0.949	0.577	0.425	0.230	0.949	0.618	0.440
0.375	-0.757	0.569	0.466	0.375	-0.757	0.601	0.481
0.375	0.096	0.632	0.628	0.375	0.096	0.644	0.635
0.520	0.096	0.600	0.577	0.520	0.096	0.625	0.600
0.520	1.375	0.503	0.330	0.520	1.375	0.536	0.340
0.665	0.522	0.545	0.448	0.665	0.522	0.573	0.459
0.665	1.375	0.487	0.317	0.665	1.375	0.524	0.326
SM570_Rr10_T30				SBHS700_Rr10_T30			
0.085	0.096	0.776	0.776	0.085	0.096	0.761	0.743
0.085	1.375	0.571	0.358	0.085	1.375	0.587	0.336
0.230	-0.330	0.656	0.633	0.230	-0.330	0.659	0.601
0.230	0.096	0.713	0.712	0.230	0.096	0.710	0.710
0.230	0.522	0.624	0.552	0.230	0.522	0.630	0.524
0.230	0.949	0.579	0.427	0.230	0.949	0.588	0.405
0.375	-0.757	0.570	0.467	0.375	-0.757	0.575	0.444
0.375	0.096	0.633	0.628	0.375	0.096	0.627	0.625
0.520	0.096	0.602	0.579	0.520	0.096	0.591	0.558
0.520	1.375	0.505	0.331	0.520	1.375	0.513	0.314
0.665	0.522	0.547	0.449	0.665	0.522	0.546	0.436
0.665	1.375	0.488	0.318	0.665	1.375	0.498	0.305
SBHS500_Rr10_T10				SBHS700_Rr10_T50			
0.085	0.096	0.803	0.803	0.085	0.096	0.773	0.759
0.085	1.375	0.602	0.381	0.085	1.375	0.594	0.343
0.230	-0.330	0.678	0.661	0.230	-0.330	0.666	0.614
0.230	0.096	0.730	0.729	0.230	0.096	0.716	0.716
0.230	0.522	0.647	0.580	0.230	0.522	0.637	0.534
0.230	0.949	0.605	0.451	0.230	0.949	0.580	0.370
0.375	-0.757	0.594	0.492	0.375	-0.757	0.581	0.453
0.375	0.096	0.645	0.636	0.375	0.096	0.631	0.627
0.520	0.096	0.625	0.602	0.520	0.096	0.600	0.569
0.520	1.375	0.524	0.349	0.520	1.375	0.519	0.321
0.665	0.522	0.566	0.464	0.665	0.522	0.553	0.442
0.665	1.375	0.509	0.332	0.665	1.375	0.504	0.311

R_R = 1.2							
$x_1 = \sigma_{rc}/\sigma_y$	$x_2 = 1000\delta_{0l}/a$	σ_{ULS}/σ_y	σ_{SLS}/σ_y	$x_1 = \sigma_{rc}/\sigma_y$	$x_2 = 1000\delta_{0l}/a$	σ_{ULS}/σ_y	σ_{SLS}/σ_y
SM490Y_Rr12_T10				SBHS500_Rr12_T10			
0.085	-0.330	0.523	0.440	0.085	0.096	0.583	0.550
0.085	0.096	0.563	0.535	0.085	1.375	0.461	0.250
0.085	0.522	0.499	0.383	0.230	-0.330	0.523	0.441
0.230	-0.330	0.492	0.423	0.230	0.096	0.561	0.512
0.230	0.096	0.538	0.517	0.230	0.522	0.500	0.383
0.230	0.522	0.467	0.366	0.230	0.949	0.465	0.295
0.230	0.949	0.430	0.279	0.375	-0.757	0.453	0.318
0.375	-0.330	0.462	0.409	0.375	0.096	0.533	0.526
0.375	0.096	0.508	0.506	0.520	0.096	0.485	0.476
0.375	0.522	0.442	0.411	0.520	1.375	0.399	0.316
0.520	0.096	0.471	0.469	0.665	0.522	0.420	0.343
0.520	0.949	0.391	0.356	0.665	1.375	0.387	0.306
0.665	0.096	0.457	0.436				
SM490Y_Rr12_T20				SBHS500_Rr12_T20			
0.085	-0.330	0.522	0.441	0.085	0.096	0.674	0.647
0.085	0.096	0.564	0.536	0.085	1.375	0.514	0.295
0.085	0.522	0.498	0.384	0.230	-0.330	0.564	0.514
0.230	-0.330	0.492	0.423	0.230	0.096	0.582	0.514
0.230	0.096	0.538	0.517	0.230	0.522	0.550	0.449
0.230	0.522	0.466	0.367	0.230	0.949	0.516	0.347
0.230	0.949	0.429	0.280	0.375	-0.757	0.485	0.377
0.375	-0.330	0.458	0.436	0.375	0.096	0.520	0.425
0.375	0.096	0.508	0.507	0.520	0.096	0.531	0.509
0.375	0.522	0.442	0.361	0.520	1.375	0.436	0.260
0.520	0.096	0.391	0.307	0.665	0.522	0.482	0.386
0.520	0.949	0.449	0.438	0.665	1.375	0.423	0.255
0.665	0.096	0.457	0.436				
SM490Y_Rr12_T30				SBHS500_Rr12_T30			
0.085	-0.330	0.523	0.445	0.085	0.096	0.596	0.564
0.085	0.096	0.564	0.541	0.085	1.375	0.467	0.256
0.085	0.522	0.498	0.388	0.230	-0.330	0.530	0.439
0.230	-0.330	0.491	0.427	0.230	0.096	0.573	0.516
0.230	0.096	0.542	0.522	0.230	0.522	0.508	0.393
0.230	0.522	0.498	0.388	0.230	0.949	0.471	0.302
0.230	0.949	0.428	0.282	0.375	-0.757	0.462	0.328
0.375	-0.330	0.456	0.429	0.375	0.096	0.495	0.429
0.375	0.096	0.502	0.498	0.520	0.096	0.462	0.438
0.375	0.522	0.440	0.415	0.520	1.375	0.402	0.325
0.520	0.096	0.473	0.471	0.665	0.522	0.431	0.348
0.520	0.949	0.389	0.359	0.665	1.375	0.391	0.220
0.665	0.096	0.460	0.439				
SM570_Rr12_T10				SBHS700_Rr12_T10			
0.085	0.096	0.569	0.537	0.085	0.096	0.560	0.522
0.085	1.375	0.448	0.245	0.085	1.375	0.460	0.234
0.230	-0.330	0.511	0.430	0.230	-0.330	0.512	0.419
0.230	0.096	0.547	0.527	0.230	0.096	0.541	0.511
0.230	0.522	0.488	0.375	0.230	0.522	0.493	0.364
0.230	0.949	0.453	0.289	0.230	0.949	0.462	0.280
0.375	-0.757	0.444	0.334	0.375	-0.757	0.450	0.304
0.375	0.096	0.510	0.506	0.375	0.096	0.515	0.476

Appendix E: FEA Results for Model-2

$x_1 = \sigma_{rc}/\sigma_y$	$x_2 = 1000\delta_{0l}/a$	σ_{ULS}/σ_y	σ_{SLS}/σ_y	$x_1 = \sigma_{rc}/\sigma_y$	$x_2 = 1000\delta_{0l}/a$	σ_{ULS}/σ_y	σ_{SLS}/σ_y
0.520	0.096	0.475	0.472	0.520	0.096	0.474	0.438
0.520	1.375	0.392	0.309	0.520	1.375	0.400	0.302
0.665	0.522	0.420	0.351	0.665	0.522	0.422	0.335
0.665	1.375	0.384	0.211	0.665	1.375	0.388	0.295
SM570_Rr12_T20				SBHS700_Rr12_T20			
0.085	0.096	0.607	0.578	0.085	0.096	0.560	0.522
0.085	1.375	0.468	0.263	0.085	1.375	0.460	0.234
0.230	-0.330	0.535	0.522	0.230	-0.330	0.512	0.419
0.230	0.096	0.568	0.522	0.230	0.096	0.541	0.518
0.230	0.522	0.512	0.403	0.230	0.522	0.493	0.364
0.230	0.949	0.474	0.310	0.230	0.949	0.462	0.280
0.375	-0.757	0.458	0.415	0.375	-0.757	0.450	0.390
0.375	0.096	0.548	0.547	0.375	0.096	0.510	0.509
0.520	0.096	0.496	0.484	0.520	0.096	0.474	0.454
0.520	1.375	0.404	0.332	0.520	1.375	0.400	0.302
0.665	0.522	0.430	0.348	0.665	0.522	0.422	0.335
0.665	1.375	0.398	0.226	0.665	1.375	0.406	0.306
SM570_Rr12_T30				SBHS700_Rr12_T30			
0.085	0.096	0.578	0.547	0.085	0.096	0.563	0.525
0.085	1.375	0.450	0.250	0.085	1.375	0.461	0.236
0.230	-0.330	0.516	0.438	0.230	-0.330	0.514	0.422
0.230	0.096	0.557	0.529	0.230	0.096	0.545	0.512
0.230	0.522	0.492	0.381	0.230	0.522	0.495	0.367
0.230	0.949	0.456	0.294	0.230	0.949	0.463	0.282
0.375	-0.757	0.444	0.398	0.375	-0.757	0.449	0.387
0.375	0.096	0.507	0.499	0.375	0.096	0.519	0.406
0.520	0.096	0.482	0.474	0.520	0.096	0.474	0.458
0.520	1.375	0.391	0.315	0.520	1.375	0.400	0.304
0.665	0.522	0.430	0.341	0.665	0.522	0.418	0.306
0.665	1.375	0.380	0.214	0.665	1.375	0.389	0.295
				SBHS700_Rr12_T50			
				0.085	0.096	0.555	0.517
				0.085	1.375	0.456	0.233
				0.230	-0.330	0.507	0.415
				0.230	0.096	0.537	0.501
				0.230	0.522	0.489	0.361
				0.230	0.949	0.458	0.278
				0.375	-0.757	0.448	0.293
				0.375	0.096	0.512	0.424
				0.520	0.096	0.472	0.456
				0.520	1.375	0.395	0.296
				0.665	0.522	0.423	0.323
				0.665	1.375	0.385	0.291

R_R = 1.4							
$x_1 = \sigma_{rc}/\sigma_y$	$x_2 = 1000\delta_{0l}/a$	σ_{ULS}/σ_y	σ_{SLS}/σ_y	$x_1 = \sigma_{rc}/\sigma_y$	$x_2 = 1000\delta_{0l}/a$	σ_{ULS}/σ_y	σ_{SLS}/σ_y
SM490Y_Rr14_T10				SBHS500_Rr14_T10			
0.085	-0.330	0.412	0.331	0.085	0.096	0.426	0.393
0.085	0.096	0.435	0.404	0.085	1.375	0.355	0.178
0.085	0.522	0.397	0.287	0.230	-0.330	0.397	0.310
0.230	-0.330	0.386	0.307	0.230	0.096	0.435	0.371
0.230	0.096	0.438	0.366	0.230	0.522	0.383	0.268
0.230	0.522	0.370	0.267	0.230	0.949	0.355	0.267
0.230	0.949	0.345	0.201	0.375	-0.757	0.360	0.220
0.375	-0.330	0.368	0.301	0.375	0.096	0.392	0.365
0.375	0.096	0.396	0.376	0.520	0.096	0.372	0.359
0.375	0.522	0.361	0.262	0.520	1.375	0.310	0.146
0.520	0.096	0.378	0.371	0.665	0.522	0.323	0.187
0.520	0.949	0.314	0.189	0.665	1.375	0.322	0.143
0.665	0.096	0.361	0.348				
SM490Y_Rr14_T20				SBHS500_Rr14_T20			
0.085	-0.330	0.412	0.332	0.085	0.096	0.426	0.394
0.085	0.096	0.435	0.405	0.085	1.375	0.355	0.178
0.085	0.522	0.396	0.289	0.230	-0.330	0.390	0.309
0.230	-0.330	0.396	0.332	0.230	0.096	0.436	0.371
0.230	0.096	0.435	0.363	0.230	0.522	0.376	0.268
0.230	0.522	0.375	0.330	0.230	0.949	0.355	0.267
0.230	0.949	0.345	0.205	0.375	-0.757	0.350	0.221
0.375	-0.330	0.373	0.291	0.375	0.096	0.392	0.368
0.375	0.096	0.404	0.393	0.520	0.096	0.372	0.359
0.375	0.522	0.362	0.263	0.520	1.375	0.317	0.145
0.520	0.096	0.378	0.373	0.665	0.522	0.329	0.186
0.520	0.949	0.317	0.185	0.665	1.375	0.322	0.142
0.665	0.096	0.366	0.349				
SM490Y_Rr14_T30				SBHS500_Rr14_T30			
0.085	-0.330	0.398	0.321	0.085	0.096	0.455	0.421
0.085	0.096	0.421	0.391	0.085	1.375	0.375	0.190
0.085	0.522	0.384	0.279	0.230	-0.330	0.423	0.333
0.230	-0.330	0.374	0.302	0.230	0.096	0.436	0.401
0.230	0.096	0.413	0.353	0.230	0.522	0.402	0.288
0.230	0.522	0.363	0.319	0.230	0.949	0.375	0.218
0.230	0.949	0.334	0.197	0.375	-0.757	0.364	0.237
0.375	-0.330	0.364	0.272	0.375	0.096	0.416	0.389
0.375	0.096	0.383	0.363	0.520	0.096	0.394	0.386
0.375	0.522	0.358	0.255	0.520	1.375	0.342	0.159
0.520	0.096	0.366	0.359	0.665	0.522	0.362	0.191
0.520	0.949	0.310	0.214	0.665	1.375	0.322	0.154
0.665	0.096	0.353	0.340				
SM570_Rr14_T10				SBHS700_Rr14_T10			
0.085	0.096	0.444	0.411	0.085	0.096	0.441	0.405
0.085	1.375	0.366	0.187	0.085	1.375	0.377	0.180
0.230	-0.330	0.407	0.350	0.230	-0.330	0.410	0.318
0.230	0.096	0.432	0.332	0.230	0.096	0.423	0.378
0.230	0.522	0.389	0.289	0.230	0.522	0.394	0.274
0.230	0.949	0.366	0.216	0.230	0.949	0.375	0.212
0.375	-0.757	0.359	0.231	0.375	-0.757	0.364	0.228
0.375	0.096	0.408	0.381	0.375	0.096	0.406	0.356

Appendix E: FEA Results for Model-2

$x_1 = \sigma_{rc}/\sigma_y$	$x_2 = 1000\delta_{01}/a$	σ_{ULS}/σ_y	σ_{SLS}/σ_y	$x_1 = \sigma_{rc}/\sigma_y$	$x_2 = 1000\delta_{01}/a$	σ_{ULS}/σ_y	σ_{SLS}/σ_y
0.520	0.096	0.386	0.376	0.520	0.096	0.386	0.370
0.520	1.375	0.318	0.153	0.520	1.375	0.342	0.224
0.665	0.522	0.337	0.177	0.665	0.522	0.339	0.255
0.665	1.375	0.320	0.149	0.665	1.375	0.319	0.145
SM570_Rr14_T20				SBHS700_Rr14_T20			
0.085	0.096	0.430	0.398	0.085	0.096	0.440	0.404
0.085	1.375	0.355	0.181	0.085	1.375	0.377	0.179
0.230	-0.330	0.392	0.191	0.230	-0.330	0.410	0.318
0.230	0.096	0.427	0.379	0.230	0.096	0.423	0.378
0.230	0.522	0.382	0.329	0.230	0.522	0.395	0.271
0.230	0.949	0.356	0.208	0.230	0.949	0.375	0.212
0.375	-0.757	0.351	0.223	0.375	-0.757	0.363	0.224
0.375	0.096	0.398	0.384	0.375	0.096	0.407	0.322
0.520	0.096	0.374	0.363	0.520	0.096	0.386	0.370
0.520	1.375	0.325	0.146	0.520	1.375	0.342	0.151
0.665	0.522	0.330	0.260	0.665	0.522	0.339	0.255
0.665	1.375	0.299	0.139	0.665	1.375	0.319	0.145
SM570_Rr14_T30				SBHS700_Rr14_T30			
0.085	0.096	0.440	0.408	0.085	0.096	0.432	0.396
0.085	1.375	0.362	0.185	0.085	1.375	0.372	0.178
0.230	-0.330	0.404	0.322	0.230	-0.330	0.400	0.313
0.230	0.096	0.450	0.380	0.230	0.096	0.414	0.332
0.230	0.522	0.390	0.328	0.230	0.522	0.387	0.265
0.230	0.949	0.362	0.277	0.230	0.949	0.368	0.207
0.375	-0.757	0.357	0.234	0.375	-0.757	0.359	0.222
0.375	0.096	0.367	0.288	0.375	0.096	0.406	0.292
0.520	0.096	0.365	0.179	0.520	0.096	0.379	0.362
0.520	1.375	0.317	0.178	0.520	1.375	0.324	0.181
0.665	0.522	0.332	0.257	0.665	0.522	0.339	0.255
0.665	1.375	0.312	0.146	0.665	1.375	0.315	0.143

APPENDIX F

FEA Results for Model-3

R_R = 0.4

$x_1 = \sigma_{rc}/\sigma_y$	$x_2 = 1000\delta_{01}/a$	$x_3 = 150 \Delta_{ini} /b_s$	σ_{ULS}/σ_y	$x_1 = \sigma_{rc}/\sigma_y$	$x_2 = 1000\delta_{01}/a$	$x_3 = 150 \Delta_{ini} /b_s$	σ_{ULS}/σ_y
SM490Y_R _R 0.4_T40				SM570_R _R 0.4_T40			
0.230	0.096	0.138	1.003	0.230	0.096	0.138	1.004
0.375	0.096	0.138	1.003	0.375	0.096	0.138	1.002
0.230	0.522	0.138	1.002	0.230	0.522	0.138	1.004
0.230	0.096	0.245	1.001	0.230	0.096	0.245	1.003
0.085	0.096	0.138	1.001	0.085	0.096	0.138	1.004
0.230	-0.330	0.138	1.002	0.230	-0.330	0.138	1.001
0.230	0.096	0.032	1.003	0.230	0.096	0.032	1.006
SBHS500_R _R 0.4_T50				SBHS700_R _R 0.4_T50			
0.230	0.096	0.138	1.005	0.230	0.096	0.138	1.026
0.375	0.096	0.138	1.002	0.375	0.096	0.138	1.024
0.230	0.522	0.138	1.004	0.230	0.522	0.138	1.020
0.230	0.096	0.245	1.003	0.230	0.096	0.245	1.023
0.085	0.096	0.138	1.004	0.085	0.096	0.138	1.022
0.230	-0.330	0.138	1.003	0.230	-0.330	0.138	1.019
0.230	0.096	0.032	1.005	0.230	0.096	0.032	1.019

R_R = 0.6

$x_1 = \sigma_{rc}/\sigma_y$	$x_2 = 1000\delta_{01}/a$	$x_3 = 150 \Delta_{ini} /b_s$	σ_{ULS}/σ_y	$x_1 = \sigma_{rc}/\sigma_y$	$x_2 = 1000\delta_{01}/a$	$x_3 = 150 \Delta_{ini} /b_s$	σ_{ULS}/σ_y
SM490Y_R _R 0.6_T30				SM570_R _R 0.6_T30			
0.230	0.096	0.138	1.001	0.230	0.096	0.138	1.001
0.375	0.096	0.138	0.988	0.375	0.096	0.138	1.002
0.230	0.522	0.138	0.959	0.230	0.522	0.138	0.996
0.230	0.096	0.245	0.988	0.230	0.096	0.245	0.996
0.085	0.096	0.138	0.984	0.085	0.096	0.138	0.974
0.230	-0.330	0.138	0.972	0.230	-0.330	0.138	0.973
0.230	0.096	0.032	0.986	0.230	0.096	0.032	0.937
SBHS500_R _R 0.6_T30				SBHS700_R _R 0.6_T30			
0.230	0.096	0.138	1.002	0.230	0.096	0.138	1.000
0.375	0.096	0.138	1.000	0.375	0.096	0.138	0.994
0.230	0.522	0.138	0.963	0.230	0.522	0.138	0.957
0.230	0.096	0.245	0.987	0.230	0.096	0.245	0.990
0.085	0.096	0.138	0.993	0.085	0.096	0.138	1.002
0.230	-0.330	0.138	0.999	0.230	-0.330	0.138	0.967
0.230	0.096	0.032	0.957	0.230	0.096	0.032	1.000

R_R = 0.8

$x_1 = \sigma_{rc}/\sigma_y$	$x_2 = 1000\delta_{0l}/a$	$x_3 = 150 \Delta_{ini} /b_s$	σ_{ULS}/σ_y	$x_1 = \sigma_{rc}/\sigma_y$	$x_2 = 1000\delta_{0l}/a$	$x_3 = 150 \Delta_{ini} /b_s$	σ_{ULS}/σ_y
SM490Y_R_R 0.8_T20				SM570_R_R 0.8_T20			
0.230	0.096	0.138	0.874	0.230	0.096	0.138	0.865
0.375	0.096	0.138	0.859	0.375	0.096	0.138	0.860
0.230	0.522	0.138	0.833	0.230	0.522	0.138	0.838
0.230	0.096	0.245	0.851	0.230	0.096	0.245	0.847
0.085	0.096	0.138	0.922	0.085	0.096	0.138	0.923
0.230	-0.330	0.138	0.843	0.230	-0.330	0.138	0.845
0.230	0.096	0.032	0.884	0.230	0.096	0.032	0.883
SBHS500_R_R 0.8_T20				SBHS700_R_R 0.8_T20			
0.230	0.096	0.138	0.907	0.230	0.096	0.138	0.877
0.375	0.096	0.138	0.863	0.375	0.096	0.138	0.876
0.230	0.522	0.138	0.839	0.230	0.522	0.138	0.845
0.230	0.096	0.245	0.857	0.230	0.096	0.245	0.879
0.085	0.096	0.138	0.926	0.085	0.096	0.138	0.929
0.230	-0.330	0.138	0.847	0.230	-0.330	0.138	0.853
0.230	0.096	0.032	0.882	0.230	0.096	0.032	0.884

R_R = 1.0

$x_1 = \sigma_{rc}/\sigma_y$	$x_2 = 1000\delta_{0l}/a$	$x_3 = 150 \Delta_{ini} /b_s$	σ_{ULS}/σ_y	σ_{SLS}/σ_y	$x_1 = \sigma_{rc}/\sigma_y$	$x_2 = 1000\delta_{0l}/a$	$x_3 = 150 \Delta_{ini} /b_s$	σ_{ULS}/σ_y	σ_{SLS}/σ_y
SM490Y_R_R 1.0_T15					SM570_R_R 1.0_T20				
0.230	0.096	0.138	0.718	0.689	0.230	0.096	0.138	0.716	0.686
0.375	0.096	0.138	0.679	0.601	0.375	0.096	0.138	0.675	0.596
0.230	0.522	0.138	0.703	0.628	0.230	0.522	0.138	0.701	0.638
0.230	0.096	0.245	0.707	0.651	0.230	0.096	0.245	0.705	0.649
0.085	0.096	0.138	0.805	0.793	0.085	0.096	0.138	0.805	0.674
0.230	-0.330	0.138	0.704	0.673	0.230	-0.330	0.138	0.704	0.653
0.230	0.096	0.032	0.736	0.735	0.230	0.096	0.032	0.731	0.729
SBHS500_R_R 1.0_T20					SBHS700_R_R 1.0_T20				
0.230	0.096	0.138	0.716	0.690	0.230	0.096	0.138	0.711	0.687
0.375	0.096	0.138	0.673	0.596	0.375	0.096	0.138	0.666	0.595
0.230	0.522	0.138	0.702	0.621	0.230	0.522	0.138	0.700	0.599
0.230	0.096	0.245	0.706	0.650	0.230	0.096	0.245	0.703	0.637
0.085	0.096	0.138	0.809	0.789	0.085	0.096	0.138	0.811	0.709
0.230	-0.330	0.138	0.706	0.651	0.230	-0.330	0.138	0.706	0.645
0.230	0.096	0.032	0.736	0.736	0.230	0.096	0.032	0.736	0.736

R_R = 1.2

$x_1 = \sigma_{rc}/\sigma_y$	$x_2 = 1000\delta_{01}/a$	$x_3 = 150 \Delta_{ini} /b_s$	σ_{ULS}/σ_y	σ_{SLS}/σ_y	$x_1 = \sigma_{rc}/\sigma_y$	$x_2 = 1000\delta_{01}/a$	$x_3 = 150 \Delta_{ini} /b_s$	σ_{ULS}/σ_y	σ_{SLS}/σ_y
SM490Y_R_R 1.2_T15					SM570_R_R 1.2_T15				
0.230	0.096	0.138	0.583	0.533	0.230	0.096	0.138	0.580	0.483
0.375	0.096	0.138	0.558	0.443	0.375	0.096	0.138	0.555	0.431
0.230	0.522	0.138	0.578	0.422	0.230	0.522	0.138	0.575	0.419
0.230	0.096	0.245	0.578	0.490	0.230	0.096	0.245	0.576	0.475
0.085	0.096	0.138	0.650	0.573	0.085	0.096	0.138	0.654	0.563
0.230	-0.330	0.138	0.580	0.469	0.230	-0.330	0.138	0.576	0.461
0.230	0.096	0.032	0.586	0.554	0.230	0.096	0.032	0.584	0.531
SBHS500_R_R 1.2_T15					SBHS700_R_R 1.2_T15				
0.230	0.096	0.138	0.581	0.486	0.230	0.096	0.138	0.580	0.461
0.375	0.096	0.138	0.554	0.436	0.375	0.096	0.138	0.547	0.428
0.230	0.522	0.138	0.576	0.413	0.230	0.522	0.138	0.572	0.416
0.230	0.096	0.245	0.577	0.504	0.230	0.096	0.245	0.575	0.450
0.085	0.096	0.138	0.651	0.570	0.085	0.096	0.138	0.649	0.566
0.230	-0.330	0.138	0.577	0.460	0.230	-0.330	0.138	0.573	0.460
0.230	0.096	0.032	0.585	0.537	0.230	0.096	0.032	0.584	0.527

R_R = 1.4

$x_1 = \sigma_{rc}/\sigma_y$	$x_2 = 1000\delta_{01}/a$	$x_3 = 150 \Delta_{ini} /b_s$	σ_{ULS}/σ_y	σ_{SLS}/σ_y	$x_1 = \sigma_{rc}/\sigma_y$	$x_2 = 1000\delta_{01}/a$	$x_3 = 150 \Delta_{ini} /b_s$	σ_{ULS}/σ_y	σ_{SLS}/σ_y
SM490Y_R_R 1.4_T10					SM570_R_R 1.4_T15				
0.230	0.096	0.138	0.497	0.431	0.230	0.096	0.138	0.495	0.404
0.375	0.096	0.138	0.474	0.336	0.375	0.096	0.138	0.474	0.301
0.230	0.522	0.138	0.492	0.315	0.230	0.522	0.138	0.491	0.308
0.230	0.096	0.245	0.497	0.363	0.230	0.096	0.245	0.494	0.391
0.085	0.096	0.138	0.539	0.491	0.085	0.096	0.138	0.539	0.505
0.230	-0.330	0.138	0.494	0.358	0.230	-0.330	0.138	0.493	0.345
0.230	0.096	0.032	0.497	0.435	0.230	0.096	0.032	0.495	0.411
SBHS500_R_R 1.4_T15					SBHS700_R_R 1.4_T15				
0.230	0.096	0.138	0.494	0.400	0.230	0.096	0.138	0.488	0.380
0.375	0.096	0.138	0.472	0.300	0.375	0.096	0.138	0.465	0.314
0.230	0.522	0.138	0.490	0.306	0.230	0.522	0.138	0.486	0.292
0.230	0.096	0.245	0.493	0.388	0.230	0.096	0.245	0.489	0.374
0.085	0.096	0.138	0.537	0.488	0.085	0.096	0.138	0.534	0.480
0.230	-0.330	0.138	0.492	0.341	0.230	-0.330	0.138	0.487	0.333
0.230	0.096	0.032	0.494	0.409	0.230	0.096	0.032	0.491	0.447